ON THE IMPORTANCE OF POLARIZATION IN RADAR SCATTERING PROBLEMS.

Thesis by

Jakob Johannes van Zyl

In Partial Fulfillment of the Requirements

for the Degree of

Doctor of Philosophy

California Institute of Technology

Pasadena, California

1986

(Submitted December 10, 1985)

ACKNOWLEDGEMENTS

I would like to express my sincere gratitude to my advisor, Professor Charles Herach Papas, and Dr. Charles Elachi for their guidance, encouragement and support during the course of this work. I would also like to thank Dr. Howard Zebker (Jet Propulsion Laboratory) and Dr. Nader Engheta for many helpful discussions regarding the contents of this thesis.

Many thanks to Dr. Dan Held, Dr. Howard Zebker and the rest of the Radar Science Group at the Jet Propulsion Laboratory for allowing me to use the multipolarization synthetic aperture radar data.

This thesis is dedicated to my wife, Kalfie, whose loving support and encouragement helped to make producing this work a pleasure.

ABSTRACT

In this thesis, the importance of polarization in radar scattering problems is investigated. The different matrix characterizations of scatterers are discussed in detail. The problem of finding the polarizations which would yield an optimum amount of power received from the scatterer is solved for the most general case. This shows that for certain classes of scatterers six optimum polarizations exist. The concept of a polarization spectrum to characterize a scatterer is introduced. The usefulness of these spectrums is illustrated when results, using measured multipolarization synthetic aperture radar data, are discussed. Another useful parameter, the coefficient of variation, is introduced. Measured results show that this parameter may be used to form an idea of the scale over which the scattering properties of the scene being imaged vary. The problem of finding the effective scattering operator of a slab filled with different scatterers is formulated. Detailed expressions are given for the effective single scattering operators. This formulation is illustrated by calculating the effective single scattering operators for models of different types of vegetation.

TABLE OF CONTENTS

CHAPTER 1

INTRODUCTION.

The analysis of the scattering of electromagnetic waves by rough surfaces has been the subject of many studies during the past four decades. It received its biggest impetus from the advent of radar and the subsequent need to know more about the radar returns from terrain and the sea. In recent years, the increasing use of spaceborne radars to map the surface of the earth once more focussed attention on the problem of radar backscatter from different types of terrain. The appearance of multipolarization imaging radars added a new dimension to this problem, and may provide scientists with some valuable new information about the terrains currently under investigation.

The problem of radar backscatter from natural surfaces is inherently different from, and usually much more complicated than that of scattering by other bodies. For instance, the exact shape of a natural surface is usually not known, and in many cases may not be of concern to scientists involved in radar imaging. Instead, only average properties of the surface shape usually enter into the problem. Since the exact boundaries of the surface are not known, a boundary-value approach cannot be used to solve the problem of radar backscatter from natural surfaces. Rather, one is usually more interested in the relationship between the average properties of the natural surface and the average radar return observed.

In radar imaging, the average properties of the radar backscatter are known, and one wants to obtain some information about the scattering terrain from these known properties. Due to the complexity of the problem, it is obvious that every possible piece of information available to the scientists involved should be utilized fully to extract the required information from the

measured data. In this thesis, the optimum use of the polarization properties of the scattering terrain will be discussed in detail.

The pioneering works in this field include that of Kennaugh [25],[10] on the effects of the type of polarization on the radar echo characteristics and that of Huynen [2] on the phenomenological theory of radar targets. Recently, the calculation of the optimum polarizations of a scatterer received intense attention [2],[3],[4],[9],[22], especially when coherent measurements are considered. A few attempts were made to find the polarizations which would optimize the amount of power received from the scatterer when the scattered waves are only partially polarized [4],[22]. Since most, if not all, of the waves scattered by natural surfaces are only partially polarized, this problem will be discussed in detail in this thesis.

This thesis is divided into seven chapters. In Chapter 2, the concept of optimum polarizations is linked to the amount of power that an antenna would absorb from the scattered wave. The different characterizations that should be used for different types of scatterers are discussed in detail. Two general methods for finding the optimum polarizations of a scatterer, which applies both when the scattered waves are partially and completely polarized, are derived in this chapter. These methods show that in the general case, *six* optimum polarizations exist and not *four* as previously reported in the literature [2],[3],[4],[9],[22]. To fully utilise the polarization information contained in the scattered waves, the concept of a *polarization spectrum* is introduced in this chapter. It is shown how the information contained in this polarization spectrum may be used to form an idea of the amount by which the scattering properties of the natural terrain varies spatially. It is also shown how the polarization spectrum may be used to compare and classify different scatterers. Finally, the problem of finding the optimum polarization for

discrimination between different scatterers is solved.

In radar imaging of natural terrain, one invariably encounters scattering from vegetated surfaces. One way to model scattering from such vegetated surfaces, is to consider the scattering from a layer of volume scatterers covering a rough surface [11]. In Chapter 3, the problem of finding the effective scattering operators of such a combination is formulated. Detailed expressions for these effective scattering operators when only single reflections of the incident wave is considered, are listed in this chapter.

In Chapter 4, the results of Chapter 3 are illustrated by calculating the effective scattering operators for a few selected models for different types of vegetation. The results of these models are discussed in detail and are shown to agree with the physical picture of the scattering processes.

Chapter 5 shows how models, such as those calculated in Chapter 4, may be used to find some information about the scattering surface through a knowledge of measured multipolarization radar imaging data.

In Chapter 6 some polarization spectrums for different types of scattering surfaces, taken from multipolarization radar images, are shown. Also, images of the amount of spatial variation in scattering properties, using real multipolarization radar imaging data, are presented and discussed.

Some conclusions are drawn and some recommendations are made in Chapter 7.

CHAPTER 2

OPTIMUM POLARIZATIONS FOR USE IN SCATTERING PROBLEMS.

2.1 Introduction

First, it will be shown how the polarization of an antenna affects the amount of power that the antenna absorbs from an incident Electromagnetic (EM) wave. Electric fields, power and polarization vectors ***radiated*** by the antenna will be denoted by the superscript ***rad***. Likewise, electric fields, power and polarization vectors *incident* on the antenna will be denoted by a superscript *inc*.

The radial component of the radiated Poynting's vector in the far field of the antenna, expressed in spherical polar coordinates is (c.f. [1])

$$S^{rad}(r,\vartheta,\varphi) = \tfrac{1}{2}\sqrt{\frac{\varepsilon_0}{\mu_0}}\,\mathbf{E}^{rad}(r,\vartheta,\varphi)\cdot\mathbf{E}^{rad*}(r,\vartheta,\varphi)\,, \tag{2-1}$$

where $\mathbf{E}^{rad}$ denotes the far-zone radiated electric field vector and * denotes complex conjugation. The radiated field polarization vector is defined by:

$$\mathbf{p}^{rad} = \frac{\mathbf{E}^{rad}}{\sqrt{\mathbf{E}^{rad}\cdot\mathbf{E}^{rad*}}}\,. \tag{2-2}$$

Similarly, one finds for the incident plane EM wave that

$$S^{inc}(\vartheta,\varphi) = \tfrac{1}{2}\sqrt{\frac{\varepsilon_0}{\mu_0}}\,\mathbf{E}^{inc}(\vartheta,\varphi)\cdot\mathbf{E}^{inc*}(\vartheta,\varphi) \tag{2-3}$$

and

$$\mathbf{p}^{inc} = \frac{\mathbf{E}^{inc}}{\sqrt{\mathbf{E}^{inc}\cdot\mathbf{E}^{inc*}}}\,. \tag{2-4}$$

The power absorbed by a load connected to the antenna is [1]:

$$P_{rec} = \frac{\lambda^2}{4\pi} g(\vartheta,\varphi)\, S^{inc}(\vartheta,\varphi)\, |\mathbf{p}^{rad}(\vartheta,\varphi)\cdot\mathbf{p}^{inc}(\vartheta,\varphi)|^2 , \tag{2-5}$$

where $g(\vartheta,\varphi)$ is the antenna gain function and $\frac{\lambda^2}{4\pi} g(\vartheta,\varphi)$ is the effective area of the antenna. From (2-2) and (2-4) it follows that

$$|\mathbf{p}^{rad}\cdot\mathbf{p}^{inc}|^2 = \frac{|\mathbf{E}^{rad}\cdot\mathbf{E}^{inc}|^2}{|\mathbf{E}^{rad}|^2\,|\mathbf{E}^{inc}|^2} . \tag{2-6}$$

Using (2-3) and (2-6) in (2-5), one finds

$$P_{rec} = K(\lambda,\vartheta,\varphi)\,|\mathbf{E}^{rad}\cdot\mathbf{E}^{inc}|^2 , \tag{2-7}$$

where

$$K(\lambda,\vartheta,\varphi) = \frac{\tfrac{1}{2}\,\frac{\lambda^2}{4\pi}\, g(\vartheta,\varphi)\,\sqrt{\frac{\varepsilon_0}{\mu_0}}}{|\mathbf{E}^{rad}|^2} . \tag{2-8}$$

In the rest of this discussion it will be assumed that K is independent of polarization. From (2-7) and (2-8) it is clear that the direction of $\mathbf{E}^{rad}$ relative to that of $\mathbf{E}^{inc}$ plays an important role in determining how much power will be absorbed from the incident wave. From (2-5) it follows that

$$0 \le P_{rec} \le \frac{\lambda^2}{4\pi} g(\vartheta,\varphi)\, S^{inc}(\vartheta,\varphi) . \tag{2-9}$$

In the rest of this chapter the use of polarization to enhance or reduce the absorption of power from waves scattered by unknown objects will be explored in great detail. It will be shown that certain optimum polarizations exist which, if used when illuminating the scattering bodies and also to receive the scattered waves, ensure that the maximum or minimum amount of power will be absorbed from the scattered waves. It will be shown that in the most general case, *six* optimum polarizations exist and not only four as has been reported in the literature so far [2] - [4]. Finally, it will be shown that it is possible to use

polarization to discriminate between two scattering bodies.

2.2 Mathematical Characterization of Scatterers.

Let an arbitrary scatterer of finite size be illuminated by a plane EM wave of infinite extend. For the present purpose, it will be assumed that the origin of a Cartesian coordinate system is located somewhere inside the scatterer and that the plane wave is travelling in the positive z- direction of this coordinate system. In this coordinate system, the illuminating plane wave has an electric field vector of the form

$$\mathbf{E}^{inc} = [E_x^{inc}\mathbf{e}_x + E_y^{inc}\mathbf{e}_y]\, e^{i(kz-\omega t)}, \qquad (2\text{-}10)$$

where E_x and E_y are complex amplitudes in the x- and y- directions respectively, and $kz-\omega t$ is the instantaneous phase of the incident plane wave. Here ω denotes the angular frequency of the wave, t denotes time and k is the wave number of the wave.

In the far-zone of the scatterer, the scattered wave is a spherical, outgoing wave. To express the electric field of this wave mathematically at some observation point P, a second coordinate coordinate system (x',y',z') of which the origin coincides with that of the original coordinate system is introduced. To express the scattered fields in the basis of the antenna, the negative z' axis points in the direction into which the scattered wave is propagating as shown in Figure 2.1.

In this coordinate system, the scattered electric field is given by:

$$\mathbf{E}^{sc} = [E_{x'}^{sc}\mathbf{e}_{x'} + E_{y'}^{sc}\mathbf{e}_{y'}]\, \frac{e^{-i(kz+\omega t)}}{kr}, \qquad (2\text{-}11)$$

where r is the distance between the scatterer and the observation point and the k in the denominator is added to ensure that the expression is dimensionally

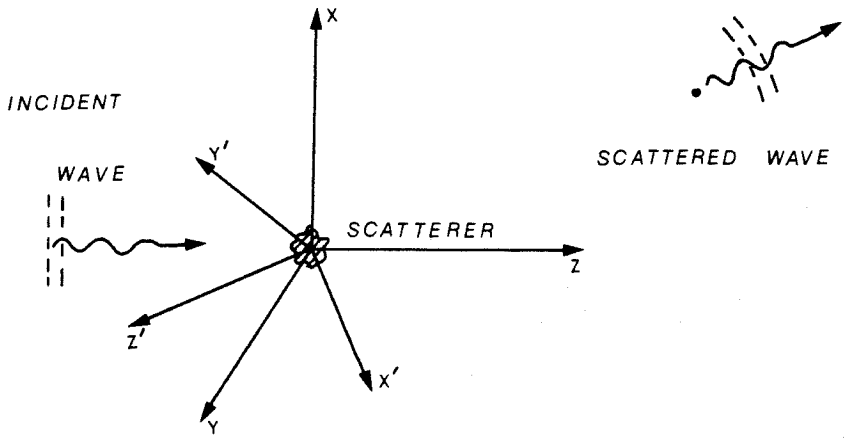

Figure 2.1. Scattering Geometry.

correct.

To characterize the scatterer, one may define a complex scattering matrix as follows:

$$\begin{bmatrix} E_{x'}^{sc} \\ E_{y'}^{sc} \end{bmatrix} = \begin{bmatrix} S_{x'x} & S_{x'y} \\ S_{y'x} & S_{y'y} \end{bmatrix} \begin{bmatrix} E_{x}^{inc} \\ E_{y}^{inc} \end{bmatrix}. \tag{2-12}$$

As will be shown shortly, it is not always possible to characterize a complex scatterer (i.e., one changing with time or one made up of a number of independent incoherent scatterers) by a single scattering matrix. For these cases, another characterization, the *Stokes Scattering Operator* (SSO) will be used. This operator describes how the Stokes parameters as opposed to the electric fields of the incident wave are transformed by the scatterer. In this discussion, the definition of Stokes parameters as found in [1] and [5] will be

used. According to this definition, an electric field of the form

$$\mathbf{E}=\mathrm{Re}\left\{\left[E_x\mathbf{e}_x+E_y\mathbf{e}_y\right]e^{i(kr-\omega t)}\right\} \tag{2-13}$$

with E_x and E_y complex quantities, is assumed. The Stokes parameters of this electric field are defined as:

$$\begin{bmatrix}S_0\\S_1\\S_2\\S_3\end{bmatrix} = \begin{bmatrix}E_xE_x^*+E_yE_y^*\\E_xE_x^*-E_yE_y^*\\2\mathrm{Re}[E_xE_y^*]\\2\mathrm{Im}[E_xE_y^*]\end{bmatrix}. \tag{2-14}$$

It is worth noting that the present definition of the Stokes parameters is the same as that used by Chandrasekhar [6] and van de Hulst [7], with the exception of a minus sign in the definition of S_3.

Now, let

$$\tilde{\mathbf{S}}^{inc} = \left[S_0^{inc}\,;\,S_1^{inc}\,;\,S_2^{inc}\,;\,S_3^{inc}\right] \tag{2-15a}$$

and

$$\tilde{\mathbf{S}}^{sc} = \left[S_0^{sc}\,;\,S_1^{sc}\,;\,S_2^{sc}\,;\,S_3^{sc}\right]. \tag{2-15b}$$

It is clear from (2-14) and (2-12) that it is possible to write

$$\mathbf{S}^{sc} = [\mathbf{M}]\mathbf{S}^{inc}, \tag{2-16}$$

where $[\mathbf{M}]$ is a 4x4 matrix with real coefficients. This matrix will be called the Stokes Scattering Operator (SSO) for obvious reasons. Following some simple algebra (shown in Appendix A) one finds that the elements of $[\mathbf{M}]$ is given, in terms of the elements of the Scattering Matrix, by:

$$M_{11} = \tfrac{1}{4}[S_{x'x}\cdot S_{x'x}^* + S_{x'y}\cdot S_{x'y}^* + S_{y'x}\cdot S_{y'x}^* + S_{y'y}\cdot S_{y'y}^*] \tag{2-17a}$$

$$M_{12} = \tfrac{1}{4}[S_{x'x}\cdot S^*_{x'x} - S_{x'y}\cdot S^*_{x'y} + S_{y'x}\cdot S^*_{y'x} - S_{y'y}\cdot S^*_{y'y}] \quad (2\text{-}17b)$$

$$M_{13} = \tfrac{1}{2}\,\mathrm{Re}[S^*_{x'x}\cdot S_{x'y}] + \tfrac{1}{2}\,\mathrm{Re}[S_{y'y}\cdot S^*_{y'x}] \quad (2\text{-}17c)$$

$$M_{14} = \tfrac{1}{2}\,\mathrm{Im}[S^*_{x'x}\cdot S_{x'y}] + \tfrac{1}{2}\,\mathrm{Im}[S_{y'y}\cdot S^*_{y'x}] \quad (2\text{-}17d)$$

$$M_{21} = \tfrac{1}{4}[S_{x'x}\cdot S^*_{x'x} + S_{x'y}\cdot S^*_{x'y} - S_{y'x}\cdot S^*_{y'x} - S_{y'y}\cdot S^*_{y'y}] \quad (2\text{-}17e)$$

$$M_{22} = \tfrac{1}{4}[S_{x'x}\cdot S^*_{x'x} - S_{x'y}\cdot S^*_{x'y} - S_{y'x}\cdot S^*_{y'x} + S_{y'y}\cdot S^*_{y'y}] \quad (2\text{-}17f)$$

$$M_{23} = \tfrac{1}{2}\,\mathrm{Re}[S^*_{x'x}\cdot S_{x'y}] - \tfrac{1}{2}\,\mathrm{Re}[S_{y'y}\cdot S^*_{y'x}] \quad (2\text{-}17g)$$

$$M_{24} = \tfrac{1}{2}\,\mathrm{Im}[S^*_{x'x}\cdot S_{x'y}] - \tfrac{1}{2}\,\mathrm{Im}[S_{y'y}\cdot S^*_{y'x}] \quad (2\text{-}17h)$$

$$M_{31} = \tfrac{1}{2}\,\mathrm{Re}[S^*_{x'x}\cdot S_{y'x}] + \tfrac{1}{2}\,\mathrm{Re}[S_{y'y}\cdot S^*_{x'y}] \quad (2\text{-}17i)$$

$$M_{32} = \tfrac{1}{2}\,\mathrm{Re}[S^*_{x'x}\cdot S_{y'x}] - \tfrac{1}{2}\,\mathrm{Re}[S_{y'y}\cdot S^*_{x'y}] \quad (2\text{-}17j)$$

$$M_{33} = \tfrac{1}{2}\,\mathrm{Re}[S^*_{x'y}\cdot S_{y'x}] + \tfrac{1}{2}\,\mathrm{Re}[S^*_{x'x}\cdot S_{y'y}] \quad (2\text{-}17k)$$

$$M_{34} = \tfrac{1}{2}\,\mathrm{Im}[S^*_{x'x}\cdot S_{y'y}] - \tfrac{1}{2}\,\mathrm{Im}[S^*_{x'y}\cdot S_{y'x}] \quad (2\text{-}17l)$$

$$M_{41} = \tfrac{1}{2}\,\mathrm{Im}[S^*_{x'x}\cdot S_{y'x}] + \tfrac{1}{2}\,\mathrm{Im}[S_{y'y}\cdot S^*_{x'y}] \quad (2\text{-}17m)$$

$$M_{42} = \tfrac{1}{2}\,\mathrm{Im}[S^*_{x'x}\cdot S_{y'x}] - \tfrac{1}{2}\,\mathrm{Im}[S_{y'y}\cdot S^*_{x'y}] \quad (2\text{-}17n)$$

$$M_{43} = \tfrac{1}{2}\,\mathrm{Im}[S^*_{x'x}\cdot S_{y'y}] + \tfrac{1}{2}\,\mathrm{Im}[S^*_{x'y}\cdot S_{y'x}] \quad (2\text{-}17o)$$

$$M_{44} = \tfrac{1}{2}\,\mathrm{Re}[S^*_{x'y}\cdot S_{y'x}] - \tfrac{1}{2}\,\mathrm{Re}[S^*_{x'x}\cdot S_{y'y}]\,. \quad (2\text{-}17p)$$

These two characterizations of a single scatterer are identical when power absorbed from the scattered wave is considered, as is shown in Appendix A. Combining the expressions (2-7), (2-12) and (2-16) with the results of Appendix A, the power absorbed by an antenna from the scattered wave is given by:

$$P_{rec} = K(\lambda,\vartheta,\varphi)\,|\mathbf{E}^{rad}\cdot[\mathbf{S}]\mathbf{E}^{rad}|^2 = K(\lambda,\vartheta,\varphi)\mathbf{S}^{rad}\cdot[\mathbf{M}]\mathbf{S}^{rad}\,. \qquad (2\text{-}18)$$

This section will be concluded by showing that any type of scatterer can be characterized by a Stokes Scattering Operator, but only certain types of scatterers can be characterized by a scattering matrix. It has already been shown that it is possible to find a Stokes Scattering Operator when the scattering matrix is known. To show that the inverse is not true, one has to consider the case of a scatterer which is made up of a number of independent, incoherent scattering centers.

In the case where an EM wave is made up by superposition of a number of EM waves with independent phases, the Stokes parameters of the resulting wave is given by ([1],[5],[6],[7]):

$$S_j = \sum_{i=1}^{N}(S_j)_i \qquad i=1,2,3\,, \qquad (2\text{-}19)$$

where the index i denotes each of the N EM waves with independent phases. Thus, if a scatterer is made up of N independent, incoherent scattering centers (i.e., there are no permanent phase relations between the waves scattered by these centers), (2-16) must read:

$$\mathbf{S}^{sc} = \sum_{i=1}^{N}\mathbf{S}_i^{sc} = \left[\sum_{i=1}^{N}[\mathbf{M}_i]\right]\mathbf{S}^{rad}\,. \qquad (2\text{-}20)$$

In the general case, there are 7 independent parameters in each scattering matrix. (A constant phase, which is lost when power measurements are made, may be neglected.) From (2-17) it is clear that each coefficient of $[\mathbf{M}_i]$ is a real number that is a nonlinear expression of the coefficients of the scattering matrix. If no assumptions are made at all, this means that there must be 9 relations between the 16 coefficients of each $[\mathbf{M}_i]$. These relations are:

$$(M_{11}-M_{22})^2-(M_{12}-M_{21})^2 = (M_{33}+M_{44})^2+(M_{34}-M_{43})^2 \qquad (2\text{-}21a)$$

$$M_{13}M_{23}+M_{14}M_{24} = M_{11}M_{21}-M_{12}M_{22} \qquad (2\text{-}21b)$$

$$M_{31}M_{32}+M_{41}M_{42} = M_{11}M_{12}-M_{21}M_{22} \qquad (2\text{-}21c)$$

$$M_{13}M_{14}-M_{23}M_{24} = M_{33}M_{34}+M_{43}M_{44} \qquad (2\text{-}21d)$$

$$M_{31}M_{41}-M_{32}M_{42} = M_{33}M_{43}+M_{34}M_{44} \qquad (2\text{-}21e)$$

$$M_{13}^2+M_{23}^2+M_{14}^2+M_{24}^2 = M_{11}^2-M_{12}^2+M_{21}^2-M_{22}^2 \qquad (2\text{-}21f)$$

$$M_{31}^2+M_{32}^2+M_{41}^2+M_{42}^2 = M_{11}^2+M_{12}^2-M_{21}^2-M_{22}^2 \qquad (2\text{-}21g)$$

$$M_{13}^2-M_{23}^2-M_{14}^2+M_{24}^2 = M_{33}^2-M_{34}^2+M_{43}^2-M_{44}^2 \qquad (2\text{-}21h)$$

$$M_{31}^2-M_{32}^2-M_{41}^2+M_{42}^2 = M_{33}^2+M_{34}^2-M_{43}^2-M_{44}^2 \,. \qquad (2\text{-}21i)$$

These relationships are all nonlinear, which means that they are lost in the addition process of (2-20). Generally, therefore, there are 16 independent parameters in the Stokes Scattering Operator. It is thus clear that it is not possible to characterize the most general scatterer (i.e., one made up of a number of independent, incoherent scattering centers) fully by a scattering matrix with only 7 independent parameters.

It is now clear that those scatterers which can be completely characterized by a scattering matrix form a rather small subset of a more general class of scatterers - those that must be characterized by a Stokes Scattering Operator. The importance of this fact is stressed by the fact that the vast majority of scatterers encountered in radar imaging are made up of a number of scattering centers. If all the information about the combination of scattering centers are to be retained, one has to characterize these scatterers by their total Stokes Scattering Operators.

2.2.1 Characterization of Scatterers in the Backscatter Case.

Since most, if not all, imaging radars use the same antenna for transmission and reception of signals, it will be worthwhile to see how the expressions of the previous section change, if any, in the backscatter case.

In the backscatter case, assuming reciprocity of the propagation path, it follows that

$$S_{x'y} = S_{y'x} . \tag{2-22}$$

In this case the primed and unprimed coordinate systems coincide. It then follows that in the backscatter case, a single scatterer may be characterized by:

$$\begin{bmatrix} E_x^{sc} \\ E_y^{sc} \end{bmatrix} = \begin{bmatrix} |S_{xx}| e^{i(\varphi_{xx}-\varphi_{xy})} & |S_{xy}| \\ |S_{xy}| & |S_{yy}| e^{i(\varphi_{yy}-\varphi_{xy})} \end{bmatrix} \begin{bmatrix} E_x^{inc} \\ E_y^{inc} \end{bmatrix} . \tag{2-23}$$

There are only five independent parameters in the scattering matrix as defined above (the *monostatic scattering matrix with relative phase only*). Using (2-23) in (2-17) one finds that in this case [**M**] becomes a symmetric real matrix with elements:

$$M_{11} = \tfrac{1}{4}[\, S_{xx}\cdot S_{xx}^* + S_{yy}\cdot S_{yy}^* + 2S_{xy}\cdot S_{xy}^* \,] \tag{2-24a}$$

$$M_{12} = \tfrac{1}{4}[\, S_{xx}\cdot S_{xx}^* - S_{yy}\cdot S_{yy}^* \,] \tag{2-24b}$$

$$M_{13} = \tfrac{1}{2} S_{xy}\, \mathrm{Re}[S_{xx}+S_{yy}] \tag{2-24c}$$

$$M_{14} = \tfrac{1}{2} S_{xy}\, \mathrm{Im}[S_{yy}-S_{xx}] \tag{2-24d}$$

$$M_{22} = \tfrac{1}{4}[\, S_{xx}\cdot S_{xx}^* + S_{yy}\cdot S_{yy}^* - 2S_{xy}\cdot S_{xy}^* \,] \tag{2-24e}$$

$$M_{23} = \tfrac{1}{2} S_{xy}\, \mathrm{Re}[S_{xx}-S_{yy}] \tag{2-24f}$$

$$M_{24} = -\tfrac{1}{2} S_{xy} \, \mathrm{Im}[S_{xx}+S_{yy}] \tag{2-24g}$$

$$M_{33} = \tfrac{1}{2} S_{xy}^2 + \tfrac{1}{2} \mathrm{Re}[S_{xx}^* \cdot S_{yy}] \tag{2-24h}$$

$$M_{34} = \tfrac{1}{2} \mathrm{Im}[S_{xx}^* \cdot S_{yy}] \tag{2-24i}$$

$$M_{44} = \tfrac{1}{2} S_{xy}^2 - \tfrac{1}{2} \mathrm{Re}[S_{xx}^* \cdot S_{yy}] \, . \tag{2-24j}$$

Since both [**M**] and the scattering matrix are now symmetric matrices, there must be five relationships between the elements of [**M**]. These are easily found from (2-21) as:

$$M_{11} = M_{22}+M_{33}+M_{44} \tag{2-25a}$$

$$M_{13}M_{23}+M_{14}M_{24} = M_{12}(M_{11}-M_{22}) \tag{2-25b}$$

$$M_{13}M_{14}-M_{23}M_{24} = M_{34}(M_{33}+M_{44}) \tag{2-25c}$$

$$M_{13}^2+M_{14}^2+M_{23}^2+M_{24}^2 = M_{11}^2-M_{22}^2 \tag{2-25d}$$

$$M_{13}^2-M_{14}^2-M_{23}^2+M_{24}^2 = M_{33}^2-M_{44}^2 \, . \tag{2-25e}$$

It is interesting to note that (2-25a) is a linear relationship, which will be retained if the summation in (2-20) is performed. The general backscatter Stokes Scattering Operator may thus contain nine independent parameters, and not ten as may be expected. Nevertheless, it is still clear that it is not possible to fully characterize the most general type of scatterer by only the five independent parameters of the scattering matrix.

To conclude this section, it will be pointed out that the elements of both the scattering matrix and the Stokes Scattering Operator are functions of, amongst other factors, frequency and the relative orientation of the scatterer with respect to the illuminating antenna (i.e., the *aspect angle* of the scatterer).

2.3 Optimum Polarizations for Power Reception.

2.3.1 Deterministic Scatterer.

A scatterer will be called a deterministic scatterer if it can be fully characterized by a complex 2x2 scattering matrix. For such a case, the power absorbed by the antenna from the scattered wave is given by

$$P_{rec} = K(\lambda,\vartheta,\varphi)\,|\mathbf{E}^{rad}.[\mathbf{S}]\mathbf{E}^{rad}|^2 . \qquad (2\text{-}26)$$

Since most current imaging (and also most other) radars use the same antenna for transmission and reception of signals, only the case of a single antenna will be considered here.

2.3.1.1 Maximum Polarizations.

P_{rec} in (2-26) will be a maximum (assuming that $K(\lambda,\vartheta,\varphi)$ is independent of polarization) if

$$[\mathbf{S}]\mathbf{E}^{rad} = t\,\mathbf{E}^{rad*}, \qquad (2\text{-}27)$$

where t is a (complex) constant. To change this into an eigenvalue problem, one simply takes the complex conjugate of both sides of (2-27) and multiply by t to find:

$$[\mathbf{S}^*][\mathbf{S}]\mathbf{E}^{rad} = \chi\mathbf{E}^{rad} \qquad (2\text{-}28)$$

where

$$\chi = t{\cdot}t^* .$$

This is now an eigenvalue problem which may be written as:

$$[\mathbf{A}]\mathbf{E}^{rad} = \chi\mathbf{E}^{rad}$$

with

$$[\mathbf{A}] = \begin{bmatrix} S_{x'x}\cdot S^{*}_{x'x}+S^{*}_{x'y}\cdot S_{y'x} & S^{*}_{x'x}\cdot S_{x'y}+S^{*}_{x'y}\cdot S_{y'y} \\ S_{x'x}\cdot S^{*}_{y'x}+S_{y'x}\cdot S^{*}_{y'y} & S_{x'y}\cdot S^{*}_{y'x}+S_{y'y}\cdot S^{*}_{y'y} \end{bmatrix} = \begin{bmatrix} A_{11} & A_{12} \\ A_{21} & A_{22} \end{bmatrix}. \quad (2\text{-}29)$$

The eigenvalues χ of [**A**] are the ***real*** roots of

$$\chi^2-(A_{11}+A_{22})\chi+A_{11}A_{22}-A_{12}A_{21} = 0. \quad (2\text{-}30)$$

The maximum polarizations are the eigenvectors of [**A**]. If one defines a polarization ratio by:

$$p_r = \frac{E_y}{E_x}, \quad (2\text{-}31)$$

it is easily shown that the two maximum polarization ratio's are:

$$p_{rmax} = \frac{A_{22}-A_{11}\pm\sqrt{(A_{22}-A_{11})^2+4A_{21}A_{12}}}{2A_{12}}. \quad (2\text{-}32)$$

In terms of the complex polarization ratio of (2-31), the Stokes parameters of an EM wave are (assuming normalized electric field amplitude):

$$S_0 = 1. \quad (2\text{-}33a)$$

$$S_1 = \frac{1-|p_r|^2}{1+|p_r|^2} \quad (3\text{-}33b)$$

$$S_2 = \frac{2Re(p_r)}{1+|p_r|^2} \quad (3\text{-}33c)$$

$$S_3 = -\frac{2Im(p_r)}{1+|p_r|^2}. \quad (3\text{-}33d)$$

Using the results of (2-32) and (2-17) one finds that the polarization ratio of the maximum polarizations can be expressed in terms of the elements of the Stokes Scattering Operator :

$$p_{rmax} = \frac{-(M_{12}+M_{21})-i(M_{43}-M_{34})}{(M_{13}+M_{23}+M_{31}-M_{32})+i(M_{14}+M_{24}-M_{42}+M_{41})}$$

$$\pm\left[\frac{[(M_{12}+M_{21})+i(M_{43}-M_{34})]^2+[(M_{13}+M_{31})+i(M_{24}-M_{42})]^2}{[(M_{13}+M_{23}+M_{31}-M_{32})+i(M_{14}+M_{24}-M_{42}+M_{41})]^2}\right.$$

$$\left.+\frac{[(M_{14}+M_{41})-i(M_{23}-M_{32})]^2}{[(M_{13}+M_{23}+M_{31}-M_{32})+i(M_{14}+M_{24}-M_{42}+M_{41})]^2}\right]^{1/2}.$$

In the backscatter case, this expression has a particularly simple form:

$$p_{rmax} = \frac{-M_{12}\pm\sqrt{M_{12}^2+M_{13}^2+M_{14}^2}}{M_{13}+iM_{14}}. \qquad (2\text{-}34)$$

If (2-34) is used in (2-33) one finds the Stokes parameters of the maximum polarizations in the backscatter case as:

$$S_{1max} = \frac{\pm M_{12}}{\sqrt{M_{12}^2+M_{13}^2+M_{14}^2}} \qquad (2\text{-}35a)$$

$$S_{2max} = \frac{\pm M_{13}}{\sqrt{M_{12}^2+M_{13}^2+M_{14}^2}} \qquad (2\text{-}35b)$$

$$S_{3max} = \frac{\pm M_{14}}{\sqrt{M_{12}^2+M_{13}^2+M_{14}^2}}. \qquad (2\text{-}35c)$$

It also follows from (2-29) that in the backscatter case [**A**] is a Hermitian matrix. This, in turn, means that the two maximum polarization vectors are orthogonal vectors, since they are the eigenvectors of a Hermitian matrix. Huynen [2] has shown that when the eigenvector corresponding to the larger eigenvalue of [**A**] is transmitted, an absolute maximum amount of power will be absorbed by the antenna.

2.3.1.2 Minimum Polarizations.

P_{rec} in (2-26) will be a minimum when

$$\mathbf{E}^{rad.}[\mathbf{S}]\mathbf{E}^{rad} = 0. \tag{2-36}$$

This occurs when

$$[\mathbf{S}]\mathbf{E}^{rad} = c\,\mathbf{E}^{rad*}_{ort}. \tag{2-37}$$

The subscript *ort* means *orthogonal to*. But, for (2-36) to be true and if

$$|\mathbf{E}^{rad}| = |\mathbf{E}^{rad}_{ort}|,$$

one must insist that

$$\mathbf{E}^{rad*}_{ort} = \pm \begin{bmatrix} 0 & -1 \\ 1 & 0 \end{bmatrix} \mathbf{E}^{rad}. \tag{2-38}$$

Using (2-38) in (2-37), one finds that the minimum polarizations are the eigenvectors of the following eigenvalue problems:

$$\pm \begin{bmatrix} 0 & 1 \\ -1 & 0 \end{bmatrix} [\mathbf{S}]\mathbf{E}^{rad} = c\,\mathbf{E}^{rad}. \tag{2-39}$$

The eigenvalues of these equations are, in general:

$$c = \pm\left[S_{y'x} - S_{x'y} \pm \sqrt{(S_{y'x}+S_{x'y})^2 - 4S_{x'x}S_{y'y}}\right]. \tag{2-40}$$

The minimum polarizations are the nonzero (complex) scalar multiples of:

$$\tilde{\mathbf{E}}_{min} = \left[\pm\tfrac{1}{2}\left\{S_{y'x} + S_{x'y} \pm \sqrt{(S_{x'y}+S_{y'x})^2 - 4S_{x'x}S_{y'y}}\right\};\ \pm S_{y'y}\right]. \tag{2-41}$$

In the backscatter case where reciprocity holds, expressions (2-40) and (2-41) become:

$$c^b = \pm\sqrt{S^2_{xy} - S_{xx}S_{yy}} \tag{2-42a}$$

$$\tilde{\mathbf{E}}^{b}_{min} = \pm[\, S_{xy} \pm \sqrt{S_{xy}^2 - S_{xx}S_{yy}}\, ;\, S_{yy}\,]\,. \qquad (2\text{-}42b)$$

Unfortunately, it is not possible to find a simple expression for the Stokes parameters of the minimum polarizations.

2.3.1.3 Polarization (Huynen) Fork.

As can be seen from (2-35) if one plots the two points corresponding to the maximum polarizations on the Poincaré sphere, (i.e., use S_1, S_2, and S_3 as the coordinates and S_0 as the radius) these points are antipodal in the backscatter case. Huynen [2] has shown that in the backscatter case, the four points corresponding to the four optimum polarizations all lie on a great circle. If a vector is formed by joining the origin of the (S_1,S_2,S_3) coordinate system with each of these points, Huynen [2] has also shown that these four vectors form a fork as shown in Figure 2.2. Furthermore, Huynen has shown that the angle γ is given by

$$\gamma = \tan^{-1}\left\{\left[\frac{\chi_1}{\chi_2}\right]^{\frac{1}{4}}\right\}, \qquad (2\text{-}43)$$

where χ_2 is the larger eigenvalue of $[\mathbf{A}]$ and χ_1 is the smaller eigenvalue.

Using (2-30) and (2-17) it is easily shown that (2-43) can be written as:

$$\gamma = \tan^{-1}\left\{\left[\frac{M_{11}-\sqrt{M_{12}^2+M_{13}^2+M_{14}^2}}{M_{11}+\sqrt{M_{12}^2+M_{13}^2+M_{14}^2}}\right]^{\frac{1}{4}}\right\}. \qquad (2\text{-}44)$$

Since (2-17) is only valid for a deterministic scatterer, it must be stressed that (2-44) is also only valid for a deterministic scatterer. From (2-44) it follows that the Huynen fork has opened completely (in the case of a deterministic scatterer) when

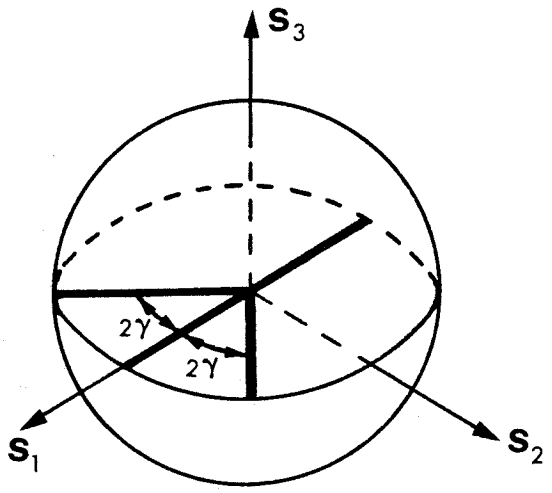

Figure 2.2. Polarization (Huynen) Fork.

$$M_{12} = M_{13} = M_{14} = 0. \tag{2-45}$$

2.3.1.4 Gamma Spheres

From (2-18) or (2-26) it is clear that for every point on the Poincaré sphere, it is possible to calculate the power received from the scatterer. It is thus possible to draw, on the Poincaré sphere, curves of constant power received by the antenna. These figures are called *Gamma Spheres* after Huynen [2]. Figure 2.3 shows the Gamma Sphere for a slightly rough surface of relative dielectric constant 3 which scatters according to the Bragg relations.

2.3.2 Distributed Scatterers.

When the aspect angle of a scatterer varies with time, or when the scattering is due to a collection of scattering centers randomly oriented and/or distributed in space, the power received by the antenna will be the averaged

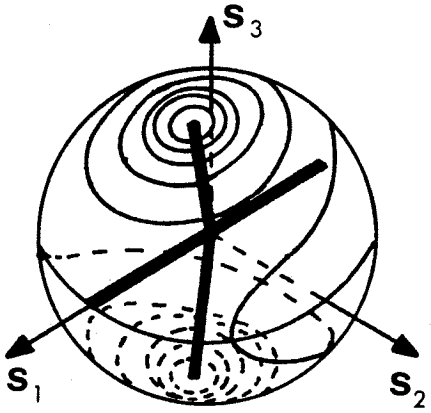

Figure 2.3. Gamma sphere for a slightly rough surface at an incidence angle of 45 degrees.

samples of scattering from a set of different single scatterers. In the case of a scatterer with time varying aspect angle, the average is taken over time. In the case of a collection of scattering centers randomly oriented and/or distributed in space, the ensemble average is taken. These classes of scatterers will be called distributed scatterers. It has been shown previously that, in general, it is not possible to completely characterize a distributed scatterer by a 2x2 scattering matrix. An alternative definition of a distributed scatterer may thus be those scatterers which can only be fully characterized by their Stokes Scattering Operator.

2.3.2.1 Optimum Polarizations.

Most scatterers encountered in radar imaging belong to this class. One may think of simple examples such as natural rough surfaces, vegetation and the

surface of the ocean. In all these cases, the properties of the scatterers within one resolution cell may vary. The question of which polarization, on the average, would yield an optimum amount of received power is therefore a very important one. To answer this question, it is remembered from (2-18) that the power received from a distributed scatterer is given by

$$P_{rec} = K(\lambda,\vartheta,\varphi)\mathbf{S}^{rad.}[\mathbf{M}]\mathbf{S}^{rad} . \qquad (2\text{-}46)$$

If it is assumed that $K(\lambda,\vartheta,\varphi)$ is constant for all polarizations, one has to solve the problem of optimizing

$$P'_{rec} = \mathbf{S}^{rad.}[\mathbf{M}]\mathbf{S}^{rad} . \qquad (2\text{-}47)$$

Two methods for solving this problem will be discussed separately.

2.3.2.1.1 Lagrange Multiplier Method.

Assuming a normalized radiated electric field amplitude, and dropping the superscript ***rad***, (2-47) may be written as

$$\begin{aligned} P'_{rec} = {} & M_{11} + (M_{12}+M_{21})S_1 + (M_{13}+M_{31})S_2 + (M_{14}+M_{41})S_3 \\ & + (M_{23}+M_{32})S_1S_2 + (M_{24}+M_{42})S_1S_3 + (M_{34}+M_{43})S_2S_3 \\ & + M_{22}S_1^2 + M_{33}S_2^2 + M_{44}S_3^2 . \end{aligned} \qquad (2\text{-}48)$$

There is a constraint on the values of S_1,S_2 and S_3 that may be used in (2-48) - they must be the components of a normalized Stokes vector ([1],[5],[6],[7]), i.e.,

$$S_1^2 + S_2^2 + S_3^2 = 1. \qquad (2\text{-}49)$$

Thus, to optimize P'_{rec} , the Lagrange Multiplier Method [8] may be used. First, the auxiliary function

$$G(S_1,S_2,S_3) = \mathbf{S}\cdot[\mathbf{M}]\mathbf{S} - \nu(S_1^2+S_2^2+S_3^2-1) \tag{2-50}$$

is formed. Then, it is required that

$$\frac{\partial G(S_1,S_2,S_3)}{\partial S_i} = 0 \qquad i=1,2,3\,. \tag{2-51}$$

Performing the indicated differentiations, one finds that the optimum values of S_1,S_2 and S_3 are the solutions to

$$\begin{bmatrix} M_{22} & \frac{1}{2}(M_{23}+M_{32}) & \frac{1}{2}(M_{24}+M_{42}) \\ \frac{1}{2}(M_{23}+M_{32}) & M_{33} & \frac{1}{2}(M_{34}+M_{43}) \\ \frac{1}{2}(M_{24}+M_{42}) & \frac{1}{2}(M_{34}+M_{43}) & M_{44} \end{bmatrix} \begin{bmatrix} S_1 \\ S_2 \\ S_3 \end{bmatrix} + \frac{1}{2} \begin{bmatrix} M_{12}+M_{21} \\ M_{13}+M_{31} \\ M_{14}+M_{41} \end{bmatrix} = \nu \begin{bmatrix} S_1 \\ S_2 \\ S_3 \end{bmatrix}. \tag{2-52}$$

This expression is of the form

$$[\mathbf{B}]\mathbf{s}+\mathbf{a} = \nu\mathbf{s} \tag{2-53}$$

and $[\mathbf{B}]$ is a real symmetric 3x3 matrix. Two cases may be identified:

(i) $\mathbf{a} = 0$: In this case the optimum polarizations are the normalized eigenvectors of $[\mathbf{B}]$. The maximum polarization is given by the eigenvector which corresponds to the maximum eigenvalue of $[\mathbf{B}]$. Likewise, the minimum polarization is given by that eigenvector which corresponds to the smallest eigenvalue of $[\mathbf{B}]$. Since $[\mathbf{B}]$ is a real symmetric matrix, these optimum polarizations are mutually orthogonal.

(ii) $\mathbf{a} \neq 0$: One may rewrite (2-53) to read

$$[\mathbf{B}-\nu\mathbf{I}]\mathbf{s} = -\mathbf{a}\,, \tag{2-54}$$

where $\mathbf{I}$ is the 3x3 identity matrix. If ν is not an eigenvalue of $[\mathbf{B}]$, (2-54) has a unique solution given by:

$$\mathbf{s} = -[\mathbf{B}-\nu\mathbf{I}]^{-1}\mathbf{a}\,. \tag{2-55}$$

However, not all values of ν which are not eigenvalues of $[\mathbf{B}]$ may be used in

(2-55). This follows from the constraint condition which requires **s** to have unit magnitude. Also, ν must be a real number; a consequence of the fact that **s** must be purely real and both [**B**] and **a** are real. If, in general, one plots the magnitude of **s** versus ν, the cases shown in Figure 2.4 may be identified.

These nine cases may occur when [**B**] has three distinct eigenvalues. If [**B**] has only two distinct eigenvalues, only three cases can arise and when [**B**] has only one eigenvalue, only one case is possible. Since these can easily be found from Figure 2.4, they will not be repeated here.

The question of how to find the correct values of ν to use in (2-55) still remains. If (2.55) is used in (2-49), one finds

$$([\mathbf{B}-\nu\mathbf{I}]^{-1}\mathbf{a})\cdot([\mathbf{B}-\nu\mathbf{I}]^{-1}\mathbf{a}) = 1. \tag{2-56}$$

Expanding this expression, one finds that the correct values of ν are the ***real*** roots of

$$p(\nu) = \nu^6 + d_1\nu^5 + d_2\nu^4 + d_3\nu^3 + d_4\nu^2 + d_5\nu + d_6 = 0, \tag{2-57}$$

where

$$d_1 = -2c_1 \tag{2-58a}$$

$$d_2 = c_1^2-q_{01}^2-q_{02}^2-q_{03}^2-2c_2 \tag{2-58b}$$

$$d_3 = 2[c_1c_2-q_{01}q_{11}-q_{02}q_{12}-q_{03}q_{13}-c_3] \tag{2-58c}$$

$$d_4 = c_2^2-q_{11}^2-q_{12}^2-q_{13}^2+2[c_1c_3-q_{01}q_{21}-q_{02}q_{22}-q_{03}q_{23}] \tag{2-58d}$$

$$d_5 = 2[c_2c_3-q_{11}q_{21}-q_{12}q_{22}-q_{13}q_{23}] \tag{2-58e}$$

$$d_6 = c_3^2-q_{21}^2-q_{22}^2-q_{23}^2 \tag{2-58f}$$

and

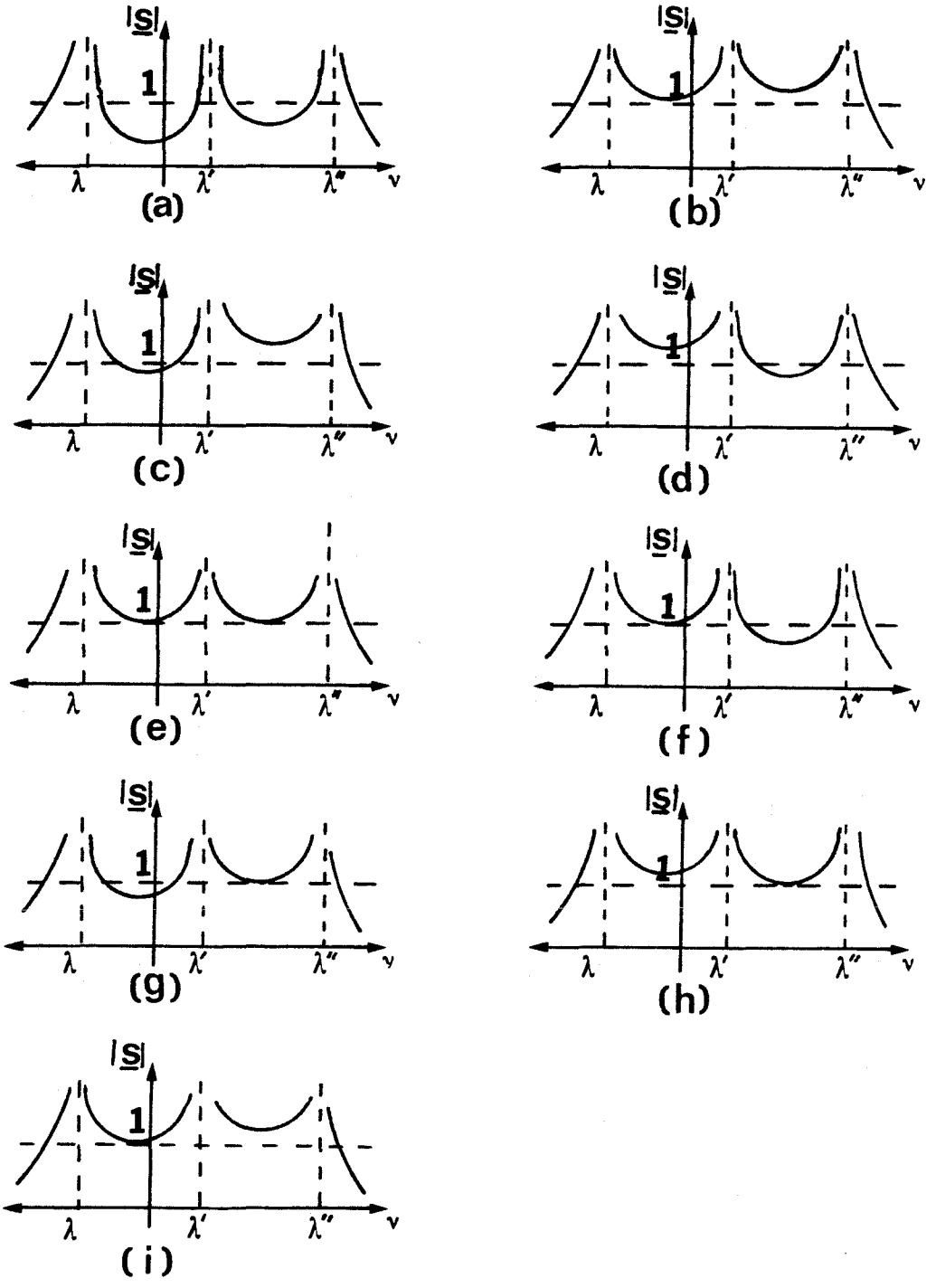

Figure 2.4. General behaviour of the magnitude of **s** as a function of ν.

$$c_1 = M_{22}+M_{33}+M_{44}$$

$$c_2 = \frac{1}{4}\left[(M_{23}+M_{32})^2+(M_{24}+M_{42})^2+(M_{34}+M_{43})^2\right]-M_{33}M_{44}-M_{22}M_{33}-M_{22}M_{44}$$

$$c_3 = M_{22}M_{33}M_{44}+\frac{1}{4}\left[(M_{23}+M_{32})(M_{24}+M_{42})(M_{34}+M_{43})\right.$$

$$\left.-M_{22}(M_{34}+M_{43})^2-M_{33}(M_{24}+M_{42})^2-M_{44}(M_{23}+M_{32})^2\right]$$

$$q_{01} = \tfrac{1}{2}(M_{12}+M_{21})$$

$$q_{11} = \frac{1}{4}\left[(M_{13}+M_{31})(M_{23}+M_{32})+(M_{14}+M_{41})(M_{24}+M_{42})\right]$$

$$-\tfrac{1}{2}(M_{12}+M_{21})(M_{33}+M_{44})$$

$$q_{21} = \tfrac{1}{2}(M_{12}+M_{21})\left[M_{33}M_{44}-\frac{1}{4}(M_{34}+M_{43})^2\right]$$

$$+\tfrac{1}{2}(M_{13}+M_{31})\left[\frac{1}{4}(M_{24}+M_{42})(M_{34}+M_{43})-\tfrac{1}{2}M_{44}(M_{23}+M_{32})\right]$$

$$+\tfrac{1}{2}(M_{14}+M_{41})\left[\frac{1}{4}(M_{23}+M_{32})(M_{34}+M_{43})-\tfrac{1}{2}M_{33}(M_{24}+M_{42})\right]$$

$$q_{02} = \tfrac{1}{2}(M_{13}+M_{31})$$

$$q_{12} = \frac{1}{4}\left[(M_{12}+M_{21})(M_{23}+M_{32})+(M_{14}+M_{41})(M_{34}+M_{43})\right]$$

$$-\tfrac{1}{2}(M_{13}+M_{31})(M_{22}+M_{44})$$

$$q_{22} = \tfrac{1}{2}(M_{12}+M_{21})\left[\tfrac{1}{4}(M_{24}+M_{42})(M_{34}+M_{43})-\tfrac{1}{2}M_{44}(M_{23}+M_{32})\right]$$

$$+\tfrac{1}{2}(M_{13}+M_{31})\left[M_{22}M_{44}-\tfrac{1}{4}(M_{24}+M_{42})^2\right]$$

$$+\tfrac{1}{2}(M_{14}+M_{41})\left[\tfrac{1}{4}(M_{23}+M_{32})(M_{24}+M_{42})-\tfrac{1}{2}M_{22}(M_{34}+M_{43})\right]$$

$$q_{03} = \tfrac{1}{2}(M_{14}+M_{41})$$

$$q_{13} = \tfrac{1}{4}\left[(M_{12}+M_{21})(M_{24}+M_{42})+(M_{13}+M_{31})(M_{34}+M_{43})\right]$$

$$-\tfrac{1}{2}(M_{14}+M_{41})(M_{22}+M_{33})$$

$$q_{23} = \tfrac{1}{2}(M_{12}+M_{21})\left[\tfrac{1}{4}(M_{23}+M_{32})(M_{34}+M_{43})-\tfrac{1}{2}M_{33}(M_{24}+M_{42})\right]$$

$$+\tfrac{1}{2}(M_{13}+M_{31})\left[\tfrac{1}{4}(M_{24}+M_{42})(M_{23}+M_{32})-\tfrac{1}{2}M_{22}(M_{34}+M_{43})\right]$$

$$+\tfrac{1}{2}(M_{14}+M_{41})\left[M_{22}M_{33}-\tfrac{1}{4}(M_{23}+M_{32})^2\right].$$

Once the real roots of $p(\nu)$ are known, the optimum polarizations can easily be calculated using (2-55).

2.3.2.1.2 Direct Method.

Since every polarization can be viewed as a point on the Poincaré sphere, [1], one may rewrite (2-48), assuming a normalized radiated electric field amplitude, as:

$$P'_{rec} = M_{11}+(M_{12}+M_{21})\sin(\vartheta)\cos(\varphi)+(M_{13}+M_{31})\sin(\vartheta)\sin(\varphi)$$

$$+(M_{14}+M_{41})\cos(\vartheta)+(M_{23}+M_{32})\sin^2(\vartheta)\sin(\varphi)\cos(\varphi)$$

$$+(M_{24}+M_{42})\sin(\vartheta)\cos(\vartheta)\cos(\varphi)+(M_{34}+M_{43})\sin(\vartheta)\cos(\vartheta)\sin(\varphi)$$

$$+M_{22}\sin^2(\vartheta)\cos^2(\varphi)+M_{33}\sin^2(\vartheta)\sin^2(\varphi)+M_{44}\cos^2(\vartheta)\,. \qquad (2\text{-}59)$$

The problem now becomes one of finding the values of ϑ and φ which would optimize (2-59). These values of ϑ and φ are the solutions to the following two nonlinear equations:

$$[(M_{12}+M_{21})\cos(\varphi)+(M_{13}+M_{31})\sin(\varphi)]\cos(\vartheta)-(M_{14}+M_{41})\sin(\vartheta)$$

$$+2(M_{23}+M_{32})\sin(\vartheta)\cos(\vartheta)\sin(\varphi)\cos(\varphi)+[(M_{24}+M_{42})\cos(\varphi)$$

$$+(M_{34}+M_{43})\sin(\varphi)](\cos^2(\vartheta)-\sin^2(\vartheta))+[M_{22}\cos^2(\varphi)$$

$$+M_{33}\sin^2(\varphi)-M_{44}]2\sin(\vartheta)\cos(\vartheta) = 0. \qquad (2\text{-}60)$$

and

$$[(M_{13}+M_{31})\cos(\varphi)-(M_{12}+M_{21})\sin(\varphi)]+(M_{23}+M_{32})\sin(\vartheta)\cos(2\varphi)$$

$$+\cos(\vartheta)[(M_{34}+M_{43})\cos(\varphi)-(M_{24}+M_{42})\sin(\varphi)]$$

$$+(M_{33}-M_{22})\sin(\vartheta)\sin(2\varphi) = 0. \qquad (2\text{-}61)$$

It is clear that both these methods may involve a considerable amount of numerical work. A close examination of the two procedures reveal that in both cases a total of ***six*** solutions may be possible. This point will be discussed in more detail in the next section.

2.3.2.2 Number of Optimum Polarizations.

As noted in the previous section, a total of six optimum polarizations are possible. In this section an example will be given of one such case.

In order to elliminate speckle noise in radar imaging, it is common to average over a number of measurements. To simulate the properties of Gaussian background noise in such a setup, a Stokes Scattering Operator was made up using four samples of scattering matrices generated by a random number generator. The Stokes Scattering Operator for each sample was calculated and the averaging was finally done on these four Stokes Scattering Operators. The resulting Stokes Scattering Operator is:

$$[\mathbf{M}] = \begin{bmatrix} .55561 & .03679 & .00965 & .09070 \\ .03679 & .13667 & .09300 & -.00076 \\ .00965 & .09300 & .19990 & .18815 \\ .09070 & -.00076 & .18815 & .21904 \end{bmatrix}. \qquad (2\text{-}62)$$

If the Lagrange Multiplier method is used, and the magnitude of **s** is plotted versus ν, one finds the result in Figure 2.5. This figure clearly shows that there are *six* optimum polarizations for this case. The optimum polarizations for this case, together with the value of P'_{rec} for each optimum polarization, are:

P_{rec}	S_1	S_2	S_3
1.12393	0.26069	0.60262	0.75086
0.81770	−.19429	−.81363	−.53817
0.61632	0.44170	−.79392	0.35366
0.51523	−.53607	−.56997	0.31221
0.45692	0.67213	−.36791	−.26797
0.40265	−.43148	0.57816	−.68090

Figure 2.6 shows these optimum polarizations when plotted on the Poincaré sphere.

Not only are there now six optimum polarizations, but the Huynen fork no

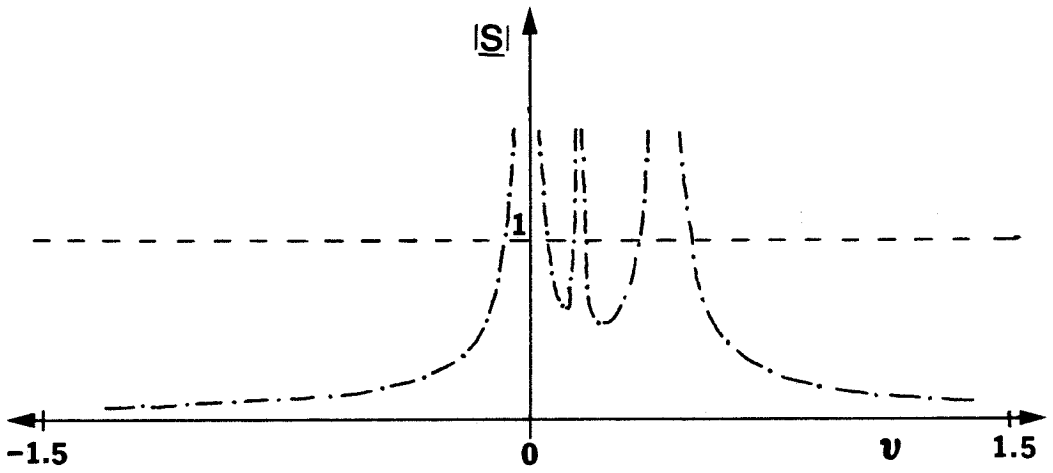

Figure 2.5. Magnitude of **s** as a function of ν.

longer exists too. Up to now, only four optimum polarizations have been mentioned in the literature [2],[3],[4],[10]. Mieras [9] shows six optimum polarizations in a figure, but shows two pairs of these to be antipodal. This is obviously not the case for the most general scatterer. Nespor, *et al.* observed that for cases where noise is present, the two maximum polarizations sometimes appear not to be antipodal on the Poincaré sphere, but did not solve the problem [22].

Two important conclusions can be drawn from the results of this section:

(i) The Huynen fork no longer exists in the general case. Instead, six optimum polarizations appear and no two optimum polarizations are antipodal when plotted on the Poincaré sphere.

(ii) There is no polarization for which the received power is zero. Also, the two nulls are not equally deep as in the case of a deterministic scatterer. It is

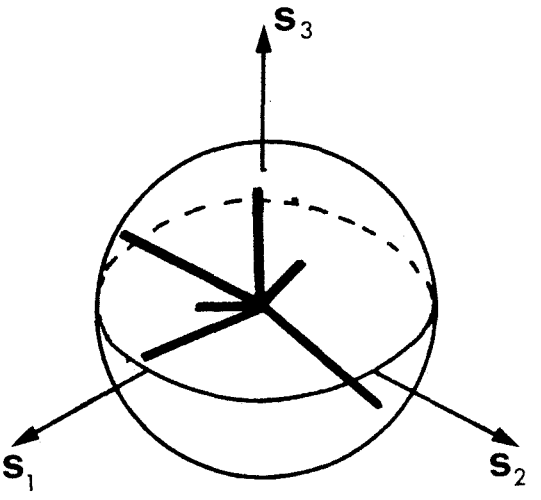

Figure 2.6. Optimum polarizations.

easily seen why physically it is no longer possible to find a polarization which yields zero received power. For each of the four samples one can find two polarizations which yield zero received power. If these four samples are combined, however, there is no guarantee that the minimum polarizations of these four samples will coincide. Thus, one may conclude that the minimum amount of received power contains some information about the amount of variation in the properties of the different samples.

2.3.2.3 Coefficient of Variation and Coherency Factor.

In the case of a distributed scatterer, the properties of the scatterers change (usually in a random fashion) either with time or spatially. It is thus clear why no single polarization can be the zero polarization of all these possibly different scatterers at once. Thus, the closer the minimum amount of received power is to zero, the less variation in scattering properties are there temporally

or spatially. Formally, this measure of variation may be expressed by introducing a *coefficient of variation* , v, defined by:

$$\text{coefficient of variation} = v = \frac{\text{minimum received power}}{\text{maximum received power}}. \qquad (2\text{-}63)$$

Note that this means that

$$0 \leq v \leq 1.$$

A value of v = 0 means no variation, or a deterministic scatterer. A value of v = 1, on the other hand, means that the received power is constant, independent of polarization. Considering either (2-48) or (2-59) it is clear that the only case for which this can be true in general, is when the Stokes Scattering Operator is of the form:

$$[\mathbf{M}] = \begin{bmatrix} a & 0 & 0 & 0 \\ 0 & b & 0 & 0 \\ 0 & 0 & b & 0 \\ 0 & 0 & 0 & b \end{bmatrix}.$$

In the backscatter case, there is a relationship between the elements of $[\mathbf{M}]$ as given by (2-25a). This means that in the backscatter case, the only distributed scatterer with a coefficient of variation of 1 must be of the form

$$[\mathbf{M}] = c \begin{bmatrix} 1 & 0 & 0 & 0 \\ 0 & \frac{1}{3} & 0 & 0 \\ 0 & 0 & \frac{1}{3} & 0 \\ 0 & 0 & 0 & \frac{1}{3} \end{bmatrix}.$$

One may also introduce a *coherency factor* [11]. This coherency factor is analogous to the *visibility* used in optics [1],[5] and is defined as:

$$\text{coherency factor} = \frac{P_{max}-P_{min}}{P_{max}+P_{min}} = \frac{1-v}{1+v}. \qquad (2\text{-}64)$$

2.3.2.4 Polarization Spectrum.

Analogous to the frequency spectrum encountered in signal analysis, one may fully characterize any scatterer by calculating its two-dimensional polarization spectrum. This polarization spectrum immediately shows the amount of power that will be received from a given scatterer for any polarization. The two variables used in plotting the polarization spectrum are the spherical polar coordinates of the given polarization when plotted on the Poincaré sphere. Figure 2.7 shows the polarization spectrum for the slightly rough surface with Gamma Sphere shown in Figure 2.3.

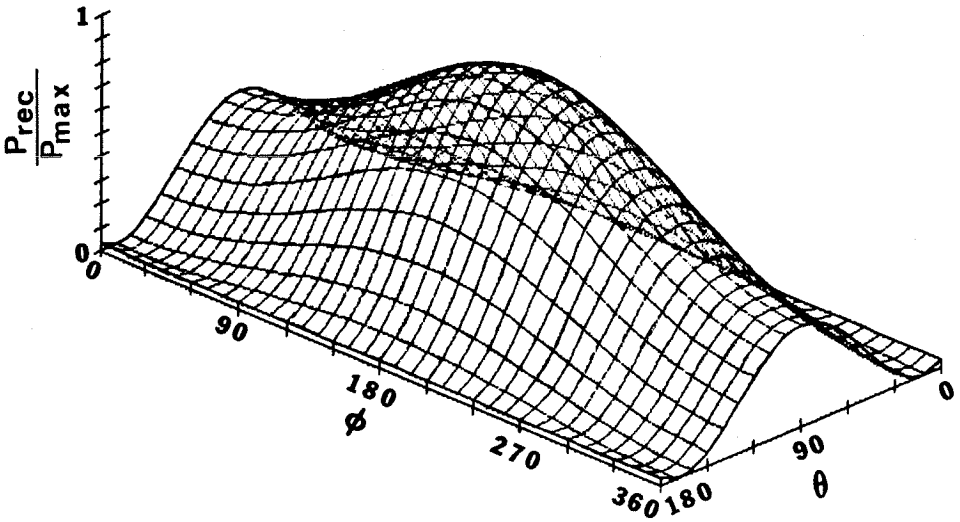

Figure 2.7. Polarization spectrum of a slightly rough surface.

It is clear by comparison of Figures 2.3 and 2.7 that the polarization spectrum conveys all the information of a Gamma Sphere and more at a glance.

In a later section the use of polarization spectrums will be discussed in more detail.

2.3.2.5 Polarization Spectrum and Optimum Polarizations.

The polarization spectrum allows a simple explanation of the various different cases of optimum polarizations shown in Figure 2.4.

(i) Two optimum polarizations. (Figure 2.4 (b)) This is the simplest polarization spectrum and contains one absolute maximum polarization and one absolute minimum polarization.

(ii) Three optimum polarizations. (Figure 2.4 (h) and (i)) In this case one finds an inflection point somewhere between the one absolute maximum and the one absolute minimum.

(iii) Four optimum polarizations. (Figure 2.4 (c), (d) and (e)) Two cases may arise. In the one case the optimum polarizations consist of one absolute maximum, two local minima and one saddle point. In the second case, the four optimum polarizations consist of one absolute maximum, one absolute minimum and two inflection points.

(iv) Five optimum polarizations. (Figure 2.4 (f) and (g)) The optimum polarizations consist of one absolute maximum, two local minima, one saddle point and one inflection point.

(v) Six optimum polarizations. (Figure 2.4 (a)) The optimum polarizations are two local maxima, two local minima and two saddle points. Figure 2.8 shows the polarization spectrum of the scatterer with six optimum polarizations discussed in Section 2.3.2.2 and clearly shows two local maxima, two local minima and two saddle points.

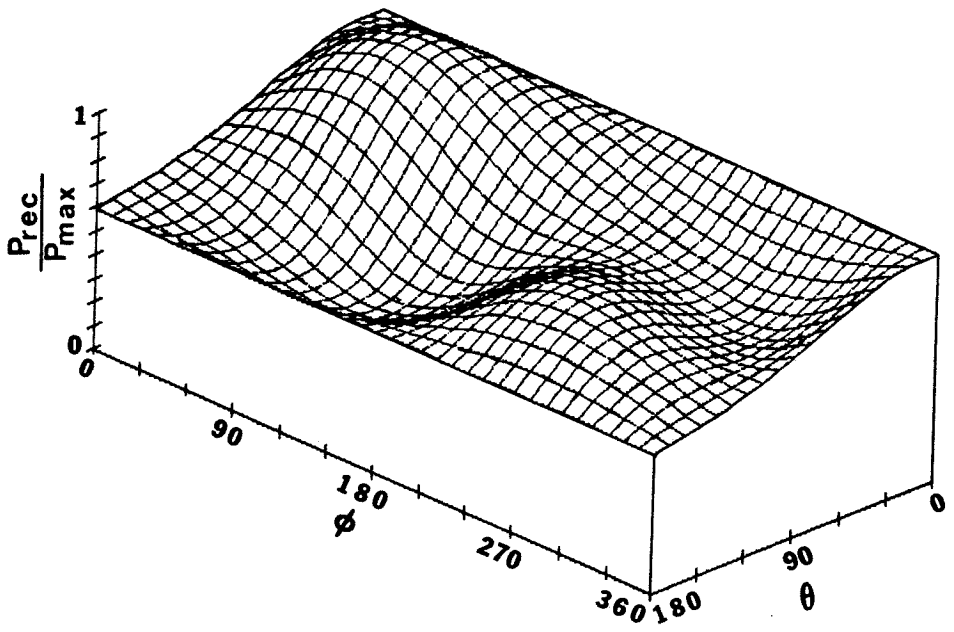

Figure 2.8. Polarization spectrum showing six optimum polarizations.

2.3.2.6 Decomposition of Scatterers.

From the discussion in Section 2.3.2.3 it is clear that every distributed scatterer can be viewed as a scatterer with a coherency factor of 1 with "noise" added to it. In fact, it has been proven by Huynen [2] that one can always decompose a distributed scatterer into a single, deterministic scatterer plus "noise." Using the polarization spectrum, it is easy to see that it is possible to decompose any scatterer into two scatterers: one with a coherency factor of 1 (coefficient of variation = 0) and one with a coherency factor of 0 (coefficient of variation = 1). The second scatterer is one with received power independent of polarization and can be viewed analogous to "white" noise in frequency spectrums. It is easily seen that in the backscatter case this decomposition will be unique, since the constant c (Section 2.3.2.3) is uniquely determined by the minimum received power. In general, however, the decomposition will not be

unique, and one has the freedom of choosing the two constants a and b to yield the minimum received power. In the backscatter case the unique decomposition is:

$$[\mathbf{M}] = P'_{min} \begin{bmatrix} \frac{3}{4} & 0 & 0 & 0 \\ 0 & \frac{1}{4} & 0 & 0 \\ 0 & 0 & \frac{1}{4} & 0 \\ 0 & 0 & 0 & \frac{1}{4} \end{bmatrix}$$

$$+ \begin{bmatrix} M_{11}-\frac{3}{4}P'_{min} & M_{12} & M_{13} & M_{14} \\ M_{12} & M_{22}-\frac{1}{4}P'_{min} & M_{23} & M_{24} \\ M_{13} & M_{23} & M_{33}-\frac{1}{4}P'_{min} & M_{34} \\ M_{14} & M_{24} & M_{34} & M_{44}-\frac{1}{4}P'_{min} \end{bmatrix}. \quad (2\text{-}65)$$

2.3.2.7 Comparison and Classification of Scatterers.

The polarization spectrum provides one with a simple and efficient way to compare different scatterers. This comparison is based on the normalized root mean-square difference between the scatterers. The difference is calculated for N points on the Poincaré sphere and is given by:

$$\text{Normalized Difference} = \frac{1}{N} \frac{\left[\sum_{i=1}^{N} (P'_{rec1}-P'_{rec2})_i^2\right]^{1/2}}{P'_{max1}+P'_{max2}}. \quad (2\text{-}66)$$

The difference is normalized with respect to the sum of the two maximum received powers to ensure that the final result will be independent of the absolute values of the polarization spectrums.

This way of comparing different scatterers also provides one with an easy

way to classify scatterers. To do this, one needs a few reference scatterers, which will typically be contained in a library. Either these reference scatterers may be models of certain physical scattering processes or they may be some previously measured polarization spectrums. The classification is then based on the normalized difference (ND) values of the scatterer under consideration when compared to the various reference scatterers [11]. This technique will be used in Chapter 6 to classify different scatterers in radar images.

2.4 Optimum Polarization for Discrimination between Scatterers.

In radar problems it is often necessary to discriminate between different sources of backscattered power. It is not always possible to do this on the basis of a difference in range or azimuth, and in these cases polarization may prove to be a valuable tool for discriminating between scatterers.

The problem of discriminating between two scatterers using polarization has been discussed by Ionannidis and Hammers [12] for the case of two different antennas used for transmission and reception. Here, the further restriction of a single antenna will be introduced, and it will be shown that the resulting problem can be reduced to one of finding the optimum polarizations for power reception. In addition, two different ways of discrimination will be considered:

(i) The first method maximizes the ratio

$$F_1 = \frac{P_{rec1}}{P_{rec2}}. \tag{2-67}$$

The disadvantage of this method is that F_1 may be large, but both P_{rec1} and P_{rec2} may be relatively small. In practice, this may mean that unacceptably low powers may be received from both sources when the optimum polarization is used.

(ii) The second method maximizes the difference,

$$F_2 = P_{rec1} - P_{rec2} . \tag{2-68}$$

In these expressions the subscript 1 denotes the source of primary interest and the subscript 2 denotes the unwanted source. The following different cases may be identified:

2.4.1 Two Deterministic Scatterers.

2.4.1.1 F_1

When the unwanted source is a deterministic scatterer, there are two polarizations which yield zero power received from this source. For these two polarizations the ratio F_1 becomes infinite and hence the minimum polarizations of the unwanted source maximizes F_1.

2.4.1.2 F_2

To maximize F_2, one may rewrite (2-68) using (2-18) as:

$$F_2 = K(\lambda,\vartheta,\varphi)\mathbf{S}^{rad.}[\mathbf{M}_1 - \mathbf{M}_2]\mathbf{S}^{rad} . \tag{2-69}$$

It is then clear that F_2 will be maximized in all cases by the maximum polarization of $[\mathbf{M}_1 - \mathbf{M}_2]$.

2.4.2 Two Distributed Scatterers.

To maximize F_1 for this case, first rewrite (2-67) as:

$$F_1 = \frac{\mathbf{S}^{rad.}[\mathbf{M}_1]\mathbf{S}^{rad}}{\mathbf{S}^{rad.}[\mathbf{M}_2]\mathbf{S}^{rad}} . \tag{2-70}$$

This function must be maximized subject to the constraint condition that S^{rad} must be a normalized Stokes vector. (A normalized radiated electric field is assumed.) This suggests that the Lagrange Multiplier Method should be used

to solve this problem. Accordingly, the auxilliary function

$$G(S_1,S_2,S_3) = F_1 - \mu(S_1^2+S_2^2+S_3^2-1.) \tag{2-71}$$

is formed. Furthermore, it is required that

$$\frac{\partial G(S_1,S_2,S_3)}{\partial S_i} = 0. \qquad i=1,2,3\ . \tag{2-72}$$

Performing the differentiations, one finds that the optimum polarizations are the solutions to

$$(\mathbf{S}\cdot[\mathbf{M}_2]\mathbf{S})[\mathbf{B}_1]\mathbf{s} + (\mathbf{S}\cdot[\mathbf{M}_2]\mathbf{S})\mathbf{a}_1 - (\mathbf{S}\cdot[\mathbf{M}_1]\mathbf{S})[\mathbf{B}_2]\mathbf{s} - (\mathbf{S}\cdot[\mathbf{M}_1]\mathbf{S})\mathbf{a}_2$$

$$= \mu\mathbf{s}(\mathbf{S}\cdot[\mathbf{M}_2]\mathbf{S})^2 \tag{2-73}$$

where $[\mathbf{B}]$ and $\mathbf{a}$ have the same meaning as in (2-52) and the subscripts denote the two different scatterers. Dividing both sides by $\mathbf{S}\cdot[\mathbf{M}_2]\mathbf{S}$, which is permissible since the unwanted scatterer is a distributed scatterer and hence has a minimum received power different from zero, one finds

$$[\mathbf{B}_1-\alpha\mathbf{B}_2-\nu\mathbf{I}]\mathbf{s} = -(\mathbf{a}_1-\alpha\mathbf{a}_2) \tag{2-74}$$

with

$$\alpha \equiv F_1 \tag{2-75}$$

and

$$\nu = \mu(\mathbf{S}\cdot[\mathbf{M}_2]\mathbf{S})\ . \tag{2-76}$$

In these expressions the superscript rad has been dropped from the elements of the Stokes vector. Since α and ν are just variables, one may perfectly well consider them to be Lagrange multipliers. One may then rewrite (2-74) to read

$$[\mathbf{B}(\alpha)-\nu\mathbf{I}]\mathbf{s} = -\mathbf{a}(\alpha) . \tag{2-77}$$

Now, given a value of α , the resulting maximum polarization is simply the maximum polarization of

$$[\mathbf{M}(\alpha)] = [\mathbf{M}_1]-\alpha[\mathbf{M}_2] \tag{2-78}$$

and can be found using the procedure described earlier in section 2.3.2.1.1. The largest value of α for which such a maximum polarization can be found, is also the maximum value of F_1. However, α cannot take on just any value. The range of values that α can take follows directly from (2-70):

$$\alpha_{max} = \frac{(P'_{rec1})_{max}}{(P'_{rec2})_{min}} . \tag{2-79}$$

Since the unwanted source is a distributed scatterer, $(P'_{rec2})_{min} \neq 0$ and α_{max} is finite. Of course, α_{max} can only be achieved if the maximum polarization of $[\mathbf{M}_1]$ coincides with the minimum polarization of $[\mathbf{M}_2]$.

Similarly, from (2-70) one finds that

$$\alpha_{min} = \frac{(P'_{rec1})_{min}}{(P'_{rec2})_{max}} . \tag{2-80}$$

Since for both sources distributed scatterers $(P'_{rec1})_{min}$ and $(P'_{rec2})_{max}$ are both strictly positive, it follows that α_{min} is strictly positive. Also, α_{min} will be achieved if and only if the maximum polarization of $[\mathbf{M}_2]$ coincides with the minimum polarization of $[\mathbf{M}_1]$. In the general case, however, it is possible to state that

$$\frac{(P'_{rec1})_{min}}{(P'_{rec2})_{max}} \leq \alpha \leq \frac{(P'_{rec1})_{max}}{(P'_{rec2})_{min}} . \tag{2-81}$$

2.4.3 One Deterministic Scatterer and One Distributed Scatterer.

If the unwanted source is a distributed scatterer, the solution is the same as that of the previous section. If the unwanted source is a deterministic scatterer, the solution is the same as that of section 2.4.1.

2.4.4 Numerical Example.

As an example, consider the problem discussed by Ioannidis and Hammers [12]. The two scatterers have Stokes Scattering Operators,

$$[\mathbf{M}_1] = \begin{bmatrix} 1 & 0 & 0 & 0 \\ 0 & \frac{5}{8} & \frac{\sqrt{3}}{8} & \frac{\sqrt{3}}{4} \\ 0 & \frac{\sqrt{3}}{8} & \frac{3}{8} & -\frac{3}{4} \\ 0 & \frac{\sqrt{3}}{4} & -\frac{3}{4} & 0 \end{bmatrix}$$

$$[\mathbf{M}_2] = \begin{bmatrix} 1 & 0 & 0 & 0 \\ 0 & \frac{1}{2} & 0 & 0 \\ 0 & 0 & \frac{1}{2} & 0 \\ 0 & 0 & 0 & 0 \end{bmatrix}.$$

The results are:

$$(P'_{rec1})_{max} = 2.0$$

$$(P'_{rec2})_{min} = 1.0$$

$$\alpha_{max} = 2.0$$

$$(P'_{rec1})_{min} = .25$$

$$(P'_{rec2})_{max} = 1.5$$

$$\alpha_{min} = \frac{1}{6}.$$

The maximum ratio is found to be

$$F_{1max} = 1.62 .$$

This maximum ratio is obtained by using the Stokes vector

$$\tilde{\mathbf{S}} = [\ 1. ; 0.3214 ; -0.5567 ; 0.7660\ ] .$$

Figure 2.9 shows the result when the polarization spectrum of $[\mathbf{M}_1]$ is divided by the polarization spectrum of $[\mathbf{M}_2]$.

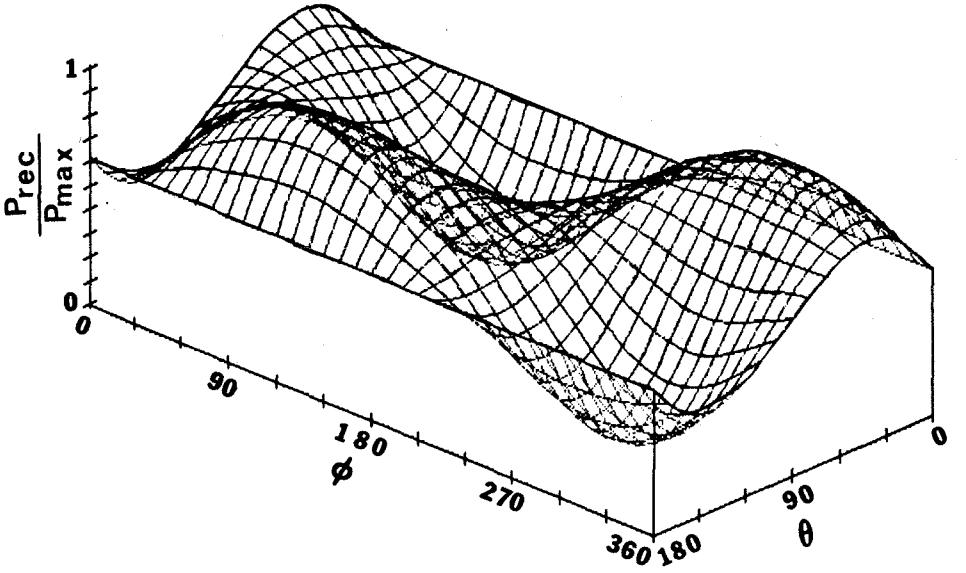

Figure 2.9. Ratio of the two polarization spectrums.

Ioannidis and Hammers reported a maximum ratio of 2.5 when two different antennas are used. The current result is still much better than would have been found if any linear or any of the two circular polarizations were used.

Figure 2.9 also shows that polarization alone may be a valuable tool in discriminating between different scatterers.

2.5 Conclusion.

In this chapter, the concepts of optimum polarizations and scatterer characterization were discussed in detail. Some techniques that use polarization to the advantage of scientists involved in radar imaging were introduced. In the subsequent chapters, these concepts will be applied to some scattering problems of interest in radar imaging.

CHAPTER 3

EFFECTIVE SCATTERING OPERATORS OF A SLAB OF SCATTERERS.

3.1 Introduction

In this chapter, the problem of finding the effective scattering operators to describe volume scattering inside a slab of scatterers will be formulated. The formulation will be done in terms of the bistatic scattering operators of the single scatterers inside the slab, and will be done in such a way that the effects of multiple scattering are included in the formal result. The formulation will also allow for more than one type of scatterer in the same slab, and effective scattering operators for both the fields and the incoherent components of the scattered radiation will be defined. This represents an advantage over the usual radiative transfer formulation [6]. Also, using this formulation, it is easy to calculate results when only single reflections are considered. This will be the subject of the last section of this chapter. The disadvantage of this formulation is that it is hard to calculate the multiple scattering results. This issue will be addressed in a later chapter.

3.2 Mathematical Formulation.

The problem to be considered is that of a plane electromagnetic wave incident upon a volume containing a number of scatterers. It will be assumed that the volume is in the form of a slab of thickness L and that only a finite part of the slab is illuminated at any instant in time. To formulate the problem mathematically, it will be assumed that the origin of the coordinate system in which the calculations are to be performed lies in the center of the illuminated area on top of the slab. The layer containing the scatterers thus occupies the region $0 \leq z \leq -L$ as shown in Figure 3.1.

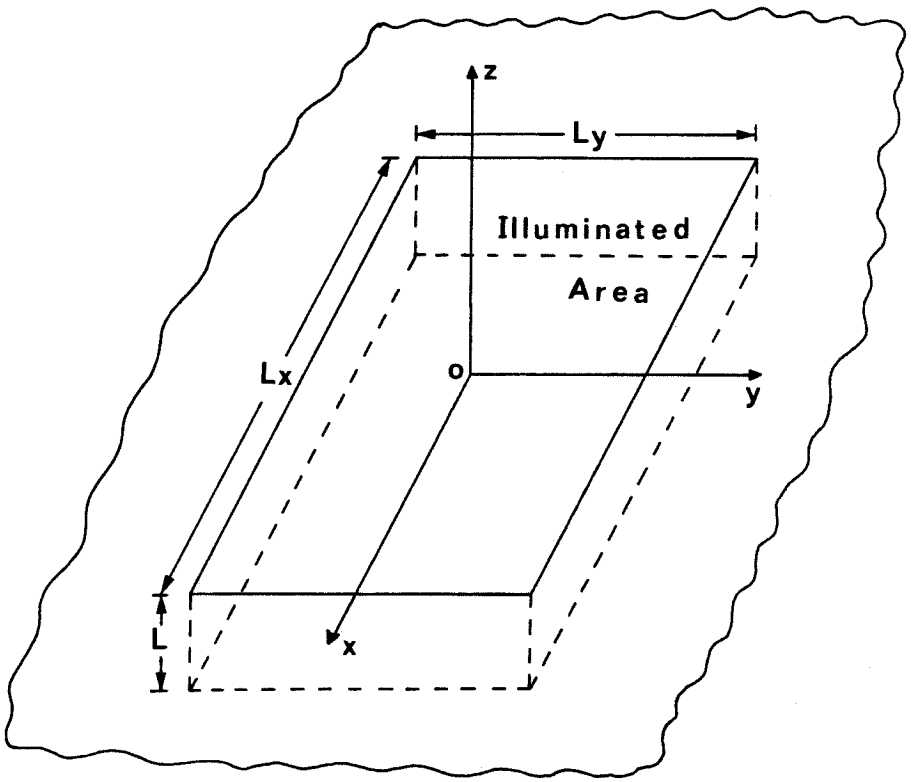

Figure 3.1. Scattering Geometry.

Here, it will be assumed that the spacing between scatterers is large enough so that the interaction between scatterers is due to far-zone fields only. Also, it will be assumed that shadowing of one scatterer by another may be neglected and that the bistatic scattering matrix of every scatterer in the volume under consideration is known. This bistatic scattering matrix relates the electric field scattered by the scatterer, $\mathbf{E}^{sc}$, into a direction (ϑ_s,φ_s) to the electric field incident on the scatterer, $\mathbf{E}^{inc}$, from a direction (ϑ_i,φ_i) (see Figure 3.2) as follows:

$$\mathbf{E}^{sc}(\mathbf{r},\vartheta_s,\varphi_s) = [\mathbf{S}(\vartheta_i,\varphi_i,\vartheta_s,\varphi_s)]\,\mathbf{E}^{inc}(\mathbf{r}',\vartheta_i,\varphi_i)\,\frac{e^{ik|\mathbf{r}-\mathbf{r}'|}}{k|\mathbf{r}-\mathbf{r}'|}. \qquad (3\text{-}1)$$

In the far zone, $r \gg r'$, this becomes:

$$\mathbf{E}^{sc}(\mathbf{r},\vartheta_s,\varphi_s) = [\mathbf{S}(\vartheta_i,\varphi_i,\vartheta_s,\varphi_s)]\, \mathbf{E}^{inc}(\mathbf{r}',\vartheta_i,\varphi_i)\, h(kr)\, \exp\left[-ik\mathbf{e}_r\cdot\mathbf{r}'\right] \qquad (3\text{-}2)$$

with

$$h(kr) = \frac{e^{ikr}}{kr}. \qquad (3\text{-}3)$$

In this discussion, the transverse components of $\mathbf{E}^{inc}$ and $\mathbf{E}^{sc}$ will be expressed in the two right-handed bases shown in Figure 3.2.

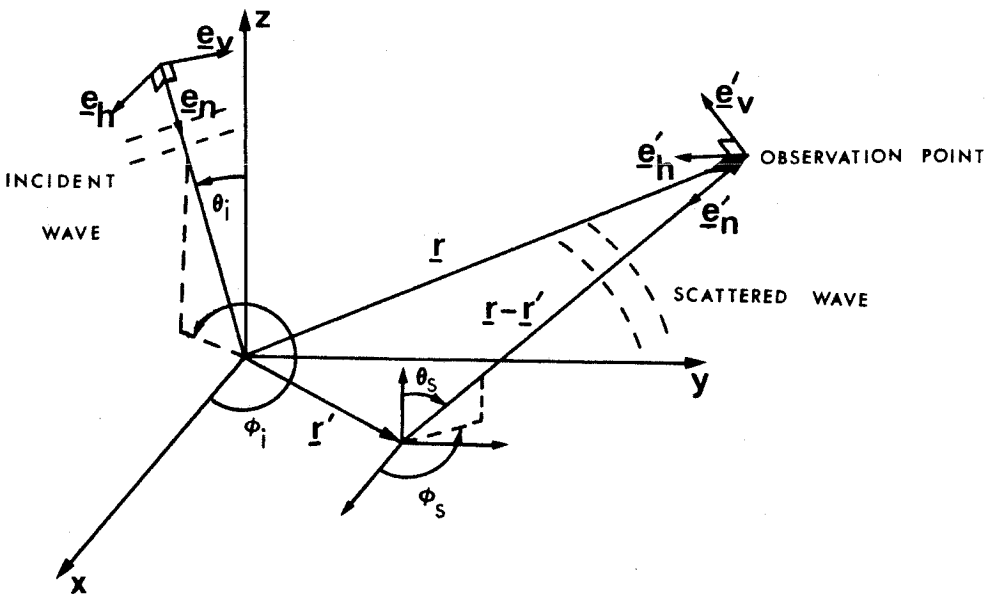

Figure 3.2. Bistatic scattering.

In these bases

$$\mathbf{e}_v = \text{unit vector in } \mathbf{e}_z\text{–}\mathbf{k} \text{ plane.} \tag{3-4}$$

In both cases the $\mathbf{e}_n$ vector points towards the scatterer. In these bases, the transverse components of the incident and scattered electric fields can be written as:

$$\mathbf{E}^{inc} = (E_v^{inc}\mathbf{e}_v + E_h^{inc}\mathbf{e}_h)\exp\left[i(\mathbf{k}_i\cdot\mathbf{r}-\omega t)\right] \tag{3-5}$$

$$\mathbf{E}^{sc}(\mathbf{r}') = (E_v^{sc}\mathbf{e}'_v + E_h^{sc}\mathbf{e}'_h)\frac{\exp\left[i(\mathbf{k}_s\cdot\mathbf{r}'-\omega t)\right]}{kr}. \tag{3-6}$$

The primes on the second set of basis vectors serve as a reminder that these are different from the first set as shown in Figure 3.2. It will be assumed that the bistatic scattering matrix as defined in (3-1) relates $\mathbf{E}^{sc}$ as expressed in the primed basis to $\mathbf{E}^{inc}$ in the unprimed basis.

Once the electric fields are related by a bistatic scattering matrix, it is easy to relate the Stokes parameters of the scattered wave to that of the incident wave. This has already been discussed in the previous chapter. For the moment it will merely be repeated that the relationship can be expressed by:

$$\mathbf{S}^{sc} = [\mathbf{M}]\mathbf{S}^{inc}. \tag{3-7}$$

The problem now is to find effective operators $[\mathbf{S}]$ and $[\mathbf{M}]$ for the whole volume of scatterers.

3.3 Positions of Scatterers are Known.

The total electric field at any position $\mathbf{r}$ follows from superposition to be:

$$\mathbf{E}(\mathbf{r}) = \mathbf{E}^{inc}(\mathbf{r}) + \mathbf{E}^{sc}(\mathbf{r}) \tag{3-8}$$

where $\mathbf{E}^{sc}(\mathbf{r})$ is the total scattered field at point $\mathbf{r}$ due to all the scatterers in the volume V under consideration. Since all the scatterers are assumed to be of

finite size, $\mathbf{E}^{sc}$ consists of a collection of spherical waves travelling away from each scattering center in all directions. It will now be defined, analogous to (3-1) that

$$\mathbf{E}^{sc}(\mathbf{r}) = [\mathbf{S}_e(\vartheta_i,\varphi_i,\vartheta_s,\varphi_s)]\,\mathbf{E}^{inc}(0)\,h(kr) \tag{3-9}$$

where $\mathbf{E}^{inc}(0)$ denotes the incident electric field at the origin of the coordinate system shown in Figure 3.1.

The total electric field incident on the j^{th} scatterer at position $\mathbf{r}_j$ is:

$$\mathbf{E}^{in}(\mathbf{r}_j) = \mathbf{E}^{inc}(\mathbf{r}_j) + \sum_{\substack{n=1 \\ n\neq j}}^{M} \mathbf{E}_n^{sc}(\mathbf{r}_j)\,. \tag{3-10}$$

The second term represents the total scattered field at point $\mathbf{r}_j$ due to all the other scatterers in the volume. Here, it was assumed that there are M scattering centers in the volume. There may, of course, also be an electric field due to scattering centers outside the illuminated volume, particularly when higher-order reflections are considered. Since these contributions are expected to be small when the scatterers are relatively far apart, except maybe near the boundaries of the volume, they will be ignored here.

From (3-10) it is clear that one needs to know $\mathbf{E}^{inc}$, both magnitude and phase, at every point $\mathbf{r}_j$ inside the medium. Since energy is taken out of the incident wave when the scattering centers are excited, the incident wave will be attenuated as it propagates through the medium. Depending on the geometry and the orientation of the various scatterers relative to the direction of the incident electric field, the two transverse components of the incident wave will suffer different attenuations. To incorporate this type of loss in this discussion, it is defined that

$$\exp\left[-\frac{\alpha_v|z|}{\cos(\vartheta_i)}\right] = \begin{cases}\text{loss suffered by } E_v \text{ component of } \mathbf{E}^{inc} \text{ when}\\ \text{travelling at an angle } \vartheta_i \text{ to the z-axis}\\ \text{for a vertical distance } |z| \text{ into the medium.}\end{cases} \quad (3\text{-}11a)$$

$$\exp\left[-\frac{\alpha_h|z|}{\cos(\vartheta_i)}\right] = \text{Same as (3-11a), but for horizontal component.} \quad (3\text{-}11b)$$

It must be noted that although this energy is taken out of the incident wave, it is not necessarily lost. Some of this energy will indeed reappear as the scattered wave.

Since it was assumed that the scattering centers are fairly far apart and that the scatterers are small, it will be assumed that the phase of the incident wave changes in the same way as if it was travelling in air when travelling in the volume of scatterers. To relate the phase of the $\mathbf{E}^{inc}$ at different positions, the plane of constant phase that goes through the origin of the coordinate system will be used as a reference. The equation describing this plane is

$$x\sin(\vartheta_i)\cos(\varphi_i) + y\sin(\vartheta_i)\sin(\varphi_i) + z\cos(\vartheta_i) = 0. \quad (3\text{-}12)$$

Taking proper care of the sign of the phase (points on the same side of the reference plane as the source of the incident wave have "negative" distance to this plane), one finds that the phase of the incident wave at $\mathbf{r}_j$ relative to the reference phase is:

$$\xi_j = -k\mathbf{e}_i\cdot\mathbf{r}_j \quad (3\text{-}13)$$

with

$$\mathbf{e}_i = \sin(\vartheta_i)\cos(\varphi_i)\mathbf{e}_x + \sin(\vartheta_i)\sin(\varphi_i)\mathbf{e}_y + \cos(\vartheta_i)\mathbf{e}_z .$$

Thus, at every point inside the medium

$$\mathbf{E}^{inc}(\mathbf{r}_j) = [\alpha_i]\mathbf{E}^{inc}(0)\exp\left[-ik\mathbf{e}_i\cdot\mathbf{r}_j\right] \tag{3-14}$$

where

$$[\alpha_i] = \begin{bmatrix} \exp\left(\dfrac{\alpha_h z_j}{\cos(\vartheta_i)}\right) & 0 \\ 0 & \exp\left(\dfrac{\alpha_v z_j}{\cos(\vartheta_i)}\right) \end{bmatrix}. \tag{3-15}$$

An argument similar to the one above gives the scattered electric field, in the far zone, due to the scattering center at $\mathbf{r}_j$ as:

$$\mathbf{E}_j^{sc}(\mathbf{r},\vartheta_s,\varphi_s) = [\alpha_s]\,\mathbf{E}_j^{sc}(\mathbf{r}_j,\vartheta_s,\varphi_s)\exp\left[-ik\mathbf{e}_r\cdot\mathbf{r}_j\right] h(kr) \tag{3-16}$$

where $[\alpha_s]$ is the same as $[\alpha_i]$, but with $\cos(\vartheta_i)$ replaced by $\cos(\vartheta_s)$. The total scattered field at point $\mathbf{r}$ is

$$\mathbf{E}^{sc}(\mathbf{r},\vartheta_s,\varphi_s) = \sum_{j=1}^{M}\mathbf{E}_j^{sc}(\mathbf{r},\vartheta_s,\varphi_s)\,. \tag{3-17}$$

In the same way as before, one can write the scattered electric field at a position $\mathbf{r}_n$ due to a scattering center at point $\mathbf{r}_j$ as:

$$\mathbf{E}_j^{sc}(\mathbf{r}_n) = [\alpha_{jn}]\,\mathbf{E}_j^{sc}(\mathbf{r}_j)\,h(k|\mathbf{r}_j-\mathbf{r}_n|) \tag{3-18}$$

where

$$[\alpha_{jn}] = \begin{bmatrix} \exp\left(-\alpha_h|\mathbf{r}_j-\mathbf{r}_n|\right) & 0 \\ 0 & \exp\left(-\alpha_v|\mathbf{r}_j-\mathbf{r}_n|\right) \end{bmatrix}.$$

Using (3-16), (3-2) and (3-10) in (3-17), one finds that:

$$\mathbf{E}^{sc}(\mathbf{r},\vartheta_s,\varphi_s) = \sum_{j=1}^{M}[\alpha_s]\,[\mathbf{S}_j(\vartheta_i,\varphi_i,\vartheta_s,\varphi_s)]\,\mathbf{E}^{inc}(\mathbf{r}_j)\,e^{-ik\mathbf{e}_r\cdot\mathbf{r}_j}\,h(kr)$$

$$+ \sum_{j=1}^{M} \sum_{\substack{n=1 \\ n\neq j}}^{M} [\alpha_s]\,[\mathbf{S}_j(\vartheta_j,\varphi_j,\vartheta_s,\varphi_s)]\,\mathbf{E}_n^{sc}(\mathbf{r}_j)\,e^{-ik\mathbf{e}_r\cdot\mathbf{r}_j}\,h(kr)\,. \quad (3\text{-}19)$$

With the help of (3-14), the first term may be written as:

$$\sum_{j=1}^{M} [\alpha_s]\,[\mathbf{S}_j(\vartheta_i,\varphi_i,\vartheta_s,\varphi_s)]\,\mathbf{E}^{inc}(\mathbf{r}_j)\,e^{-ik\mathbf{e}_r\cdot\mathbf{r}_j}\,h(kr)$$

$$= \left\{ \sum_{j=1}^{M} [\alpha_s]\,[\mathbf{S}_j(\vartheta_i,\varphi_i,\vartheta_s,\varphi_s)]\,[\alpha_i]\,e^{-ik(\mathbf{e}_r\cdot\mathbf{r}_j+\mathbf{e}_i\cdot\mathbf{r}_j)} \right\} \mathbf{E}^{inc}(0)\,h(kr)$$

$$\equiv [\mathbf{S}_e^{(1)}(\vartheta_i,\varphi_i,\vartheta_s,\varphi_s)]\,\mathbf{E}^{inc}(0)\,h(kr)\,. \quad (3\text{-}20)$$

If (3-2), (3-16), (3-10), (3-14) and (3-18) are used repeatedly in (3-19) one finds that

$$\mathbf{E}^{sc}(\mathbf{r},\vartheta_s,\varphi_s) = [\mathbf{S}_e(\vartheta_i,\varphi_i,\vartheta_s,\varphi_s)]\,\mathbf{E}^{inc}(0)\,h(kr) \quad (3\text{-}21)$$

with

$$[\mathbf{S}_e(\vartheta_i,\varphi_i,\vartheta_s,\varphi_s)] = \sum_{m=1}^{\infty} [\mathbf{S}_e^{(m)}(\vartheta_i,\varphi_i,\vartheta_s,\varphi_s)] \quad (3\text{-}22)$$

and

$$[\mathbf{S}_e^{(1)}(\vartheta_i,\varphi_i,\vartheta_s,\varphi_s)] = \sum_{j=1}^{M} [\alpha_s]\,[\mathbf{S}_j(\vartheta_i,\varphi_i,\vartheta_s,\varphi_s)]\,[\alpha_i]\,\exp\left[-ik(\mathbf{e}_r\cdot\mathbf{r}_j+\mathbf{e}_i\cdot\mathbf{r}_j)\right] \quad (3\text{-}23a)$$

$$[\mathbf{S}_e^{(2)}(\vartheta_i,\varphi_i,\vartheta_s,\varphi_s)] = \sum_{j=1}^{M} \sum_{\substack{n=1 \\ n\neq j}}^{M} \left\{ [\alpha_s]\,[\mathbf{S}_j(\vartheta_j,\varphi_j,\vartheta_s,\varphi_s)]\,[\alpha_{jn}] \right.$$

$$\left. \times \begin{bmatrix} -1 & 0 \\ 0 & 1 \end{bmatrix} [\mathbf{S}_n(\vartheta_i,\varphi_i,\vartheta_j,\varphi_j)]\,[\alpha_i]\,\exp\left[-ik(\mathbf{e}_r\cdot\mathbf{r}_j+\mathbf{e}_i\cdot\mathbf{r}_n)\right]\,h(k\,|\mathbf{r}_j-\mathbf{r}_n|) \right\}. \quad (3\text{-}23b)$$

The extra matrix with diagonal elements -1 and 1 is needed to correctly change coordinate bases between the two scatterers.

It is clear that the superscript (m) denotes the number of reflections that the electric field has suffered inside the slab before reaching the observation point. Although this is an infinite series, the higher-order terms will be important only when the scattering centers are fairly close together. In general, it is expected that the series will converge in most cases with only a few terms.

If one is interested in the energy transmitted through the slab, the only modification to (3-23) needed is to replace the subscript s with a subscript t and to replace $[\alpha_s]$ by $[\alpha_t]$, where

$$[\alpha_t] = \begin{bmatrix} \exp\left(-\frac{\alpha_h(L-|z_j|)}{|\cos(\vartheta_t)|}\right) & 0 \\ 0 & \exp\left(-\frac{\alpha_v(L-|z_j|)}{|\cos(\vartheta_t)|}\right) \end{bmatrix}. \qquad (3\text{-}24)$$

3.4 Scatterers Distributed Statistically

In the vast majority of the cases encountered in radar imaging, scattering centers are distributed statistically. In these cases, it is not possible to calculate the exact field scattered by the slab of scatterers, and one has to settle for information about the *average* fields or powers reflected or transmitted.

It will be assumed that in these cases, some information about the distribution of scattering centers is already known. In particular,

$$p_i(\mathbf{r}) = \begin{cases} \text{Three-dimensional probability density function (p.d.f.) for} \\ \text{the location of a scatterer of the } i^{th} \text{ kind.} \end{cases}$$

$$p_{ij}(\mathbf{r}_j/\mathbf{r}_i) = \begin{cases} \text{Three-dimensional conditional p.d.f. expressing the} \\ \text{probability to find a scatterer of the } j^{th} \text{ kind at } \mathbf{r}_j \\ \text{given that a scatterer of the } i^{th} \text{ kind is located at } \mathbf{r}_i. \end{cases}$$

should be known. Similar functions should also be known for combinations of three, four, five, etc. scatterers.

It is easily seen that in general the fields scattered by such a slab will be partially coherent [13]. If there are some permanent phase relations between the different waves scattered, one must add the fields in such a fashion that these permanent phase relations are not lost. For the incoherent part of the power, there are no such permanent phase relations, and powers may be added. In general [5],

$$\langle P_{tot} \rangle = P_{coherent} + P_{incoherent} . \tag{3-25}$$

Here, it will be understood that

$$P_{incoherent} \alpha \langle |\mathbf{E}_{tot}^{sc}|^2 \rangle . \tag{3-26}$$

It is clear that in order to characterize the slab completely, effective operators for both the average field and the average intensity must be found.

3.4.1 Effective Operator for the Average Electric Field.

Let ρ be the average volume density of the scatterers in the volume. Then, if an electric field travels a distance d through the medium, the resulting attenuation matrix which describes the attenuation of the electric field *per unit area normal to the direction of propagation* is:

$$[\alpha(d)] = \begin{bmatrix} \exp\left[-\alpha_h \rho d\right] & 0 \\ 0 & \exp\left[-\alpha_v \rho d\right] \end{bmatrix} . \tag{3-27}$$

Thus, $[\alpha_i]$, $[\alpha_s]$ and $[\alpha_t]$ are:

$$[\alpha_i] = \begin{bmatrix} \exp\left(\frac{\alpha_h \rho z}{\cos(\vartheta_i)}\right) & 0 \\ 0 & \exp\left(\frac{\alpha_v \rho z}{\cos(\vartheta_i)}\right) \end{bmatrix} \tag{3-28a}$$

$$[\alpha_s] = \begin{bmatrix} \exp\left(\frac{\alpha_h \rho z}{\cos(\vartheta_s)}\right) & 0 \\ 0 & \exp\left(\frac{\alpha_v \rho z}{\cos(\vartheta_s)}\right) \end{bmatrix} \tag{3-28b}$$

$$[\alpha_t] = \begin{bmatrix} \exp\left(-\frac{\alpha_h \rho (L+z)}{|\cos(\vartheta_t)|}\right) & 0 \\ 0 & \exp\left(-\frac{\alpha_v \rho (L+z)}{|\cos(\vartheta_t)|}\right) \end{bmatrix} \tag{3-28c}$$

The effective scattering matrix for the average of the reflected fields, ***per unit scattering area projected normal to the direction of propagation*** , follows from the same arguments as in the previous section to be given by (3-22). In this case, however,

$$[\mathbf{S}_e^{(1)}] = \frac{\sqrt{\cos(\vartheta_s)}}{A_l} \left\{ \sum_{i=1}^{N} N_i \int p_i(\mathbf{r}) \, [\alpha_s] \, [\mathbf{S}_i] \, [\alpha_i] \exp\left[-ik(\mathbf{e}_r \cdot \mathbf{r} + \mathbf{e}_i \cdot \mathbf{r})\right] dv \right\} \tag{3-29}$$

with A_l the total illuminated area and assuming that there are N different types of scatterers present in the volume. N_i is the number of scatterers of the i^{th} type present in the volume. The integration must include the whole illuminated volume. Similarly,

$$[\mathbf{S}_e^{(2)}] = \frac{\sqrt{\cos(\vartheta_s)}}{A_l} \sum_{i=1}^{N} \left\{ N_i(N_i-1) \int p_i(\mathbf{r}) \int p_{ii}(\mathbf{r}'/\mathbf{r}) \, [\mathbf{S}_{ii}] \right.$$

$$\times \exp\left[-ik(\mathbf{e}_r \cdot \mathbf{r} + \mathbf{e}_i \cdot \mathbf{r}')\right] h(|\mathbf{r}-\mathbf{r}'|) dv'dv$$

$$\left. + \sum_{\substack{j=1 \\ j \neq i}}^{N} N_i \, N_j \int p_i(\mathbf{r}) \int p_{ij}(\mathbf{r}'/\mathbf{r}) \, [\mathbf{S}_{ij}] \exp\left[-ik(\mathbf{e}_r \cdot \mathbf{r} + \mathbf{e}_i \cdot \mathbf{r}')\right] h(|\mathbf{r}-\mathbf{r}'|) \, dv'dv \right\} \qquad (3\text{-}30)$$

with

$$[\mathbf{S}_{xy}] = [\alpha_s] \, [\mathbf{S}_x(\vartheta', \varphi', \vartheta_s, \varphi_s)] \, [\alpha_{\mathbf{r},\mathbf{r}'}] \begin{bmatrix} -1 & 0 \\ 0 & 1 \end{bmatrix} [\mathbf{S}_y(\vartheta_i, \varphi_i, \vartheta', \varphi')] \, [\alpha_i] \, .$$

3.4.2 Effective Operator for Incoherently Reflected Intensity.

It was already shown in section 2.2 that for incoherent scattering, the total Stokes vector is the sum of the individual Stokes vectors. Hence, in terms of incoherently reflected (or transmitted) intensities, the slab of scatterers is best characterized by an effective Stokes Scattering Operator. Using (3-27) and (2-17) one finds that the attenuation matrix for this case is $[\beta_x]$ with elements:

$$\beta_{x11} = \tfrac{1}{2} \exp\left[\frac{2\alpha_h \rho z}{\cos(\vartheta_x)}\right] + \tfrac{1}{2} \exp\left[\frac{2\alpha_v \rho z}{\cos(\vartheta_x)}\right] \qquad (3\text{-}31a)$$

$$\beta_{x12} = \tfrac{1}{2} \exp\left[\frac{2\alpha_h \rho z}{\cos(\vartheta_x)}\right] - \tfrac{1}{2} \exp\left[\frac{2\alpha_v \rho z}{\cos(\vartheta_x)}\right] \qquad (3\text{-}31b)$$

$$\beta_{x33} = \exp\left[\frac{(\alpha_h + \alpha_v)\rho z}{\cos(\vartheta_x)}\right] \qquad (3\text{-}31c)$$

$$\beta_{x22} = \beta_{x11} \qquad (3\text{-}31d)$$

$$\beta_{x21} = \beta_{x12} \tag{3-31e}$$

$$\beta_{x44} = \beta_{x33} \cdot \tag{3-31f}$$

$$\text{All other } \beta_{xij} = 0. \tag{3-31g}$$

Here, x may either be s or i. For transmission, the x is replaced by t, z is replaced by -(L+z) and $\cos(\vartheta_x)$ is replaced by $|\cos(\vartheta_t)|$.

Then, in the same way as for the fields, one finds that the effective Stokes Scattering Operator for reflection, *per unit illuminated area projected normal to the direction of propagation*, is of the form:

$$[\mathbf{M}_e(\vartheta_i,\varphi_i,\vartheta_s,\varphi_s)] = \sum_{m=1}^{\infty} [\mathbf{M}_e^{(m)}(\vartheta_i,\varphi_i,\vartheta_s,\varphi_s)] \tag{3-32}$$

with

$$[\mathbf{M}_e^{(1)}] = \frac{\cos(\vartheta_s)}{A_l} \sum_{i=1}^{N} N_i \int p_i(\mathbf{r})[\beta_s][\mathbf{M}_i][\beta_i]\, dv \tag{3-33a}$$

$$[\mathbf{M}_e^{(2)}] = \frac{\cos(\vartheta_s)}{A_l} \sum_{i=1}^{N} \Bigg\{ N_i(N_i-1) \int p_i(\mathbf{r}) \int \frac{p_{ij}(\mathbf{r}'/\mathbf{r})}{|\mathbf{r}-\mathbf{r}'|^2} [\mathbf{M}_{ii}]\, dv'\, dv$$

$$+ \sum_{\substack{j=1 \\ j\neq i}}^{N} N_i N_j \int p_i(\mathbf{r}) \int \frac{p_{ij}(\mathbf{r}'/\mathbf{r})}{|\mathbf{r}'-\mathbf{r}|^2} [\mathbf{M}_{ij}]\, dv'\, dv \tag{3-33b}$$

where $[\mathbf{M}_{xy}]$ has the same form as $[\mathbf{S}_{ij}]$ of the previous section, but with the $[\alpha]$ matrices replaced by the corresponding $[\beta]$ matrices and the $[\mathbf{S}]$ matrices replaced by the $[\mathbf{M}]$ matrices. The matrix to take care of the change in basis should be replaced by its equivalent Stokes Scattering Operator. The effective operator for the transmitted energy can be found by replacing $[\beta_s]$ by $[\beta_t]$ in the expressions above.

3.5 General Results for Single Reflections.

In the rest of this chapter, it will be assumed that the scattering centers are distributed uniformly and randomly; i.e.,

$$p_i(\mathbf{r}) = \frac{f_i}{V} \tag{3-34}$$

where f_i represents the fraction of the the total amount of scatterers, which are of the i^{th} type and V is the total illuminated volume.

3.5.1 Reflection Operators.

3.5.1.1 Intensities.

Following the procedure described in the previous section, one finds that the elements of the effective Stokes Scattering Operator are:

$$M_{e11}^{(1)} = \frac{\cos(\vartheta_i)\cos^2(\vartheta_s)}{4}\sum_{i=1}^{N} f_i \left\{ A(|S_{h'h}|^2)_i + B(|S_{v'h}|^2)_i \right.$$

$$\left. + C(|S_{h'v}|^2)_i + D(|S_{v'v}|^2)_i \right\} \tag{3-35a}$$

$$M_{e12}^{(1)} = \frac{\cos(\vartheta_i)\cos^2(\vartheta_s)}{4}\sum_{i=1}^{N} f_i \left\{ A(|S_{h'h}|^2)_i + B(|S_{v'h}|^2)_i \right.$$

$$\left. - C(|S_{h'v}|^2)_i - D(|S_{v'v}|^2)_i \right\} \tag{3-35b}$$

$$M_{e13}^{(1)} = \cos(\vartheta_i)\cos^2(\vartheta_s)\sum_{i=1}^{N} f_i \left\{ E\,\mathrm{Re}(S_{h'h}^{*}S_{h'v})_i + F\,\mathrm{Re}(S_{v'v}S_{v'h}^{*})_i \right\} \tag{3-35c}$$

$$M_{e14}^{(1)} = \cos(\vartheta_i)\cos^2(\vartheta_s)\sum_{i=1}^{N} f_i \left\{ E\,\mathrm{Im}(S_{h'h}^{*}S_{h'v})_i + F\,\mathrm{Im}(S_{v'v}S_{v'h}^{*})_i \right\} \tag{3-35d}$$

$$M_{e21}^{(1)} = \frac{\cos(\vartheta_i)\cos^2(\vartheta_s)}{4}\sum_{i=1}^{N} f_i \left\{ A(|S_{h'h}|^2)_i - B(|S_{v'h}|^2)_i \right.$$

$$\left. + C(|S_{h'v}|^2)_i - D(|S_{v'v}|^2)_i \right\} \qquad (3\text{-}35e)$$

$$M_{e22}^{(1)} = \frac{\cos(\vartheta_i)\cos^2(\vartheta_s)}{4}\sum_{i=1}^{N} f_i \left\{ A(|S_{h'h}|^2)_i - B(|S_{v'h}|^2)_i \right.$$

$$\left. - C(|S_{h'v}|^2)_i + D(|S_{v'v}|^2)_i \right\} \qquad (3\text{-}35f)$$

$$M_{e23}^{(1)} = \cos(\vartheta_i)\cos^2(\vartheta_s)\sum_{i=1}^{N} f_i \left\{ E\,\mathrm{Re}(S_{h'h}^{*}S_{h'v})_i - F\,\mathrm{Re}(S_{v'v}S_{v'h}^{*})_i \right\} \qquad (3\text{-}35g)$$

$$M_{e24}^{(1)} = \cos(\vartheta_i)\cos^2(\vartheta_s)\sum_{i=1}^{N} f_i \left\{ E\,\mathrm{Im}(S_{h'h}^{*}S_{h'v})_i - F\,\mathrm{Im}(S_{v'v}S_{v'h}^{*})_i \right\} \qquad (3\text{-}35h)$$

$$M_{e31}^{(1)} = \cos(\vartheta_i)\cos^2(\vartheta_s)\sum_{i=1}^{N} f_i \left\{ G\,\mathrm{Re}(S_{h'h}^{*}S_{v'h})_i + H\,\mathrm{Re}(S_{v'v}S_{h'v}^{*})_i \right\} \qquad (3\text{-}35i)$$

$$M_{e32}^{(1)} = \cos(\vartheta_i)\cos^2(\vartheta_s)\sum_{i=1}^{N} f_i \left\{ G\,\mathrm{Re}(S_{h'h}^{*}S_{v'h})_i - H\,\mathrm{Re}(S_{v'v}S_{h'v}^{*})_i \right\} \qquad (3\text{-}35j)$$

$$M_{e33}^{(1)} = \cos(\vartheta_i)\cos^2(\vartheta_s)\sum_{i=1}^{N} f_i\, I \left\{ \mathrm{Re}(S_{h'v}^{*}S_{v'h})_i + \mathrm{Re}(S_{h'h}^{*}S_{v'v})_i \right\} \qquad (3\text{-}35k)$$

$$M_{e34}^{(1)} = \cos(\vartheta_i)\cos^2(\vartheta_s)\sum_{i=1}^{N} f_i\, I \left\{ \mathrm{Im}(S_{h'h}^{*}S_{v'v})_i - \mathrm{Im}(S_{h'v}^{*}S_{v'h})_i \right\} \qquad (3\text{-}35l)$$

$$M_{e41}^{(1)} = \cos(\vartheta_i)\cos^2(\vartheta_s)\sum_{i=1}^{N} f_i \left\{ G\,\mathrm{Im}(S_{h'h}^{*}S_{v'h})_i + H\,\mathrm{Im}(S_{v'v}S_{h'v}^{*})_i \right\} \qquad (3\text{-}35m)$$

$$M_{e42}^{(1)} = \cos(\vartheta_i)\cos^2(\vartheta_s)\sum_{i=1}^{N} f_i \left\{ G\,\mathrm{Im}(S_{h'h}^{*}S_{v'h})_i - H\,\mathrm{Im}(S_{v'v}S_{h'v}^{*})_i \right\} \qquad (3\text{-}35n)$$

$$M_{e43}^{(1)} = \cos(\vartheta_i)\cos^2(\vartheta_s)\sum_{i=1}^{N} f_i\, I \left\{ \mathrm{Im}(S_{h'h}^{*}svv)_i + \mathrm{Im}(S_{h'v}^{*}S_{v'h})_i \right\} \qquad (3\text{-}35o)$$

$$M_{e44}^{(1)} = \cos(\vartheta_i)\cos^2(\vartheta_s)\sum_{i=1}^{N} f_i I\left\{ \mathrm{Re}(S^*_{h'v}S_{v'h})_i - \mathrm{Re}(S^*_{h'h}S_{v'v})_i \right\}, \tag{3-35p}$$

where

$$A = \frac{1-\exp\left[-\alpha_1 L\right]}{\alpha_h^i\cos(\vartheta_s) + \alpha_h^s\cos(\vartheta_i)} \tag{3-36a}$$

$$B = \frac{1-\exp\left[-\alpha_2 L\right]}{\alpha_h^i\cos(\vartheta_s) + \alpha_v^s\cos(\vartheta_i)} \tag{3-36b}$$

$$C = \frac{1-\exp\left[-\alpha_3 L\right]}{\alpha_v^i\cos(\vartheta_s) + \alpha_h^s\cos(\vartheta_i)} \tag{3-36c}$$

$$D = \frac{1-\exp\left[-\alpha_4 L\right]}{\alpha_v^i\cos(\vartheta_s) + \alpha_v^s\cos(\vartheta_i)} \tag{3-36d}$$

$$E = \frac{1-\exp\left[-\alpha_5 L\right]}{(\alpha_h^i+\alpha_v^i)\cos(\vartheta_s) + 2\alpha_h^s\cos(\vartheta_i)} \tag{3-36e}$$

$$F = \frac{1-\exp\left[-\alpha_6 L\right]}{(\alpha_h^i+\alpha_v^i)\cos(\vartheta_s) + 2\alpha_v^s\cos(\vartheta_i)} \tag{3-36f}$$

$$G = \frac{1-\exp\left[-\alpha_7 L\right]}{2\alpha_h^i\cos(\vartheta_s) + (\alpha_h^s+\alpha_v^s)\cos(\vartheta_i)} \tag{3-36g}$$

$$H = \frac{1-\exp\left[-\alpha_8 L\right]}{2\alpha_v^i\cos(\vartheta_s) + (\alpha_h^s+\alpha_v^s)\cos(\vartheta_i)} \tag{3-36h}$$

$$I = \frac{1-\exp\left[-\alpha_9 L\right]}{(\alpha_h^i+\alpha_v^i)\cos(\vartheta_s) + (\alpha_h^s+\alpha_v^s)\cos(\vartheta_i)} \tag{3-36i}$$

and

$$\alpha_1 = 2\rho\left\{\frac{\alpha_h^i}{\cos(\vartheta_i)} + \frac{\alpha_h^s}{\cos(\vartheta_s)}\right\} \tag{3-37a}$$

$$\alpha_2 = 2\rho\left\{\frac{\alpha_h^i}{\cos(\vartheta_i)} + \frac{\alpha_v^s}{\cos(\vartheta_s)}\right\} \tag{3-37b}$$

$$\alpha_3 = 2\rho\left\{\frac{\alpha_v^i}{\cos(\vartheta_i)} + \frac{\alpha_h^s}{\cos(\vartheta_s)}\right\} \tag{3-37c}$$

$$\alpha_4 = 2\rho\left\{\frac{\alpha_v^i}{\cos(\vartheta_i)} + \frac{\alpha_v^s}{\cos(\vartheta_s)}\right\} \tag{3-37d}$$

$$\alpha_5 = \rho\left\{\frac{\alpha_v^i+\alpha_h^i}{\cos(\vartheta_i)} + \frac{2\alpha_h^s}{\cos(\vartheta_s)}\right\} \tag{3-37e}$$

$$\alpha_6 = \rho\left\{\frac{\alpha_v^i+\alpha_h^i}{\cos(\vartheta_i)} + \frac{2\alpha_v^s}{\cos(\vartheta_s)}\right\} \tag{3-37f}$$

$$\alpha_7 = \rho\left\{\frac{2\alpha_h^i}{\cos(\vartheta_i)} + \frac{\alpha_v^s+\alpha_h^s}{\cos(\vartheta_s)}\right\} \tag{3-37g}$$

$$\alpha_8 = \rho\left\{\frac{2\alpha_v^i}{\cos(\vartheta_i)} + \frac{\alpha_v^s+\alpha_h^s}{\cos(\vartheta_s)}\right\} \tag{3-37h}$$

$$\alpha_9 = \rho\left\{\frac{\alpha_h^i+\alpha_v^i}{\cos(\vartheta_i)} + \frac{\alpha_h^s+\alpha_v^s}{\cos(\vartheta_s)}\right\}. \tag{3-37i}$$

Also,

$$\alpha_x^y = \sum_{j=1}^{N} f_j \, (\alpha_x^y)_j \tag{3-38}$$

where x may be either h or v and y may be either i or s.

Here, a distinction is made between the attenuation constants for the incident and scattered waves. This must be done since, in general, the relative orientation of the scatterer with respect to the incident and scattered waves may be different. This will lead to different amounts of energy absorbed from the two waves or, equivalently, different attenuations suffered by the two waves.

3.5.1.2 Electric Fields.

In a similar fashion, it is found that the effective scattering matrix has elements

$$S_{ehh}^{(1)} = J \left\{ \frac{1 - \exp\left[-\left[\frac{\alpha_h^i}{\cos(\vartheta_i)} + \frac{\alpha_h^s}{\cos(\vartheta_s)} \right] \rho \, L + ik(\cos(\vartheta_i)+\cos(\vartheta_s))L \right]}{\left[\frac{\alpha_h^i}{\cos(\vartheta_i)} + \frac{\alpha_h^s}{\cos(\vartheta_s)} \right] \rho - ik(\cos(\vartheta_i)+\cos(\vartheta_s))} \right\}$$

$$\times \sum_{i=1}^{N} f_i \, (S_{h'h})_i \tag{3-39a}$$

$$S_{ehv}^{(1)} = J \left\{ \frac{1 - \exp\left[-\left[\frac{\alpha_v^i}{\cos(\vartheta_i)} + \frac{\alpha_h^s}{\cos(\vartheta_s)} \right] \rho \, L + ik(\cos(\vartheta_i)+\cos(\vartheta_s))L \right]}{\left[\frac{\alpha_v^i}{\cos(\vartheta_i)} + \frac{\alpha_h^s}{\cos(\vartheta_s)} \right] \rho - ik(\cos(\vartheta_i)+\cos(\vartheta_s))} \right\}$$

$$\times \sum_{i=1}^{N} f_i \, (S_{h'v})_i \tag{3-39b}$$

$$S_{evh}^{(1)} = J\left\{\frac{1-\exp\left[-\left[\frac{\alpha_h^i}{\cos(\vartheta_i)}+\frac{\alpha_v^s}{\cos(\vartheta_s)}\right]\rho\, L + ik(\cos(\vartheta_i)+\cos(\vartheta_s))L\right]}{\left[\frac{\alpha_h^i}{\cos(\vartheta_i)}+\frac{\alpha_v^s}{\cos(\vartheta_s)}\right]\rho - ik(\cos(\vartheta_i)+\cos(\vartheta_s))}\right\}$$

$$\times \sum_{i=1}^{N} f_i\,(S_{v'h})_i \qquad (3\text{-}39c)$$

$$S_{evv}^{(1)} = J\left\{\frac{1-\exp\left[-\left[\frac{\alpha_v^i}{\cos(\vartheta_i)}+\frac{\alpha_v^s}{\cos(\vartheta_s)}\right]\rho\, L + ik(\cos(\vartheta_i)+\cos(\vartheta_s))L\right]}{\left[\frac{\alpha_v^i}{\cos(\vartheta_i)}+\frac{\alpha_v^s}{\cos(\vartheta_s)}\right]\rho - ik(\cos(\vartheta_i)+\cos(\vartheta_s))}\right\}$$

$$\times \sum_{i=1}^{N} f_i(S_{v'v})_i \qquad (3\text{-}39d)$$

with

$$J = \sqrt{\cos(\vartheta_s)}\,\rho\, Sa[k(\sin(\vartheta_i)\cos(\varphi_i)+\sin(\vartheta_s)\cos(\varphi_s))\frac{L_x}{2}]$$

$$\times Sa[k(\sin(\vartheta_i)\sin(\varphi_i)+\sin(\vartheta_s)\sin(\varphi_s))\frac{L_y}{2}] \qquad (3\text{-}40)$$

and

$$Sa[x] \equiv \frac{\sin(x)}{x}.$$

The attenuation constants are the same as those given in (3-38).

3.5.2 Transmission Operators.

3.5.2.1 Intensities.

The effective Stokes Transmission Operator for intensities transmitted

through the slab is of the same form as given in (3-35), but with A through I replaced by:

$$A_t = \frac{\exp\left[-\frac{2\alpha_h^t}{|\cos(\vartheta_t)|}\rho L\right] - \exp\left[-\frac{2\alpha_h^i}{\cos(\vartheta_i)}\rho L\right]}{\alpha_h^i|\cos(\vartheta_t)| + \alpha_h^t\cos(\vartheta_i)} \tag{3-41a}$$

$$B_t = \frac{\exp\left[-\frac{2\alpha_v^t}{|\cos(\vartheta_t)|}\rho L\right] - \exp\left[-\frac{2\alpha_h^i}{\cos(\vartheta_i)}\rho L\right]}{\alpha_h^i|\cos(\vartheta_t)| + \alpha_v^t\cos(\vartheta_i)} \tag{3-41b}$$

$$C_t = \frac{\exp\left[-\frac{2\alpha_h^t}{|\cos(\vartheta_t)|}\rho L\right] - \exp\left[-\frac{2\alpha_v^i}{\cos(\vartheta_i)}\rho L\right]}{\alpha_v^i|\cos(\vartheta_t)| + \alpha_h^t\cos(\vartheta_i)} \tag{3-41c}$$

$$D_t = \frac{\exp\left[-\frac{2\alpha_v^t}{|\cos(\vartheta_t)|}\rho L\right] - \exp\left[-\frac{2\alpha_v^i}{\cos(\vartheta_i)}\rho L\right]}{\alpha_v^i|\cos(\vartheta_t)| + \alpha_v^t\cos(\vartheta_i)} \tag{3-41d}$$

$$E_t = \frac{\exp\left[-\frac{2\alpha_h^t}{|\cos(\vartheta_t)|}\rho L\right] - \exp\left[-\frac{\alpha_h^i+\alpha_v^i}{\cos(\vartheta_i)}\rho L\right]}{2\alpha_h^t\cos(\vartheta_i) + (\alpha_h^i+\alpha_v^i)|\cos(\vartheta_t)|} \tag{3-41e}$$

$$F_t = \frac{\exp\left[-\frac{2\alpha_v^t}{|\cos(\vartheta_t)|}\rho L\right] - \exp\left[-\frac{\alpha_h^i+\alpha_v^i}{\cos(\vartheta_i)}\rho L\right]}{2\alpha_v^t\cos(\vartheta_i) + (\alpha_v^i+\alpha_h^i)|\cos(\vartheta_t)|} \tag{3-41f}$$

$$G_t = \frac{\exp\left[-\frac{\alpha_h^t+\alpha_v^t}{|\cos(\vartheta_t)|}\rho L\right] - \exp\left[-\frac{2\alpha_h^i}{\cos(\vartheta_i)}\rho L\right]}{(\alpha_h^t+\alpha_v^t)\cos(\vartheta_i) + 2\alpha_h^i|\cos(\vartheta_t)|} \tag{3-41g}$$

$$H_t = \frac{\exp\left[-\frac{\alpha_h^t+\alpha_v^t}{|\cos(\vartheta_t)|}\rho L\right] - \exp\left[-\frac{2\alpha_v^i}{\cos(\vartheta_i)}\rho L\right]}{(\alpha_h^t+\alpha_v^t)\cos(\vartheta_i) + 2\alpha_v^i|\cos(\vartheta_t)|} \tag{3-41h}$$

$$I_t = \frac{\exp\left[-\frac{\alpha_h^t+\alpha_v^t}{|\cos(\vartheta_t)|}\rho L\right] - \exp\left[-\frac{\alpha_h^i+\alpha_v^i}{\cos(\vartheta_i)}\rho L\right]}{(\alpha_v^t+\alpha_h^t)\cos(\vartheta_i) + (\alpha_h^i+\alpha_v^i)|\cos(\vartheta_t)|}. \tag{3-41i}$$

These expressions represent the power that appears on the transmission side of the slab after suffering one reflection inside the slab. The angle ϑ_t is measured from the normal to the slab surface on the reflection side of the slab; i.e., ϑ_t>90 degrees.

Added to this component of the transmitted power is that component of the power which suffered no reflections at all. This will only appear in the same direction as the original incident plane wave and has an effective Stokes Transmission Operator $[\mathbf{T}_e^{(0)}]$ with coefficients:

$$T_{e11}^{(0)} = \tfrac{1}{2}\left\{\exp\left[-\frac{2\alpha_h^i}{\cos(\vartheta_i)}\rho L\right] + \exp\left[-\frac{2\alpha_v^i}{\cos(\vartheta_i)}\rho L\right]\right\} \tag{3-42a}$$

$$T_{e12}^{(0)} = \tfrac{1}{2}\left\{\exp\left[-\frac{2\alpha_h^i}{\cos(\vartheta_i)}\rho L\right] - \exp\left[-\frac{2\alpha_v^i}{\cos(\vartheta_i)}\rho L\right]\right\} \tag{3-42b}$$

$$T_{e33}^{(0)} = -\exp\left[-\frac{\alpha_h^i+\alpha_v^i}{\cos(\vartheta_i)}\rho L\right] \tag{3-42c}$$

$$T_{e22}^{(0)} = T_{e11}^{(0)} \tag{3-42d}$$

$$T_{e21}^{(0)} = T_{e12}^{(0)} \tag{3-42e}$$

$$T_{e44}^{(0)} = T_{e33}^{(0)} . \tag{3-42f}$$

$$\text{All other } T_{eij}^{(0)} = 0. \tag{3-42g}$$

3.5.2.2 Electric Fields.

The effective transmission matrix is of the form

$$[\mathbf{R}_e] = \begin{bmatrix} -\exp\left(-\frac{\alpha_h^i}{\cos(\vartheta)}\rho L\right) & 0 \\ 0 & \exp\left(-\frac{\alpha_v^i}{\cos(\vartheta)}\rho L\right) \end{bmatrix} e^{i\frac{kl}{\cos(\vartheta)}} \delta(\Omega-\Omega_i) + [\mathbf{R}_e^{(1)}], \tag{3-43}$$

where

$$\delta(\Omega-\Omega_i) = \begin{cases} 1 & \text{if } \vartheta=\pi-\vartheta_i \text{ and } \varphi=\varphi_i+\pi \\ 0 & \text{if } \vartheta\neq\pi-\vartheta_i \text{ or } \varphi\neq\varphi_i+\pi . \end{cases} \tag{3-44}$$

The elements of $[\mathbf{R}_e^{(1)}]$ are:

$$R_{ehh}^{(1)} = J\left\{\frac{\exp\left(-\frac{\alpha_h^t}{|\cos(\vartheta_t)|}\rho L\right) - \exp\left(-\left[\frac{\alpha_h^i}{\cos(\vartheta_i)}\rho - ik(\cos(\vartheta_i)+|\cos(\vartheta_t)|)\right]L\right)}{\left[\frac{\alpha_h^i}{\cos(\vartheta_i)}+\frac{\alpha_h^t}{|\cos(\vartheta_t)|}\right]\rho - ik(\cos(\vartheta_i)+|\cos(\vartheta_t)|)}\right\}$$

$$\times \sum_{i=1}^{N} f_i\,(S_{h'h})_i \tag{3-45a}$$

$$R_{ehv}^{(1)} = J\left\{\frac{\exp\left(-\frac{\alpha_h^t}{|\cos(\vartheta_t)|}\rho L\right) - \exp\left(-\left[\frac{\alpha_v^i}{\cos(\vartheta_i)}\rho - ik(\cos(\vartheta_i)+|\cos(\vartheta_t)|)\right]L\right)}{\left[\frac{\alpha_h^t}{|\cos(\vartheta_t)|}+\frac{\alpha_v^i}{\cos(\vartheta_i)}\right]\rho - ik(\cos(\vartheta_i)+|\cos(\vartheta_t)|)}\right\}$$

$$\times \sum_{i=1}^{N} f_i \, (S_{h'v})_i \tag{3-45b}$$

$$R_{evh}^{(1)} = J \left\{ \frac{\exp\left[-\frac{\alpha_v^t}{|\cos(\vartheta_t)|} \rho L \right] - \exp\left[-\left[\frac{\alpha_h^i}{\cos(\vartheta_i)} \rho - ik(\cos(\vartheta_i) + |\cos(\vartheta_t)|) \right] L \right]}{\left[\frac{\alpha_v^t}{|\cos(\vartheta_t)|} + \frac{\alpha_h^i}{\cos(\vartheta_i)} \right] \rho - ik(\cos(\vartheta_i) + |\cos(\vartheta_t)|)} \right\}$$

$$\times \sum_{i=1}^{N} f_i \, (S_{v'h})_i \tag{3-45c}$$

$$R_{evv}^{(1)} = J \left\{ \frac{\exp\left[-\frac{\alpha_v^t}{|\cos(\vartheta_t)|} \rho L \right] - \exp\left[-\left[\frac{\alpha_v^i}{\cos(\vartheta_i)} \rho - ik(\cos(\vartheta_i) + |\cos(\vartheta_t)|) \right] L \right]}{\left[\frac{\alpha_v^t}{|\cos(\vartheta_t)|} + \frac{\alpha_v^i}{\cos(\vartheta_i)} \right] \rho - ik(\cos(\vartheta_i) + |\cos(\vartheta_t)|)} \right\}$$

$$\times \sum_{i=1}^{N} f_i \, (S_{v'v})_i \,. \tag{3-45d}$$

J is still given by (3-40), but with ϑ_s and φ_s replaced by ϑ_t and φ_t, respectively.

A closer look at the results of the previous sections reveal a few general features of these effective operators. In the first place, it is noted that when L is made zero, all the first-order operators vanish. At the same time the total effective transmission operators describe an undisturbed wave propagating through space. This, of course, is to be expected. A slab of thickness zero simply means no scatterers present. Hence, no scattering is expected and the incident wave propagates undisturbed through space. Secondly, when ρL approaches infinity, all transmission operators vanish and all reflection operators approach limiting values. This again corresponds to the physical picture. If the slab is very thick (i.e, ρL is very large), any wave propagating

through the medium is attenuated strongly. Since the energy is only incident from one side of the slab (say the top), very little of the incident energy reaches the bottom layers of the slab. Similarly, energy scattered in the forward direction from the top layers will also be absorbed by other scatterers before it can reach the bottom layers. The result is that no energy is transmitted through a thick slab. This also explains why the reflected energy reaches a limiting value as the thickness of the slab is increased. Only energy scattered from the top layers actually manages to reach the outside of the slab. Increasing the thickness of the slab further has no effect on the amount of energy reflected by the slab, since the energy reflected off the bottom layers is absorped before it reaches either side of the slab.

3.5.3 Scattering Cross Sections.

In any basis, the Scattering Cross Section, or Radar Cross Section (RCS) of a scatterer is defined as [14]:

$$\sigma_{ij} = \lim_{r\to\infty} (4\pi r^2) \left[\frac{P_{rec\ ij}}{P_{transmitted}} \right] . \tag{3-47}$$

Here, the subscript ij means that polarization j is transmitted and polarization i is used to receive the scattered waves. It is easily seen from (2-18) and (3-2) that

$$\frac{P_{rec\ ij}}{P_{transmitted}} = \frac{1}{2(kr)^2} \mathbf{S}_i^{rad.} [\mathbf{M}] \mathbf{S}_j^{rad} . \tag{3-48}$$

Using (3-48) in (3-47), one finds that

$$\sigma_{ij} = \frac{2\pi}{k^2} \mathbf{S}_i^{rad.} [\mathbf{M}] \mathbf{S}_j^{rad} . \tag{3-49}$$

In particular, when the horizontal-vertical basis used previously is used, one finds, using the results of section 3.5.1, that

$$\sigma_{hh} = \frac{2\pi}{k^2}\cos(\vartheta_i)\cos^2(\vartheta_s)\,A\sum_{i=1}^{N} f_i\,(|S_{h'h}|^2)_i \qquad (3\text{-}50a)$$

$$\sigma_{vh} = \frac{2\pi}{k^2}\cos(\vartheta_i)\cos^2(\vartheta_s)\,B\sum_{i=1}^{N} f_i\,(|S_{v'h}|^2)_i \qquad (3\text{-}50b)$$

$$\sigma_{hv} = \frac{2\pi}{k^2}\cos(\vartheta_i)\cos^2(\vartheta_s)\,C\sum_{i=1}^{N} f_i\,(|S_{h'v}|^2)_i \qquad (3\text{-}50c)$$

$$\sigma_{vv} = \frac{2\pi}{k^2}\cos(\vartheta_i)\cos^2(\vartheta_s)\,D\sum_{i=1}^{N} f_i\,(|S_{v'v}|^2)_i\,. \qquad (3\text{-}50d)$$

In the backscatter case where reciprocity of the propagation path holds, it follows from (3-50) and (3-36) that

$$\sigma_{hv} = \sigma_{vh}\,. \qquad (3\text{-}51)$$

At this stage a few words about the units of these various parameters are in order. According to the definition of the bistatic scattering matrix given in Section 3.2, the elements of the bistatic scattering matrix are dimensionless. In Section 3.4; however, the effective operators *per unit illuminated area* are calculated. This means that in the present definition the scattering cross sections are dimensionless quantities: they are the scattering cross sections per unit illuminated area.

3.6 Conclusions.

In this chapter the effective scattering operators for a slab of scatterers were defined. General expressions in terms of the elements of the bistatic scattering matrices were derived for the case where only one reflection inside the slab is considered. In the next chapter these expressions will be used to derive some models to describe scattering from vegetation layers.

CHAPTER 4

MODELS TO DESCRIBE BACKSCATTER FROM VEGETATION LAYERS.

4.1 Introduction

In this chapter, some simple models to describe backscatter from vegetation layers will be derived. These models will include only single reflections. In the first part of this chapter, the reflection operators for slabs filled with some simple scatterers will be calculated. In the last part these models will then be combined to form models that describe backscatter from different types of vegetation.

4.2 Effective Operators for Slabs Filled with Simple Scatterers.

In this section, the single reflection effective operators for some slabs filled with simple scatterers will be derived.

4.2.1 Slab of Isotropic Scatterers.

An isotropic scatterer does not change the polarization of the incident wave and scatters equally strong in all directions. Thus, the scattering matrix of an isotropic scatterer is of the form:

$$[\mathbf{S}(\vartheta_i,\varphi_i,\vartheta_s,\varphi_s)] = \left[\frac{\tilde{\omega}}{4\pi}\right]^{1/2}\begin{bmatrix}1 & 0\\ 0 & 1\end{bmatrix}. \tag{4-1}$$

The constant $\tilde{\omega}$ is the *single scattering albedo* [6] of the scatterer, and is a measure of loss inside the scatterer. When $\tilde{\omega} = 1.$, all the energy absorbed by the scatterer is reradiated. This is the case of *perfect scattering* [6]. The effective area of an isotropic antenna with unit gain, is [1]:

$$A(\vartheta,\varphi) = \frac{\lambda^2}{4\pi}. \tag{4-2}$$

To find the attenuation constants for this type of scatterer, it is defined

that:

$$A(\vartheta,\varphi) \times \text{Incident power density}$$

$$\equiv \left[1. - e^{-2\alpha}\right] \times \text{Incident power.} \tag{4-3}$$

Assuming α for each scatterer to be small, it follows from (4-20) that, to a good approximation, *per unit area normal to the incident direction* :

$$\alpha_x(\vartheta,\varphi) = \tfrac{1}{2}A_x(\vartheta,\varphi) \qquad x = h,v\,. \tag{4-4}$$

Here, A_h must be taken as the effective area that will be "seen" by a horizontally polarized wave approaching the scatterer from a direction ϑ,φ . For the present case, it follows from (4-4) that:

$$\alpha_v^i = \alpha_h^i = \alpha_v^s = \alpha_h^s = \frac{\lambda^2}{8\pi}. \tag{4-5}$$

If one defines:

$$\mu_x = \cos(\vartheta_x) \tag{4-6}$$

and the results of Section 3.5.2 are used, it is easily shown that the effective reflection operators, per unit illuminated area, are:

$$[\mathbf{M}_e^{(1)}] = \left[\frac{\tilde{\omega}}{\lambda^2}\right]\left[\frac{\mu_i\,\mu_s^2}{\mu_i+\mu_s}\right]\left\{1-\exp\left[-\frac{\rho L\lambda^2}{4\pi}\left(\frac{1}{\mu_i}+\frac{1}{\mu_s}\right)\right]\right\}\begin{bmatrix}1&0&0&0\\0&1&0&0\\0&0&1&0\\0&0&0&-1\end{bmatrix} \tag{4-7}$$

and

$$[\mathbf{S}_e^{(1)}] = J\,\frac{\sqrt{4\pi\tilde{\omega}}}{2\lambda^2}\left\{\frac{1. - \exp\left[-\left\{\left[\frac{\lambda^2\rho}{8\pi}\left(\frac{1}{\mu_i}+\frac{1}{\mu_s}\right)-ik(\mu_i+\mu_s)\right\}L\right]\right]}{\left(\frac{1}{\mu_i}+\frac{1}{\mu_s}\right)\rho - ik(\mu_i+\mu_s)}\right\}\begin{bmatrix}1&0\\0&1\end{bmatrix}. \tag{4-8}$$

The backscatter coefficients per unit illuminated area are:

$$\sigma_{hh} = \sigma_{vv} = 2\pi\tilde{\omega}\left[\frac{\mu_i}{k\lambda}\right]^2\left\{1 - \exp\left[-\frac{\rho\lambda^2 L}{2\pi}\right]\right\} \tag{4-9}$$

and

$$\sigma_{vh} = \sigma_{hv} = 0.$$

Isotropic scatterers, like isotropic antennas, cannot, of course, exist in practice [15],[16],[17]. This model, however, allows one to compare results with other formulations. Chandrasekhar [6] gives the result for single-scattering intensity for a slab of isotropic scatterers as:

$$I = \frac{\tilde{\omega}}{4} F\left[\frac{\mu_i}{\mu_s+\mu_i}\right]\left\{1. - \exp\left[-\tau\left[\frac{1}{\mu_i}+\frac{1}{\mu_s}\right]\right]\right\}. \tag{4-10}$$

Here, F is the net flux of the incident radiation which, for a plane wave, is directly proportional to the incident intensity. Apart from a different constant, which arises because of the normalization introduced by Chandrasekhar, the only difference between (4-7) and (4-10) is the factor of μ_s^2 in (4-7), which is absent in (4-10). This difference is easily explained by the fact that in the present case a fixed illuminated area is considered. As the observation angle is increased, the "effective" illuminated area, the illuminated area projected normal to the observation direction, reduces according to a cosine law. In the case treated by Chandrasekhar, the observation area is fixed. As the observation angle is increased, the effective ground area to illuminate the complete observation area must increase according to an inverse cosine law. Thus, to compare results, one has to divide (4-10) by μ_s^2 , which clearly gives a result similar to (4-7).

4.2.2 Slab of Dipoles of Arbitrary but Similar Orientation.

Although this case will seldom be encountered in radar imaging, it is the first step towards deriving other, more realistic models. The arbitrarily oriented dipole, shown in Figure 4.1, is assumed to have an electric susceptibility χ_e. Note that χ_e may be a complex quantity. As is shown in Appendix B, the results for this case are:

$$\alpha_v^x = \frac{3\lambda^2}{16\pi} Z_x^2 \tag{4-11a}$$

$$\alpha_h^x = \frac{3\lambda^2}{16\pi} W_x^2, \tag{4-11b}$$

where

$$Z_x = \sin(\vartheta_x)\cos(\vartheta_d) - \cos(\varphi_d - \varphi_x)\sin(\vartheta_d)\cos(\vartheta_x) \tag{4-12a}$$

$$W_x = \sin(\vartheta_d)\sin(\varphi_d - \varphi_x), \tag{4-12b}$$

where x may be either i or s. Also:

$$S_{h'h} = p\, W_i\, W_s \tag{4-13a}$$

$$S_{h'v} = p\, W_s\, Z_i \tag{4-13b}$$

$$S_{v'h} = p\, W_i\, Z_s \tag{4-13c}$$

$$S_{v'v} = p\, Z_i\, Z_s\,. \tag{4-13d}$$

Using the results in Chapter 3 one can now calculate the effective operator for a slab of dipoles with arbitrary but similar orientations.

The constant p in (4-12) is a dimensionless quantity. This is easily shown when the results in Appendix B are considered. According to these,

$$p = \frac{k^3 \chi_e}{4\pi}.$$

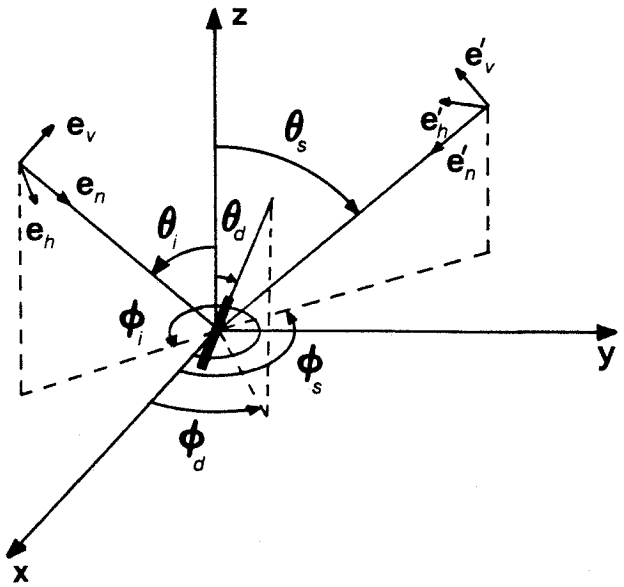

Figure 4.1. Dipole of arbitrary orientation.

(4-14)

But Schelkunoff and Friis [21] give an approximation for χ_e for a thin conducting rod of length 2l and radius a as:

$$\chi_e = \frac{4\pi l^3}{3\log(\frac{2l}{a})}. \tag{4-15}$$

Using this in (4-14) one finds:

$$p = \left[\frac{2\pi l}{\lambda}\right]^3 \frac{1}{3\log(\frac{2l}{a})}, \tag{4-16}$$

which is indeed a dimensionless quantity.

4.2.3 Dipoles Oriented Randomly Around a Fixed Angle.

In this model, it will be assumed that the dipoles are oriented around a fixed angle, ϑ_1 , according to the probability density function:

$$p_1(\vartheta,\varphi) = \frac{3\cos^2(\vartheta-\vartheta_1)}{4\pi[1+\sin^2(\vartheta)]} \qquad 0 \le \varphi \le 2\pi \ ; \ 0 \le \vartheta \le \pi \ . \tag{4-17}$$

This probability density function with $\vartheta = 0$ has been used by Peake in a model (discussed in [23]), which describes backscatter from an infinitely thick vegetation layer.

To find the effective scattering operators for this case, the ensemble average of the previous model must be calculated using (4-17). Each element of each operator must be averaged separately. The results are:

$$\langle \alpha_v^x \rangle = \frac{3\lambda^2}{80\pi}\left\{\frac{1+\sin^2(\vartheta_1)+2\sin^2(\vartheta_x)\cos^2(\vartheta_1)+2\sin^2(\vartheta_1)\cos^2(\vartheta_x)}{1+\sin^2(\vartheta_1)}\right\} \tag{4-18a}$$

$$\langle \alpha_h^x \rangle = \frac{3\lambda^2}{80\pi}\left\{\frac{1+3\sin^2(\vartheta_1)}{1+\sin^2(\vartheta_1)}\right\} . \tag{4-18b}$$

Here, x may be either i or s. The ensemble average of the elements of the scattering matrix are:

$$\langle S_{h'h} \rangle = \frac{p}{5}\cos(\varphi_s-\varphi_i)\left\{\frac{1+3\sin^2(\vartheta_1)}{1+\sin^2(\vartheta_1)}\right\} \tag{4-19a}$$

$$\langle S_{h'v} \rangle = \frac{p}{5}\sin(\varphi_i-\varphi_s)\cos(\vartheta_i)\left\{\frac{1+3\sin^2(\vartheta_1)}{1+\sin^2(\vartheta_1)}\right\} \tag{4-19b}$$

$$\langle S_{v'h} \rangle = \frac{p}{5}\sin(\varphi_s-\varphi_i)\cos(\vartheta_s)\left\{\frac{1+3\sin^2(\vartheta_1)}{1+\sin^2(\vartheta_1)}\right\} \tag{4-19c}$$

$$\langle S_{v'v} \rangle = \frac{p}{5}\cos(\varphi_s-\varphi_i)\left\{\frac{\sin(\vartheta_i)\sin(\vartheta_s)[2+\cos^2(\vartheta_1)]}{1+\sin^2(\vartheta_1)}\right.$$

$$\left. + \frac{\cos(\vartheta_i)\cos(\vartheta_s)[1+3\sin^2(\vartheta_1)]}{1+\sin^2(\vartheta_1)}\right\}. \qquad (4\text{-}19d)$$

The other quantities needed to calculate the effective scattering operator for intensities are:

$$\langle |S_{h'h}|^2 \rangle = \frac{|p|^2}{35}[1+2\cos^2(\varphi_s-\varphi_i)]\left\{\frac{1+5\sin^2(\vartheta_1)}{1+\sin^2(\vartheta_1)}\right\} \qquad (4\text{-}20a)$$

$$\langle |S_{h'v}|^2 \rangle = \frac{|p|^2}{35}\left\{\frac{\cos^2(\vartheta_i)[1+5\sin^2(\vartheta_1)][1+2\sin^2(\varphi_s-\varphi_i)]}{1+\sin^2(\vartheta_1)}\right.$$

$$\left. + \frac{\sin^2(\vartheta_i)[3+\sin^2(\vartheta_1)]}{1+\sin^2(\vartheta_1)}\right\} \qquad (4\text{-}20b)$$

$$\langle |S_{v'h}|^2 \rangle = \frac{|p|^2}{35}\left\{\frac{\cos^2(\vartheta_s)[1+5\sin^2(\vartheta_1)][1+2\sin^2(\varphi_s-\varphi_i)]}{1+\sin^2(\vartheta_1)}\right.$$

$$\left. + \frac{\sin^2(\vartheta_s)[3+\sin^2(\vartheta_1)]}{1+\sin^2(\vartheta_1)}\right\} \qquad (4\text{-}20c)$$

$$\langle |S_{v'v}|^2 \rangle = \frac{|p|^2}{35}\left\{\frac{[1+5\sin^2(\vartheta_1)][1+2\cos^2(\varphi_s-\varphi_i)]\cos^2(\vartheta_i)\cos^2(\vartheta_s)}{1+\sin^2(\vartheta_1)}\right.$$

$$+ \frac{3\sin^2(\vartheta_i)\sin^2(\vartheta_s)[2+3\cos^2(\vartheta_1)]}{1+\sin^2(\vartheta_1)} + [3+\sin^2(\vartheta_1)]$$

$$\times \frac{[\cos^2(\vartheta_i)\sin^2(\vartheta_s)+\sin^2(\vartheta_i)\cos^2(\vartheta_s)+\cos(\varphi_s-\varphi_i)\sin(2\vartheta_i)\sin(2\vartheta_s)]}{1+\sin^2(\vartheta_1)}\Bigg\} \quad (4\text{-}20d)$$

$$\langle S^*_{h'h}S_{h'v}\rangle = \frac{2|p|^2}{35}\cos(\vartheta_i)\cos(\varphi_s-\varphi_i)\sin(\varphi_i-\varphi_s)\left\{\frac{1+5\sin^2(\vartheta_1)}{1+\sin^2(\vartheta_1)}\right\} \quad (4\text{-}20e)$$

$$\langle S^*_{h'h}S_{v'h}\rangle = \frac{2|p|^2}{35}\cos(\vartheta_s)\cos(\varphi_s-\varphi_i)\sin(\varphi_s-\varphi_i)\left\{\frac{1+5\sin^2(\vartheta_1)}{1+\sin^2(\vartheta_1)}\right\} \quad (4\text{-}20f)$$

$$\langle S_{v'v}S^*_{h'v}\rangle = \frac{2|p|^2}{35}\sin(\varphi_s-\varphi_i)\cos(\vartheta_i)\left\{\frac{\sin(\vartheta_i)\sin(\vartheta_s)[3+\sin^2(\vartheta_1)]}{1+\sin^2(\vartheta_1)}\right.$$

$$\left. + \frac{\cos(\varphi_s-\varphi_i)\cos(\vartheta_i)\cos(\vartheta_s)[1+5\sin^2(\vartheta_1)]}{1+\sin^2(\vartheta_1)}\right\} \quad (4\text{-}20g)$$

$$\langle S_{v'v}S^*_{v'h}\rangle = \frac{2|p|^2}{35}\sin(\varphi_i-\varphi_s)\cos(\vartheta_s)\left\{\frac{\sin(\vartheta_i)\sin(\vartheta_s)[3+\sin^2(\vartheta_1)]}{1+\sin^2(\vartheta_1)}\right.$$

$$\left. + \frac{\cos(\varphi_s-\varphi_i)\cos(\vartheta_i)\cos(\vartheta_s)[1+5\sin^2(\vartheta_1)]}{1+\sin^2(\vartheta_1)}\right\} \quad (4\text{-}20h)$$

$$\langle S^*_{h'h}S_{v'v}\rangle = \frac{|p|^2}{35}\left\{\frac{\cos(\varphi_s-\varphi_i)\sin(\vartheta_i)\sin(\vartheta_s)[3+\sin^2(\vartheta_1)]}{1+\sin^2(\vartheta_1)}\right.$$

$$+ \frac{\cos(2\varphi_s - 2\varphi_i)\cos(\vartheta_i)\cos(\vartheta_s)[1+5\sin^2(\vartheta_1)]}{1+\sin^2(\vartheta_1)} \Bigg\} \qquad (4\text{-}20i)$$

$$\langle S_{v'h} S^*_{h'v} \rangle = \langle S^*_{h'h} S_{v'v} \rangle . \qquad (4\text{-}20j)$$

Using these expressions in the expressions of the previous chapter allows one to calculate the effective operator for incoherently reflected power.

4.2.4 Dipoles Oriented Spherically Randomly.

The probability density function which describes the orientation of the dipoles for this model is:

$$p_2(\vartheta,\varphi) = \frac{1}{4\pi} \qquad 0 \le \varphi \le 2\pi \; ; \; 0 \le \vartheta \le \pi . \qquad (4\text{-}21)$$

Using the results of Section 4.2.2 and taking ensemble averages, gives:

$$\langle \alpha^i_h \rangle = \langle \alpha^s_h \rangle = \langle \alpha^i_v \rangle = \langle \alpha^s_v \rangle = \frac{\lambda^2}{16\pi} \qquad (4\text{-}22)$$

and

$$\langle S_{h'h} \rangle = \frac{p}{3} \cos(\varphi_s - \varphi_i) \qquad (4\text{-}23a)$$

$$\langle S_{h'v} \rangle = \frac{p}{3} \sin(\varphi_i - \varphi_s) \cos(\vartheta_i) \qquad (4\text{-}23b)$$

$$\langle S_{v'h} \rangle = \frac{p}{3} \sin(\varphi_s - \varphi_i) \cos(\vartheta_s) \qquad (4\text{-}23c)$$

$$\langle S_{v'v} \rangle = \frac{p}{3} [\, \cos(\vartheta_s)\cos(\vartheta_i)\cos(\varphi_s - \varphi_i) + \sin(\vartheta_i)\sin(\vartheta_s) \,] . \qquad (4\text{-}23d)$$

Also,

$$\langle |S_{h'h}|^2 \rangle = \frac{|p|^2}{15} [1+2\cos^2(\varphi_s - \varphi_i)] \qquad (4\text{-}24a)$$

$$\langle |S_{h'v}|^2 \rangle = \frac{|p|^2}{15} [1+2\cos^2(\vartheta_i)\sin^2(\varphi_s - \varphi_i)] \qquad (4\text{-}24b)$$

$$\langle |S_{v'h}|^2 \rangle = \frac{|p|^2}{15}[1+2\cos^2(\vartheta_s)\sin^2(\varphi_s-\varphi_i)] \quad (4\text{-}24c)$$

$$\langle |S_{v'v}|^2 \rangle = \frac{|p|^2}{15}[1+2\,Z_{is}^2] \quad (4\text{-}24d)$$

$$\langle S^*_{h'h}S_{h'v} \rangle = \frac{2|p|^2}{15}\sin(\varphi_s-\varphi_i)\cos(\varphi_s-\varphi_i)\cos(\vartheta_i) \quad (4\text{-}24e)$$

$$\langle S^*_{h'h}S_{v'h} \rangle = \frac{2|p|^2}{15}\sin(\varphi_i-\varphi_s)\cos(\varphi_s-\varphi_i)\cos(\vartheta_s) \quad (4\text{-}24f)$$

$$\langle S_{v'v}S^*_{h'v} \rangle = \frac{2|p|^2}{15}\sin(\varphi_s-\varphi_i)\cos(\vartheta_i)\,Z_{is} \quad (4\text{-}24g)$$

$$\langle S_{v'v}S^*_{v'h} \rangle = \frac{2|p|^2}{15}\sin(\varphi_i-\varphi_s)\cos(\vartheta_s)\,Z_{is} \quad (4\text{-}24h)$$

$$\langle S_{v'v}S^*_{h'h} \rangle = \frac{|p|^2}{15}[\cos(\vartheta_i)\cos(\vartheta_s)\cos(2\varphi_s-2\varphi_i) + \sin(\vartheta_i)\sin(\vartheta_s)\cos(\varphi_s-\varphi_i)] \quad (4\text{-}24i)$$

$$\langle S_{v'h}S^*_{h'v} \rangle = \langle S_{v'v}S^*_{h'h} \rangle\,, \quad (4\text{-}24j)$$

where

$$Z_{is} = \cos(\vartheta_s)\cos(\vartheta_i)\cos(\varphi_s-\varphi_i)+\sin(\vartheta_i)\sin(\vartheta_s)\,. \quad (4\text{-}25)$$

4.2.5 Slab Filled with Small Dielectric Spheres.

When a plane wave is incident upon a small dielectric sphere, a dipole is created [7],[14],[21]. Comparing the first term in the Mie series solution for a wave scattered off a dielectric sphere [7],[14] with the results of Appendix B and section 4.2.2, it is clear that the constant p in this case becomes:

$$p_2 = \left[\frac{\varepsilon_r - 1}{\varepsilon_r + 2}\right] (ka)^3 , \tag{4-26}$$

where ε_r is the (complex) relative dielectric constant of the sphere and a is the radius of the sphere. In this case, the dipole created by the incident electric field is parallel to the incident electric field. Thus, using the results of Appendix B, one finds that:

$$\alpha_h^i = \alpha_h^s = \alpha_v^i = \alpha_v^s = \frac{3\lambda^2}{16\pi} \tag{4-27}$$

and

$$S_{h'h} = \left[\frac{\varepsilon_r - 1}{\varepsilon_r + 2}\right] (ka)^3 \cos(\varphi_s - \varphi_i) \tag{4-28a}$$

$$S_{h'v} = \left[\frac{\varepsilon_r - 1}{\varepsilon_r + 2}\right] (ka)^3 \cos(\vartheta_i) \sin(\varphi_i - \varphi_s) \tag{4-28b}$$

$$S_{v'h} = \left[\frac{\varepsilon_r - 1}{\varepsilon_r + 2}\right] (ka)^3 \cos(\vartheta_s) \sin(\varphi_s - \varphi_i) \tag{4-28c}$$

$$S_{v'v} = \left[\frac{\varepsilon_r - 1}{\varepsilon_r + 2}\right] (ka)^3 [\sin(\vartheta_i)\sin(\vartheta_s) + \cos(\varphi_s - \varphi_i)\cos(\vartheta_s)\cos(\vartheta_i)]. \tag{4-28d}$$

4.2.6 Slab Containing Chiral Objects.

To model a chiral medium, a slab filled with the small chiral objects shown in Figure 4.2 will be considered. The objects are assumed to be spherically randomly oriented; i.e., the probability density function describing the orientations of the objects is given by (4-21).

The results for this case are derived in detail in Appendix C. Here, the results of Appendix C will be compared with results found elsewhere in the literature [18]. To do this, a wave normally incident upon a slab of chiral

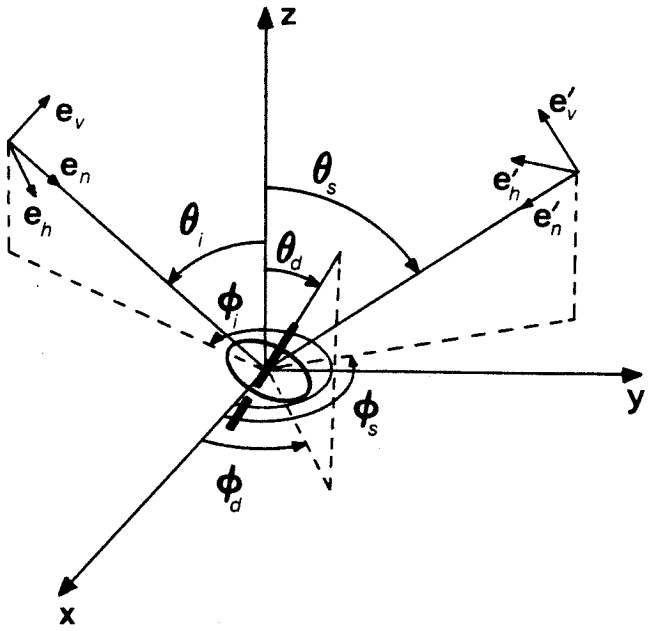

Figure 4.2. Chiral object.

objects will be assumed. The incident wave is then of the form:

$$\mathbf{E}^{inc} = (a_h \mathbf{e}_h + a_v e^{i\delta} \mathbf{e}_v)\, e^{i(kz+\omega t)} . \tag{4-29}$$

From the results of Appendix C (C-20) it follows that the reflection matrix is of the form

$$[\mathbf{S}_e^{(1)}] = c_1 \begin{bmatrix} \chi_e+\chi_m & \pm(\chi_{em}-\chi_{me}) \\ \pm i(\chi_{me}-\chi_{em}) & \chi_e+\chi_m \end{bmatrix} . \tag{4-30}$$

The constant c_1 is not important for the comparison of the results. The reflected electric field is thus:

$$\mathbf{E}^{ref} = c_1 \{ [(\chi_e+\chi_m)a_h \pm i(\chi_{em}-\chi_{me})a_v e^{i\delta}]\mathbf{e}_h$$

$$+ \left[\pm i(\chi_{me}-\chi_{em})a_h+(\chi_e+\chi_m)a_v e^{i\delta}]\mathbf{e}_v\right\} e^{-i(kz-\omega t)} .$$

For the chiral objects shown, $\chi_{em} = \chi_{me} = \chi_c$ [18]. In that case, the reflected field becomes:

$$\mathbf{E}^{ref} = c_1 (\chi_e+\chi_m) [a_h \mathbf{e}_h + a_v e^{i\delta} \mathbf{e}_v] e^{-i(kz-\omega t)} . \qquad (4\text{-}31)$$

This result is in accord with the results reported in [18]. The same result as that in [18] is also found when the transmitted wave is considered.

It must be stressed, however, that this result takes only single reflections in the slab into account. It is possible that the chiral medium may in fact alter the state of polarization of the incident wave upon reflection when higher-order reflections are considered. This is indeed the case when the incoherent component of the backscattered energy is considered. Using the results in (C-21) of Appendix C, it is easily shown that:

If the slab of chiral objects is illuminated by a linearly polarized wave, the resulting incoherently reflected wave is *elliptically* polarized. The orientation angle of this ellipse is the same as that of the incident linear polarization and the ellipse "fatness" is directly proportional to χ_c. This means that if the medium was not chiral, i.e., $\chi_c = 0$, the reflected wave would also be linearly polarized. The handedness of the elliptical polarization is the same as that of the chirality of the medium.

Now consider the case of a general elliptically polarized incident wave. The incoherently reflected wave will also be elliptically polarized, with the orientation angle of the ellipse the same as that of the ellipse of the incident wave. If the incident wave is polarized with the same handedness as the chirality of the medium, the ellipse of the reflected wave will be slightly "fatter" than that of the

incident wave. If the incident wave polarization and the chirality of the medium are of opposite handedness, the ellipse of the reflected wave will be slightly "thinner" than the ellipse of the incident wave.

Unfortunately, there are no other works currently available to compare this interesting result with.

4.3 Some Simple Models to Describe Backscatter from Vegetation Layers.

In this section, some of the models of the previous sections will be combined to describe backscatter from a few selected types of vegetation.

4.3.1 Grasslands.

4.3.1.1 Grass Only. (First Grasslands Model)

The grass-like vegetation is modelled as vertical dipoles oriented randomly around the vertical direction. In this and all other models, the ground surface will be assumed to be a slightly rough surface which scatters according to the Bragg relations [25] and with a relative dielectric constant of 3. The dipoles are assumed to have a χ_e given by (4-14) and it is assumed that $\lambda/l = l/a = 10$.

Figure 4.3. Model for grass-like vegetation layers.

Figure 4.4 shows the backscatter coefficients as a function of incidence angle for this model without the presence of a ground surface. From this it is seen that the hh and vv coefficients approach the same value for incidence

angles near normal incidence. This is, of course, to be expected since at normal incidence there is no distinction between the vertically and the horizontally polarized electric fields. Also, it is seen that for angles of incidence away from the normal, the hh coefficient is always smaller than the vv component. This is also to be expected, since the layer consists of dipoles mostly vertically oriented.

Figure 4.5 shows the backscatter coefficients as a function of incidence angle for this model with the ground surface present. This shows that for incidence angles less than 50 degrees there is an appreciable degree of interaction between the vegetation layer and waves reflected by the ground surface. Since the vegetation is mostly vertically oriented, the vv component of backscattered power from the ground surface is attenuated more than the hh component. In this area, the actual received backscattered power is predominantly due to the ground surface. For incidence angles greater than 50 degrees, the vegetation layer appears thick enough to attenuate power received from the ground surface to the extent that the received power is mainly due to the vegetation layer, and the behaviour is similar to that in Figure 4.4.

Figure 4.6 shows how the backscatter coefficients change when the layer thickness is increased. The vv component of the power scattered by the ground surface is attenuated much more than the hh component as expected. All the coefficients finally reach a limiting value as discussed in Section 3.5.2.2.

Figures 4.7 and 4.8 show the angle between the two minimum polarizations (analogous to the Huynen fork angle) and the coherency factor for this model as the layer thickness is increased. For the ground surface alone, the maximum polarization is vertical polarization. As the layer thickness increases, the vertical component of the power reflected from the ground surface is attenuated more than the hh component. When the point is reached at which

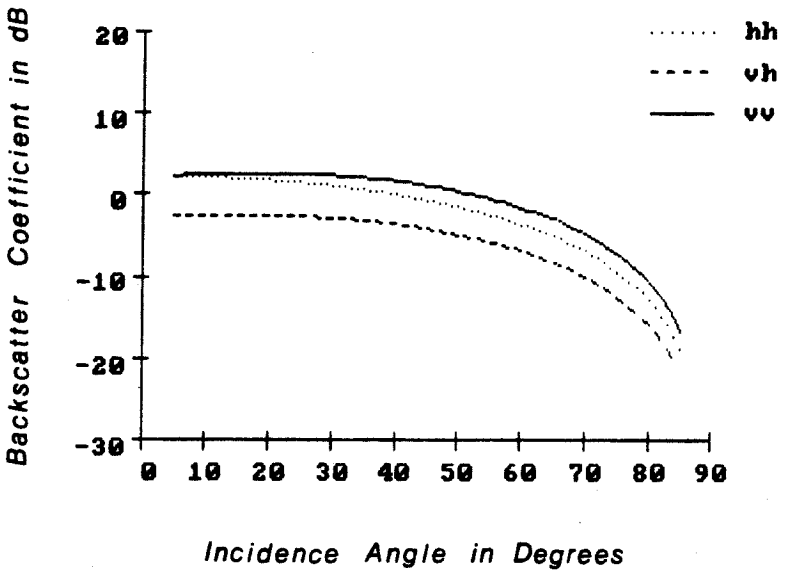

Figure 4.4. Backscatter coefficients as a function of incidence angle for the first grasslands model suspended in air. ρL = 1500.

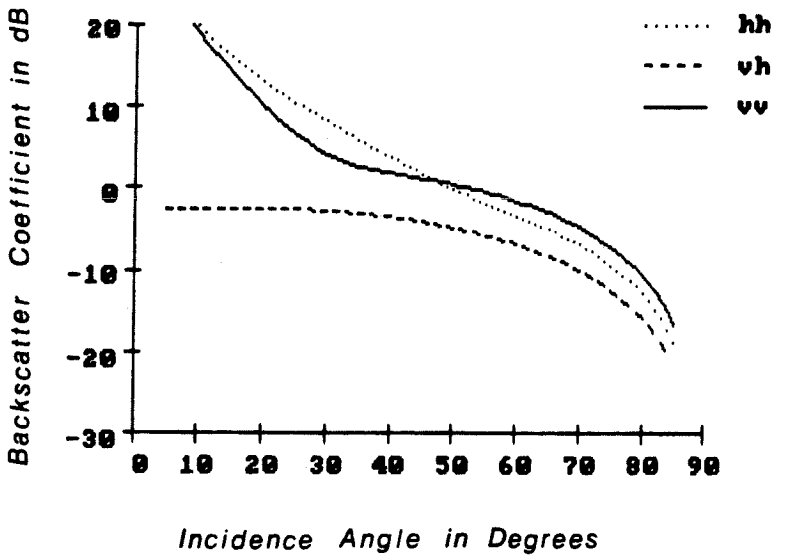

Figure 4.5. Backscatter coefficients as a function of incidence angle for the first grasslands model with a ground surface present. ρL = 1500.

received power is divided equally between the vertical and horizontal components, the "fork" has opened completely. If the layer thickness is

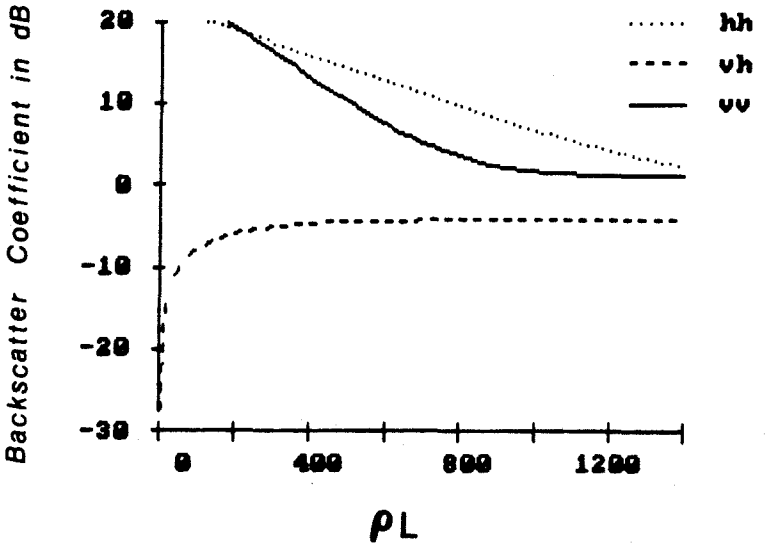

Figure 4.6. Backscatter coefficients as a function of layer thickness for the first grasslands model with a ground surface present. Incidence angle = 45 degrees.

increased beyond this point, the horizontal component of the received power becomes larger than the vertical component, and horizontal polarization becomes the maximum polarization. This situation is shown in the polarization spectrum of Figure 4.9. Here, power is still received mainly from the ground surface. As the layer thickness is increased, the difference between the vertical and the horizontal components of the received power increases to a maximum (Figure 4.6). At this point, the "fork" angle is a minimum (Figure 4.7). If the layer thickness is further increased, the power in the vertical component of the received power starts to increase relative to the power in the horizontal component. This happens because the power in the vertical component comes mainly from the vegetation layer, which increases as the layer thickness is increased. At this stage, the power in the horizontal component is still mainly due to the ground surface, and decreases as the layer thickness is increased. The result of this is that the "fork" starts to open up again, and has opened

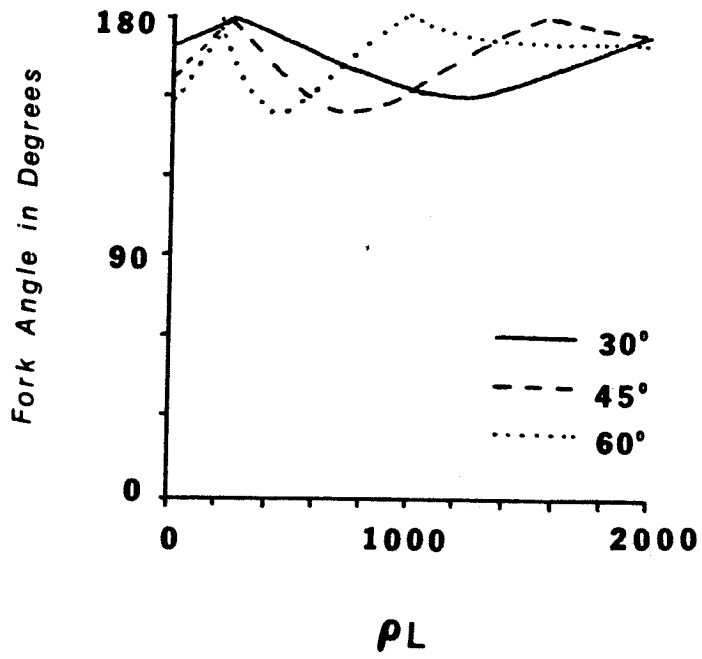

Figure 4.7. Angle between the two minimum polarization vectors as a function of layer thickness at various incidence angles for the first grasslands model.

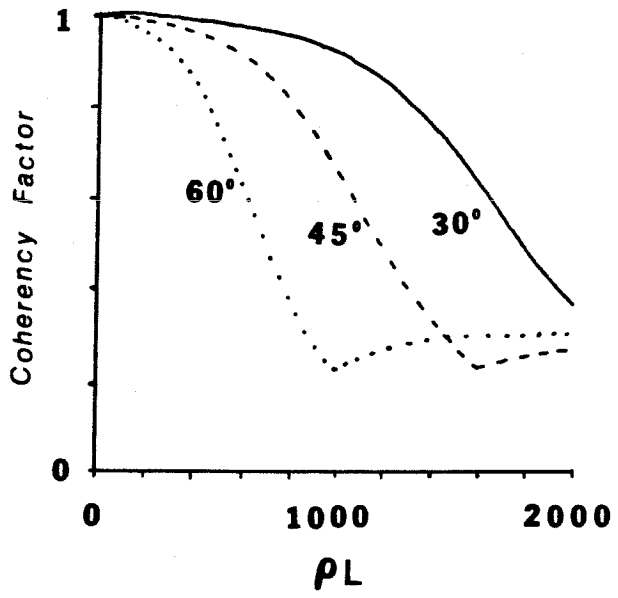

Figure 4.8. Coherency factor as a function of layer thickness at various incidence angles for the first grasslands model.

completely when the received power is divided equally between the horizontal and vertical components.

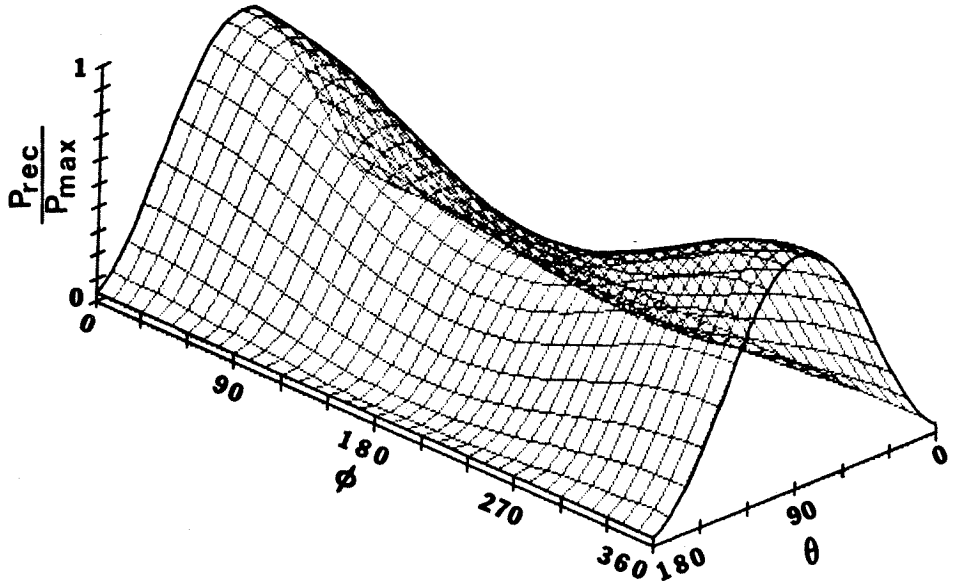

Figure 4.9. Polarization spectrum for the first grasslands model when power is received mainly from the ground surface. Incidence angle = 45 degrees and ρL = 400.

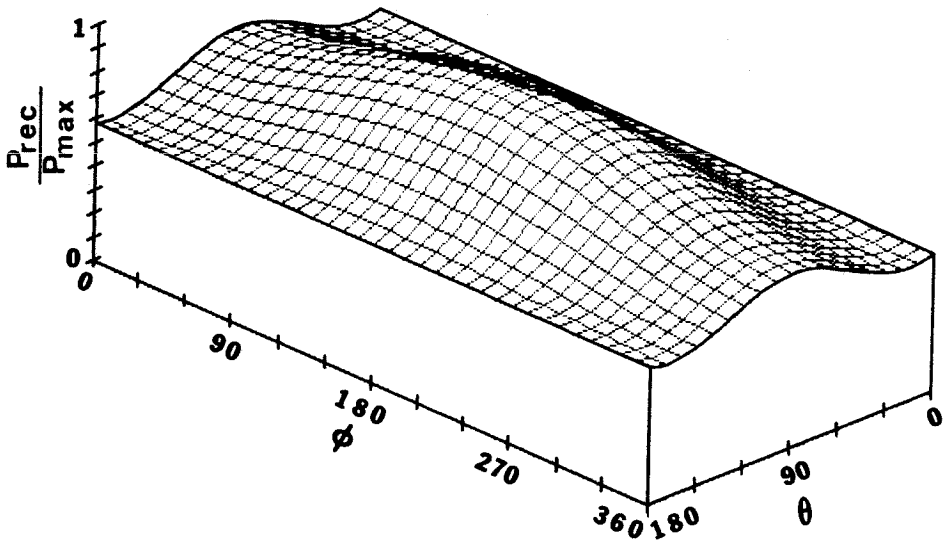

Figure 4.10. Polarization spectrum for the first grasslands model when power is received mainly from the vegetation layer. Incidence angle = 45 degrees and ρL = 2000.

At this point, seen over the whole polarization spectrum, the received power

is divided equally between that from the ground surface and that from the vegetation layer. This represents the scatterer with the biggest constant of variation or, equivalently, the smallest coherency factor. If the layer thickness is increased beyond this point, the scattering from the vegetation layer dominates. The result is that the "fork" closes to its limiting value and the coherency factor increases slowly to its limiting value. At this stage, as expected, the most power will be received if vertically polarized fields are transmitted. This situation is shown in the polarization spectrum of Figure 4.10.

4.3.1.2 Grass plus Point Scatterers. (Second Grasslands Model)

This model is an extension of the previous model to provide for any point scatterers that may exist in the vegetation layer. This is done by adding small dielectric spheres to the dipoles of the previous model. In the figures that follow it was assumed that the layer consists of 50% dipoles oriented randomly around the vertical direction and 50% small dielectric spheres with radius .075 wavelength and relative dielectric constant 6 + i0.

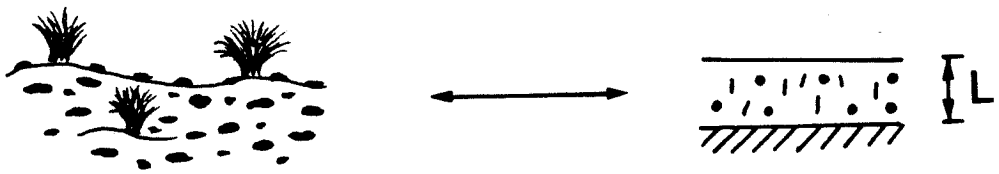

Figure 4.11. Second model for grass-like vegetation.

Figures 4.12 to 4.16 show the results for this model. Figure 4.12 shows the surprising result that at higher incidence angles the hh component of the backscatter coefficients is bigger than the vv component. This result is directly the opposite of that in Figure 4.5. The reason for this becomes apparent

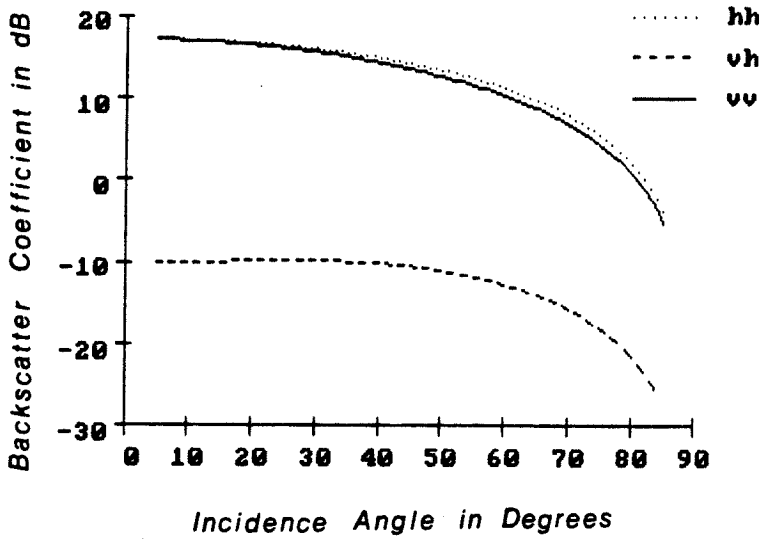

Figure 4.12. Backscatter coefficients as a function of incidence angle for the second grasslands model with a ground surface present. ρL = 1500.

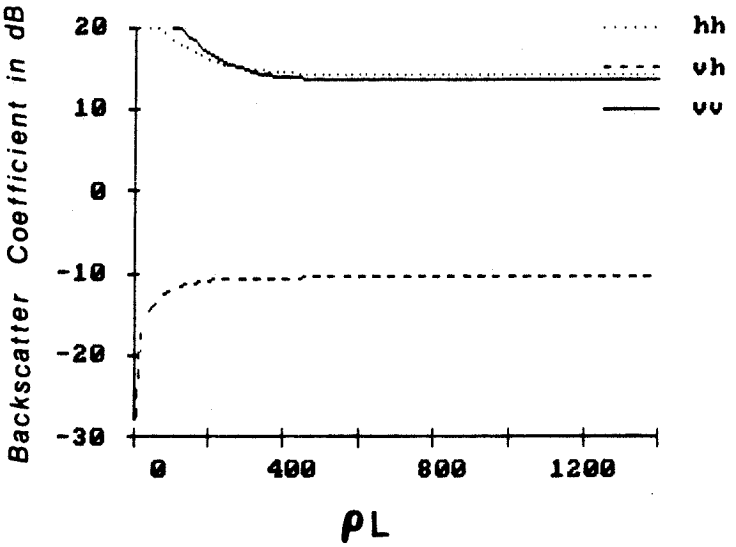

Figure 4.13. Backscatter coefficients as a function of layer thickness for the second grasslands model with a ground surface present. Incidence angle = 45 degrees.

however, when it is realized that in Figure 4.12 the backscattered power is mainly due to the spheres. If a sphere alone is considered, the hh and vv

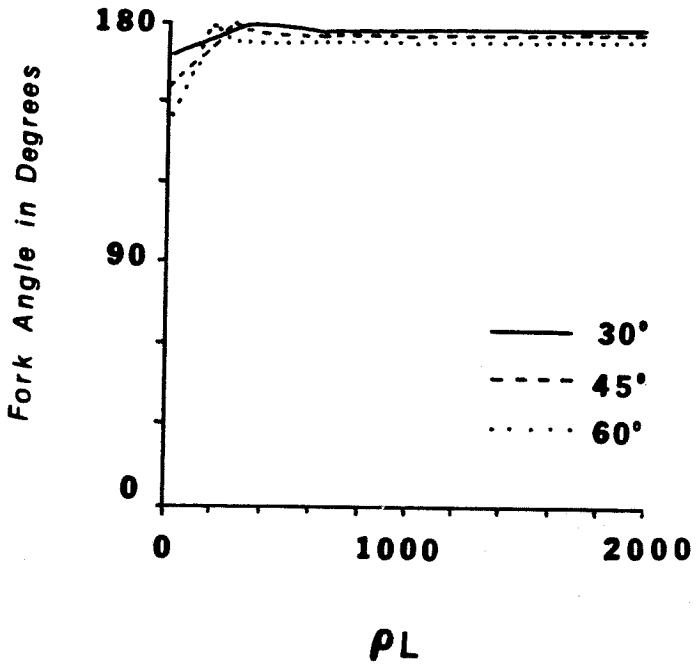

Figure 4.14. Angle between the two minimum polarization vectors as a function of layer thickness at various incidence angles for the second grasslands model.

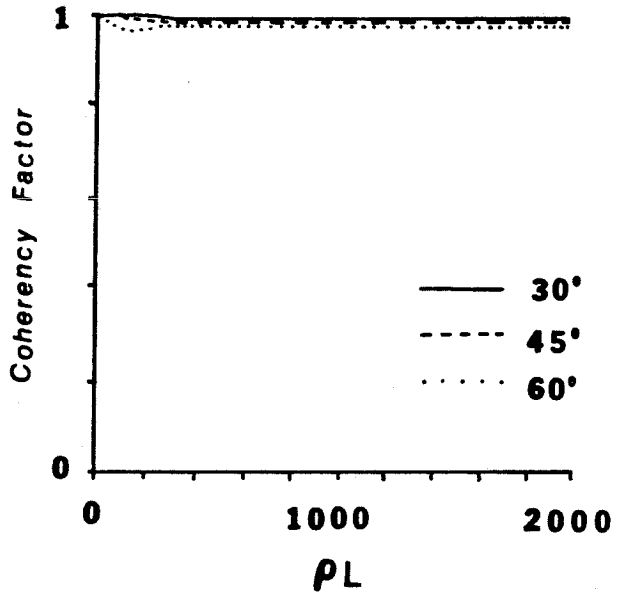

Figure 4.15. Coherency factor as a function of layer thickness at various incidence angles for the second grasslands model.

backscatter coeficients are equal. However, when the dipoles, oriented mostly vertically, are added, the vertical component of the scattered electric field is

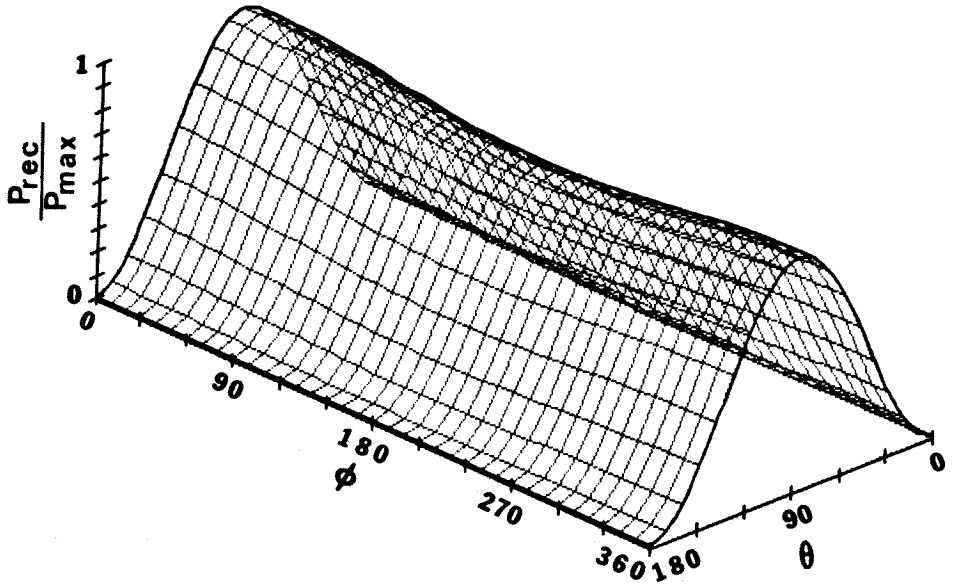

Figure 4.16. Polarization spectrum for the second grasslands model when power is received mainly from the vegetation layer. Incidence angle = 45 degrees and $\rho L = 2000$.

attenuated slightly more than the horizontal component inside the vegetation layer. The result is that the hh backscatter coefficient is slightly larger than the vv backscatter coefficient.

Figure 4.13 shows that the vertically polarized electric fields are attenuated more than the horizontally polarized ones. This fact is to be expected from the composition of the layer. Also, since the scattering from the spheres is much stronger than from the dipoles, a much lower value of ρL than before is needed for the scattered power to be received mainly from the vegetation layer.

Figures 4.14 and 4.15 show that both the "fork" angle and the coherency factor are close to that of a layer of spheres for most layer thicknesses. The "fork" angle opens completely from that of a slightly rough surface and then closes slightly. This happens because for thick layers the maximum polarization is horizontal polarization as opposed to vertical polarization for very thin layers.

The fact that horizontal polarization yields the maximum amount of received power as well as the fact that the polarization "fork" has almost opened completely for thick layers is shown in the polarization spectrum of Figure 4.16.

A comparison of the results of the two grasslands models clearly shows that changing the composition of the vegetation layer dramatically affects the results. Also, the results for the second grasslands model show that even though the scattering is mainly due to the spheres, the presence of the dipoles can be seen in the final results, albeit in an indirect manner.

4.3.2 Coniferous Trees.

The model to describe backscatter from coniferous trees consists of two layers. The top layer is made up of dipoles oriented randomly around 120 degrees from the vertical and the bottom layer is made up of dipoles oriented randomly around the vertical direction. Physically, the top layer models the branches and needles and the bottom layer models the trunks of the coniferous trees.

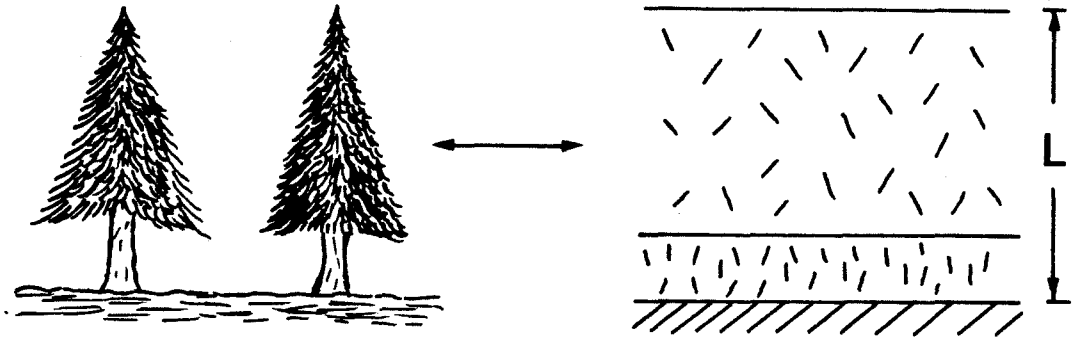

Figure 4.17. Model for coniferous trees.

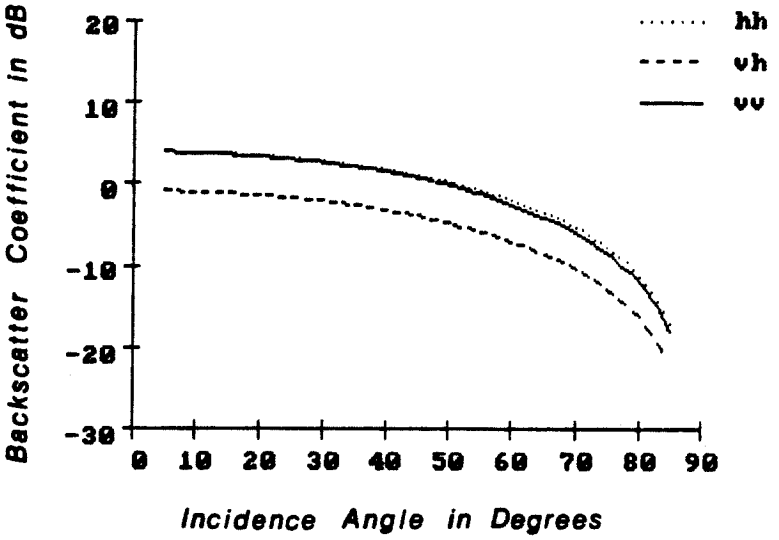

Figure 4.18. Backscatter coefficients as a function of incidence angle for the coniferous trees model suspended in air. $\rho L = 1500$.

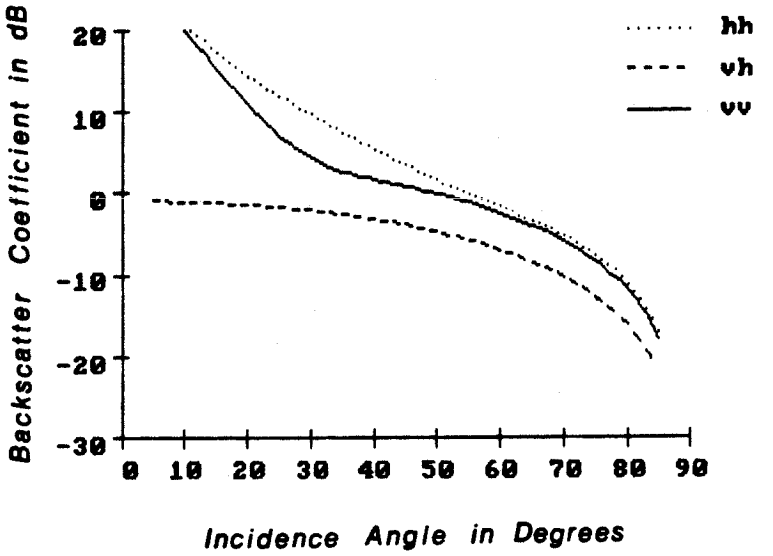

Figure 4.19. Backscatter coefficients as a function of incidence angle for the coniferous trees model with a ground surface present. $\rho L = 1500$.

To keep the model simple, it will be assumed that the two layers are of equal thickness. For thick layers, one expects the hh backscatter coefficient to

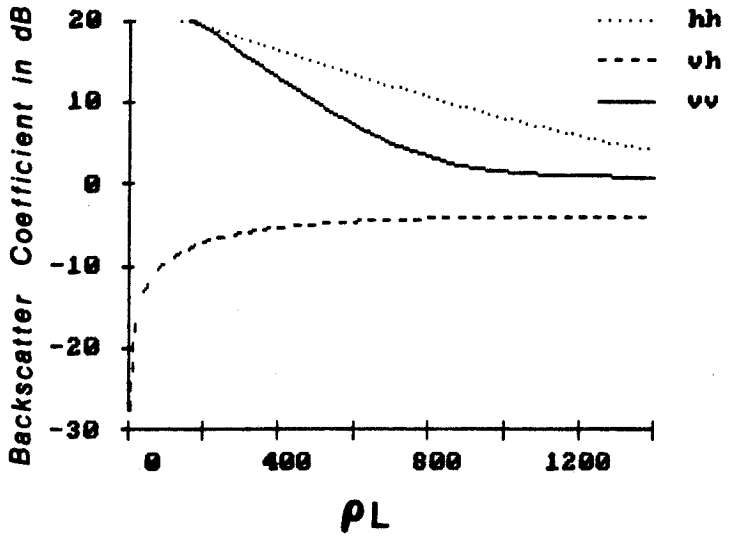

Figure 4.20. Backscatter coefficients as a function of layer thickness for the coniferous trees model with a ground surface present. Incidence angle = 45 degrees.

be larger than the vv coefficient. When the two layers are suspended in air, (Figure 4.18) the hh coefficient is only slightly larger than the vv coefficient. For the case shown, however, the top layer is not thick enough to completely attenuate returns from the bottom layer, which scatters the vertically polarized electric field more strongly than the horizontally polarized ones. These vertically polarized fields are also not strongly attenuated in the top layer, with the result that the vv coefficient is closer to the hh coefficient than would be expected if only the top layer were present.

Figure 4.20 shows the backscatter coefficients as a function of layer thickness. This figure shows that, for ρL smaller than 600, the vv coefficient decreases more rapidly than for $600 \leq \rho l \leq 800$. For $\rho L \leq 600$ this attenuation is strongly affected by the bottom layer, but as ρL grows bigger than 600 the effect of the top layer starts to dominate. The result is that seen in Figure 4.20.

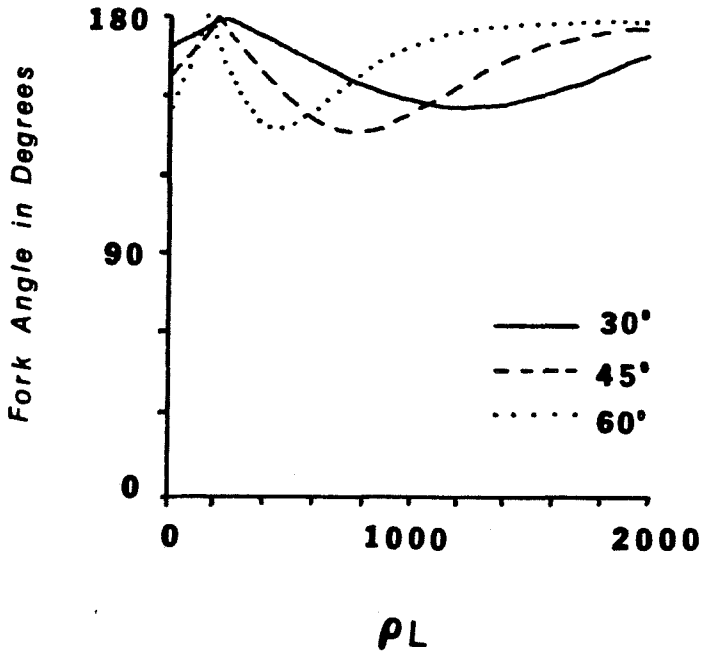

Figure 4.21. Angle between the two minimum polarization vectors as a function of layer thickness at various incidence angles for the coniferous trees model.

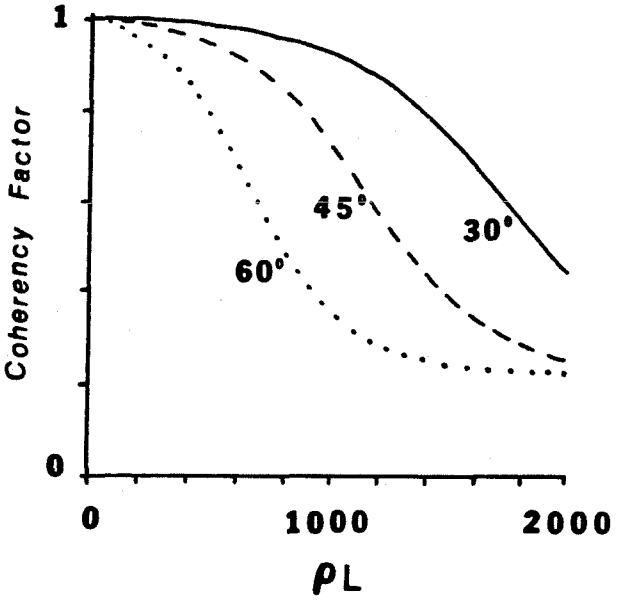

Figure 4.22. Coherency factor as a function of layer thickness at various incidence angles for the coniferous trees model.

Since the vertically polarized electric fields are attenuated more than the horizontally polarized ones in thin layers, one would expect the "fork" angle to

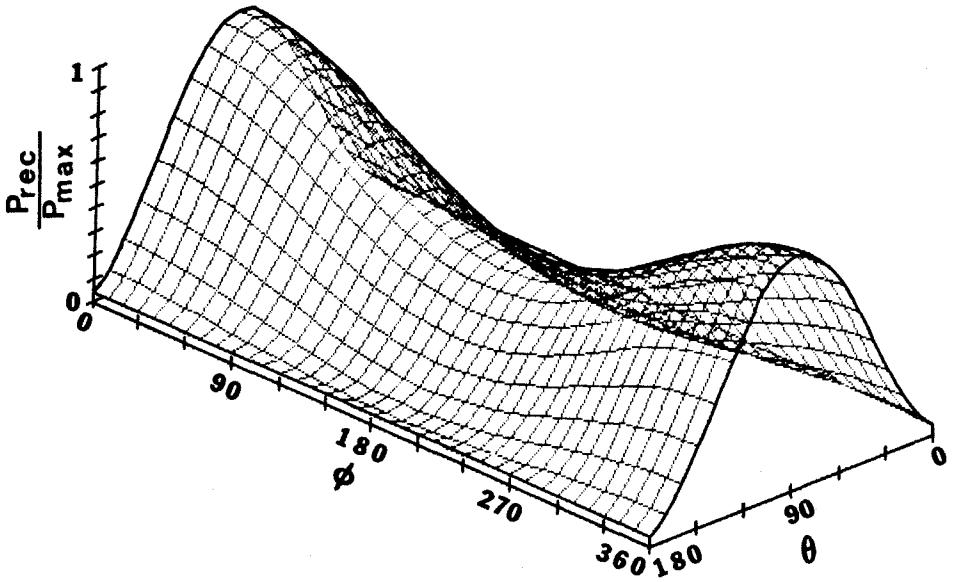

Figure 4.23. Polarization spectrum for the coniferous trees model when power is received mainly from the ground surface. Incidence angle = 45 degrees and ρL = 400.

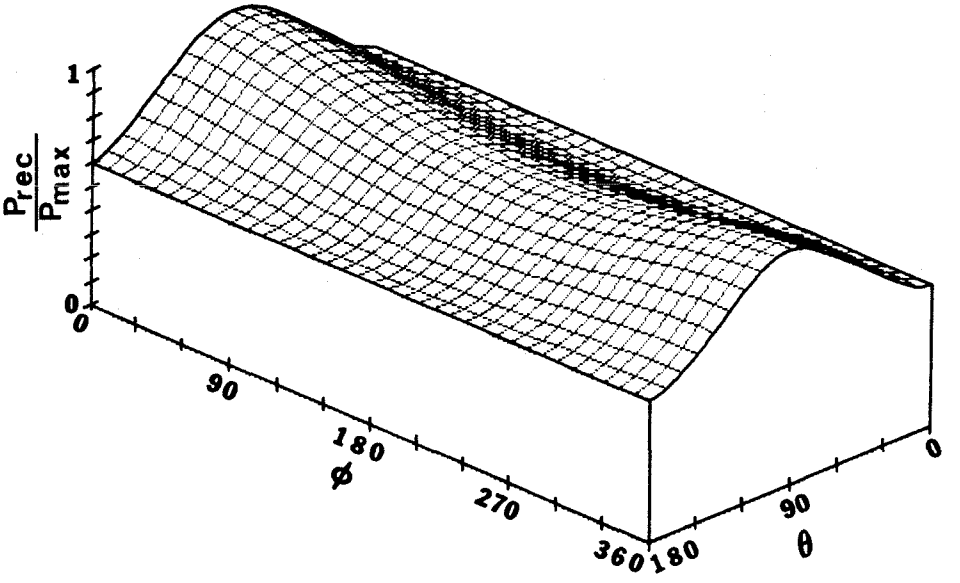

Figure 4.24. Polarization spectrum for the coniferous trees model when power is received mainly from the vegetation layer. Incidence angle = 45 degrees and ρL = 2000.

first open up and then close to a minimum value. If the layer is made even

thicker, one would expect the "fork" to start opening again, but since for this model the maximum polarization for thick layers is horizontal polarization, one would not expect the "fork" to open up completely again. Instead, the "fork" angle should approach a limiting value for thick layers. This behaviour is displayed in Figure 4.21. Similarly, one would expect the coherency factor to decrease monotonically to a limiting value. This is indeed the case, as is witnessed in Figure 4.21.

For thin layers, the effect of the bottom layer is very pronounced. Thus, one would expect that the polarization spectrum of the vegetation-ground combination for thin layers would look similar to that of the first grasslands model. This is seen to be true when Figures 4.9 and 4.23 are compared. For thick layers, one would expect that polarizations nearly horizontal would yield the most power received. This is indeed the case shown by the polarization spectrum shown in Figure 4.24.

4.3.3 Deciduous Trees.

Deciduous trees usually have leaves and branches pointing in all directions. To model this situation, the top layer of the previous model is replaced by one which contains dipoles oriented spherically randomly.

For layers thick enough so that the scattering is dominated by the top layer, one expects the hh and vv backscatter coefficients to be the same. This must be the case since the top layer presents the same characteristics to both polarizations. This result is found in Figures 4.26 and 4.27.

As the layer thickness increases, one first expects the vv backscatter coefficient to decrease more rapidly than the hh coefficient due to the presence of the mostly vertically oriented dipoles in the bottom layer. When the layers are thick enough so that the effect of the bottom layer is negligible, one expects

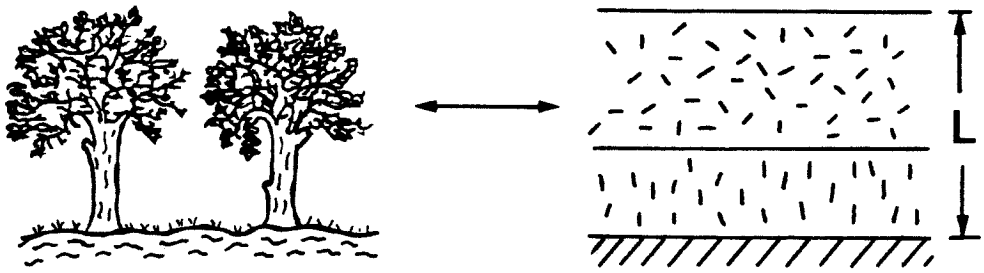

Figure 4.25. Model for deciduous trees.

the hh and vv coefficients to decrease at the same rate and finally to become equal. This behaviour is displayed in Figure 4.28.

For thin layers, vertical polarization is the maximum polarization. As in the case of the first grasslands model, for medium thick layers the maximum polarization is horizontal polarization. For very thick layers, the top layer of the model displays the same characteristics for any linear polarization. One would thus expect that the polarization "fork" should first open completely, then close to a minimum and finally open completely. This is clearly the case shown in Figure 4.29. The result in Figure 4.30 can also be explained in this way. Since the variation in scattering properties increases to a limiting value as the layer thickness is increased, one would expect the coherency factor to decrease to a limiting value as shown in Figure 4.30.

For thin layers, as in the case of the coniferous trees model, one expects that the most power will be received (mainly from the ground surface) if horizontally polarized waves are transmitted. This is clearly the case in Figure 4.31. For very thick layers, one expects that any linear polarization would yield

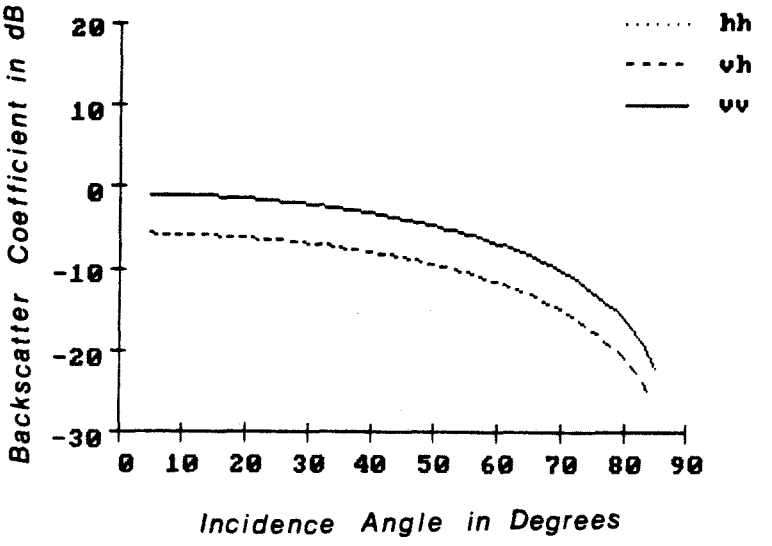

Figure 4.26. Backscatter coefficients as a function of incidence angle for the deciduous trees model suspended in air. ρL = 1500.

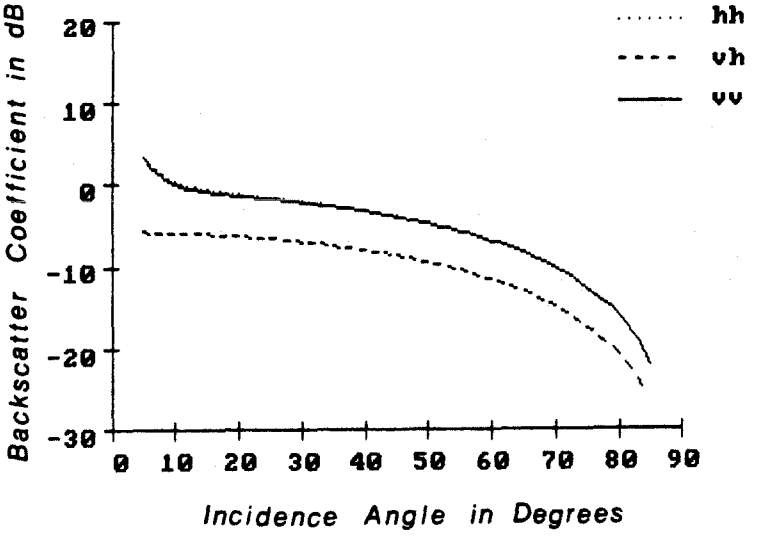

Figure 4.27. Backscatter coefficients as a function of incidence angle for the deciduous trees model with a ground surface present. ρL = 1500.

a maximum amount of power received. This result is shown in Figure 4.32.

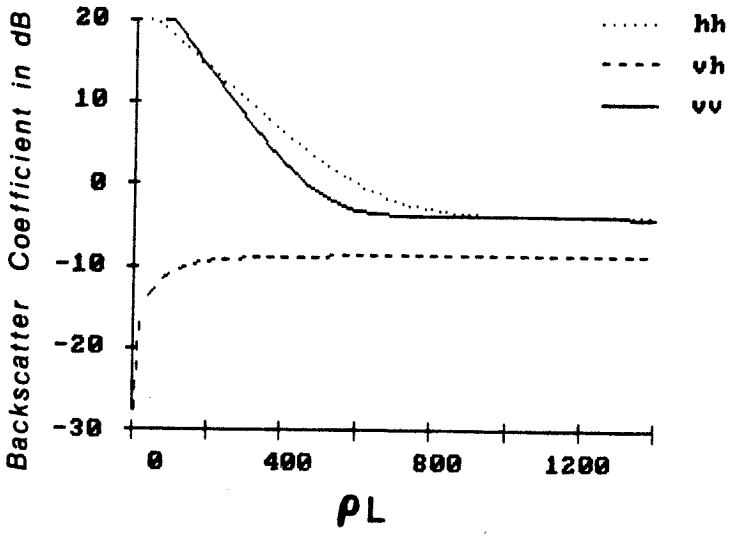

Figure 4.28. Backscatter coefficients as a function of layer thickness for the deciduous trees model with a ground surface present. Incidence angle = 45 degrees.

4.4 Conclusions.

In this chapter, some single scattering models to describe backscatter from four different types of vegetation were derived and the results discussed. It is clear that when the results of these models are compared, there is a big difference between the different models, especially when the vegetation layers are thick. This difference is easiest to see when the polarization spectrums of the models are compared. All the results found can easily be explained by the physical properties of the various models.

The models described in this chapter were chosen to be the simplest possible theoretical model which could describe scattering from different types of vegetation. When more measured data become available, more sophisticated models may be generated. To really model a physical scattering process accurately, the relative importance of the various parts of the vegetation when

the scattered fields are generated, must be known.

In the next chapter it will be shown how these models, and the difference between the various models, may be used to the advantage of scientists involved in multipolarization radar imaging.

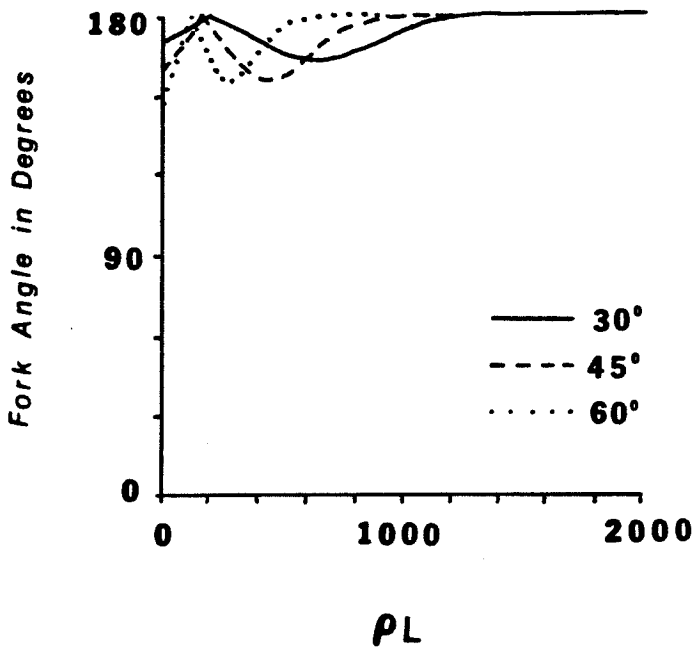

Figure 4.29. Angle between the two minimum polarization vectors as a function of layer thickness at various incidence angles for the deciduous trees model.

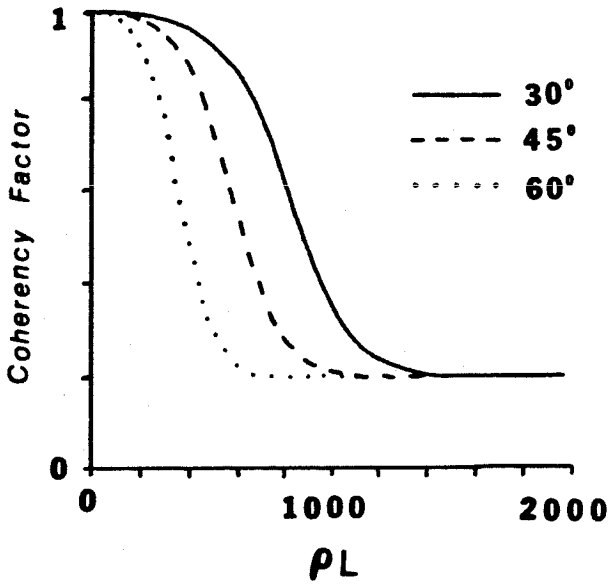

Figure 4.30. Coherency factor as a function of layer thickness at various incidence angles for the deciduous trees model.

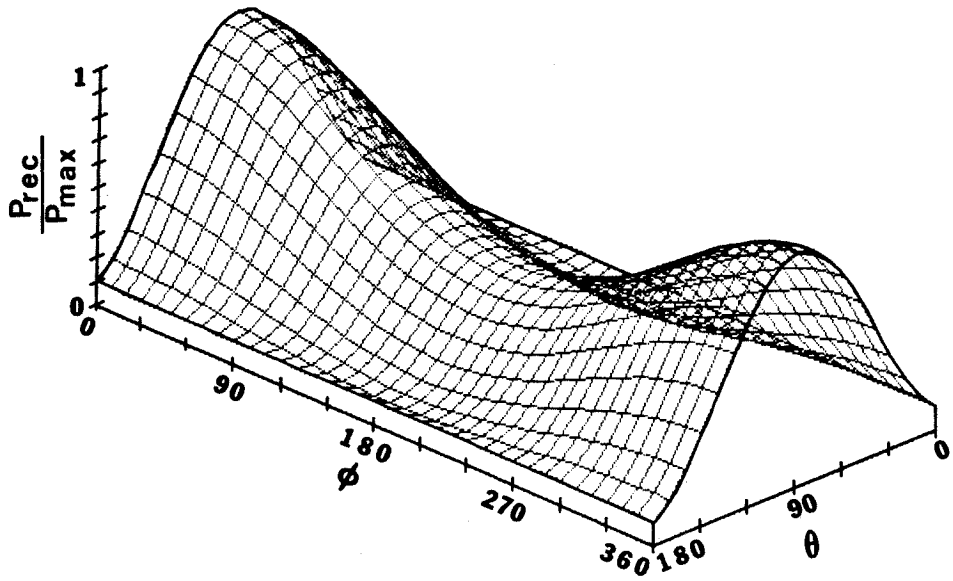

Figure 4.31. Polarization spectrum for the deciduous trees model when power is received mainly from the ground surface. Incidence angle = 45 degrees and ρL = 400.

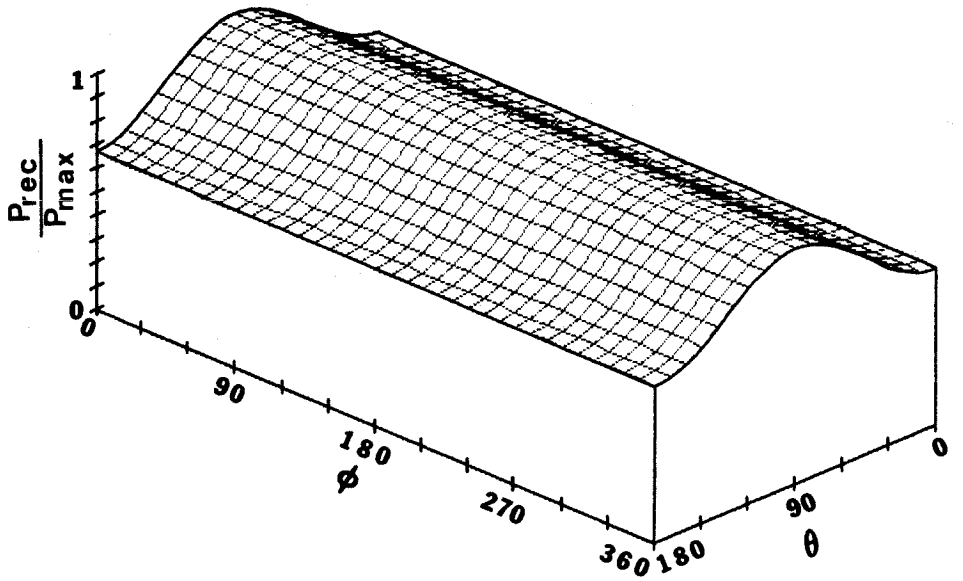

Figure 4.32. Polarization spectrum for the deciduous trees model when power is received mainly from the vegetation layer. Incidence angle = 45 degrees and ρL = 2000.

CHAPTER 5

SOLVING THE INVERSE PROBLEM.

In radar imaging, scientists usually deal with the inverse scattering problem: the average properties of the radar backscatter from the vegetation layer is known and one wants to obtain some information about certain parameters of the vegetation from these known properties. This is a very difficult problem, since it is conceivable that there may be more than one type of vegetation that may produce the same average radar backscatter as a function of incidence angle and wavelength. If one has some knowledge of the vegetation layer, it may be possible to use the measured radar backscatter to obtain more general information about the vegetation under consideration.

In this chapter, a simple way to classify measured results into different classes wil be presented. It will also be shown how this process will essentially solve the inverse problem to the accuracy permitted by the accuracy of the models used to do the classification.

In general, investigators may be interested in many different parameters characterizing a vegetation layer. Some of the most important ones are:

(a) The thickness L of the layer.

(b) The amount of absorption in the layer. This would give some information about the quantity of biomass (i.e., amount of vegetation and the water content of the vegetation) per unit volume it contained.

(c) The type (i.e., long, thin scatterers or point scatterers) and relative orientation of the scatterers in the layer. This may provide some information about the type of vegetation present in the layer.

(d) Geologists may be interested in discriminating between scattering from the ground surface and scattering from the vegetation volume.

Obviously, it would be very difficult in practice to distinguish between each and every possible type of vegetation. A promising method of obtaining a reliable solution is to build up a library of models of vegetation layers which would include the most important types of vegetation and ground surfaces. To find the parameters of the model which best approximate a measured Stokes Scattering Operator, one simply has to calculate the polarization spectrum for the measured Stokes Scattering Operator and compare the result with the polarization spectrums of the models in the library [11]. The parameters of the polarization spectrum that differs the least from the measured one may then be taken as the parameters of the vegetation layer. The advantages of this method are:

(i) All the parameters of the vegetation layer are solved for simultaneously.

(ii) Once a model has been chosen to represent the measured Stokes Scattering Operator, the polarization which would yield the optimum amount of discrimination between the power scattered by the ground surface and the power scattered by the vegetation volume can easily be calculated. Also the polarizations that would enhance or decrease the intensity of the particular pixel in the image are easy to calculate.

The main disadvantage of this method is that the accuracy that may be achieved is limited by how well the models imitate the real physical scattering processes encountered in nature.

To illustrate this method, the four models of the previous chapter will be compared. The comparison is done on the basis of their normalized difference values defined in Section 2.3.2.7. Two cases will be considered:

(i) The models all have the same thickness as the reference model. (Figure 5.1.)

(ii) A reference model of fixed layer thickness is compared to all the other models, including itself, for all possible layer thicknesses. (Figure 5.2.)

In both Figures 5.1 and 5.2, the first grasslands model was used as the reference. It is clear from both these figures, which were calculated using 200 points on the Poincaré sphere, that there is indeed a sizable difference between the various models. The real difference may, of course, be increased by using more points on the Poincaré sphere when calculating the normalized difference values.

One does not have to use models to do this type of classification, however. This technique of comparing different scatterers gives a simple way to map those parts of an image which are similar to a previously selected pixel. In that case, the reference polarization spectrum is the polarization spectrum of the selected pixel. Mapping is done by comparing the polarization spectrums of the other pixels in the image to that of the reference pixel.

For those scientists interested in the ground surface, it is important to know which polarization would give the best discrimination between the power scattered by the ground surface and the power scattered by the vegetation volume. Once a model for the measured polarization spectrum has been chosen, it is a straightforward problem to calculate this optimum polarization.

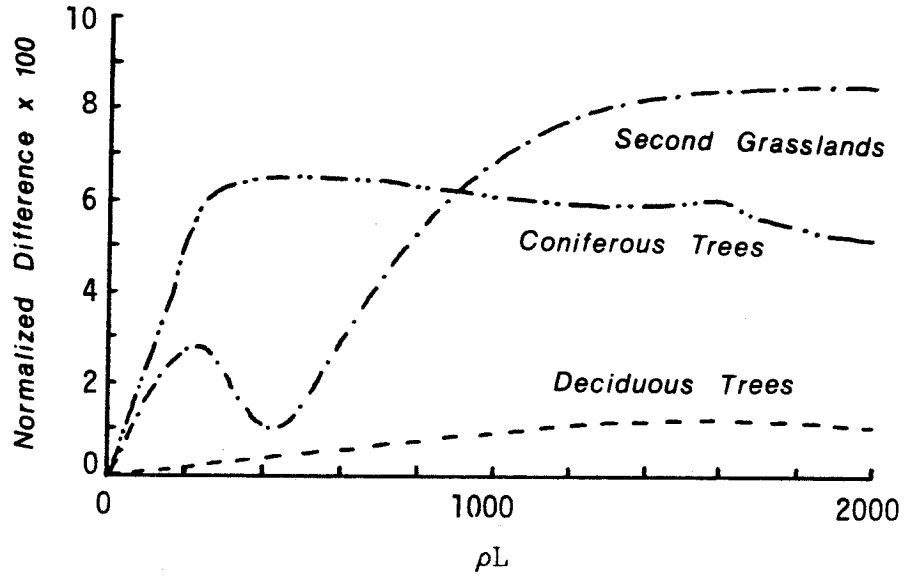

Figure 5.1. Normalized difference values when the first grasslands model is compared with other models with the same layer thickness.

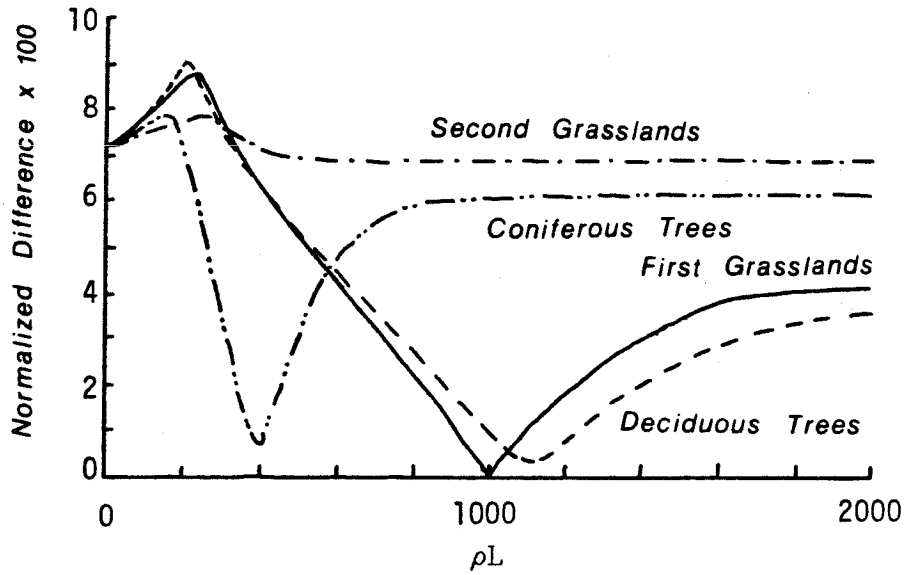

Figure 5.2. Normalized difference values as a function of layer thickness when the first grasslands model with $\rho L = 1000$ is compared with all the models.

Figures 5.3 and 5.4 show the locus of this optimum polarization for

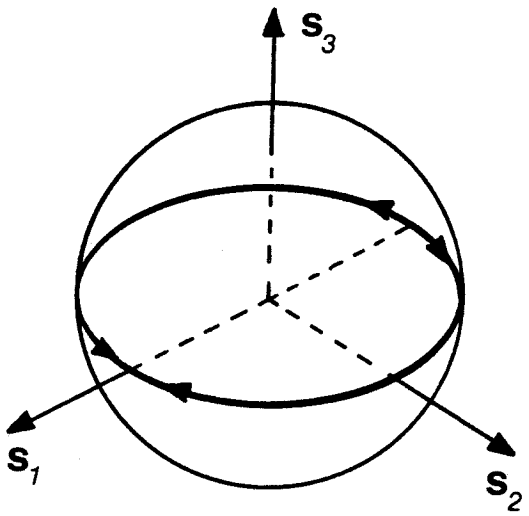

Figure 5.3. Optimum polarization for discriminating between the returns from the ground surface and the vegetation for the first grasslands model, the coniferous trees model and the deciduous trees model.

different layer thicknesses plotted on the Poincaré sphere. It is not completely surprising that the behaviour of this optimum polarization is similar for the first grasslands, the coniferous trees and the deciduous trees models. The reason for this is that the return from the ground surface in all three cases is influenced most by a layer of dipoles that are randomly oriented around the vertical direction. For these cases, it was explained earlier why horizontal polarization would yield the strongest return from the ground surface.

The optimum polarization for discriminating between returns from the ground surface and the second grasslands model exhibits an interesting behaviour. Starting off at vertical polarization (the maximum polarization of the ground surface), it soon moves to the circular polarizations. For ρL in the region of 500, it moves back to vertical polarization and then rapidly moves via the linear polarizations to horizontal polarization. After a brief stay at horizontal polarization, it moves back to the circular polarizations, where it

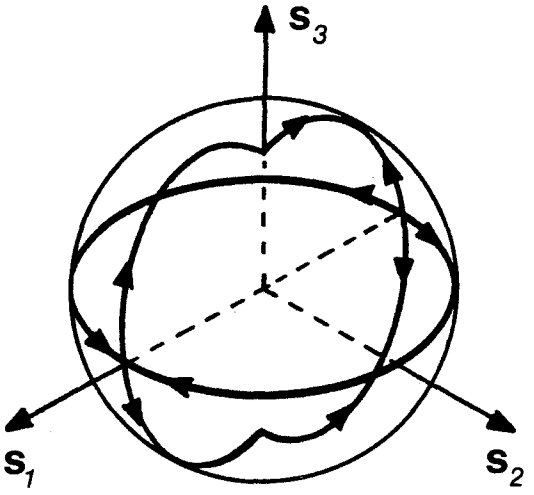

Figure 5.4. Optimum polarization for discrimination between the returns from the ground surface and the vegetation layer for the second grasslands model.

finally stays. It was remarked earlier that for this model the scattering is dominated by the spheres. Spheres, however, have their polarization nulls at the circular polarizations, and hence it is to be expected that the circular polarizations would give the best discrimination between the returns from the ground surface and the second grasslands model. The quick movements to vertical polarization and then via the linear polarizations to horizontal polarization is the result of the slight difference between the attenuation constants for vertical and horizontal polarizations due to the presence of the dipoles.

CHAPTER 6

MULTIPOLARIZATION RADAR IMAGING RESULTS.

6.1 Introduction.

In this chapter, some of the concepts defined in earlier chapters will be applied to real multipolarization synthetic aperture radar data. The data were captured by the airborne high resolution synthetic aperture radar flown by the Jet Propulsion Laboratory [25] during early summer 1985. Two areas will be investigated:

(i) The San Francisco area in California.

(ii) The Snake River Plain lava flow area in Idaho.

Here, the polarization spectrums of different scenes will be shown and discussed. Also, the coefficient of variation for these two areas will be calculated and shown in image form.

6.2 Results.

Figures 6.1 and 6.2 show images of the two areas to be investigated. Both the images were made assuming horizontal polarization for both the transmitting and the receiving antennas. In each of these areas, a strip corresponding to a quarter of the total image was selected to be investigated. For these strips, the average Stokes Scattering Operators were calculated for 16 pixels, giving a final resolution of 15 metres in the slant range direction and 22 metres in the azimuth direction. Figure 6.5 shows the definition of these directions. For each of the average Stokes Scattering Operators, the coefficient of variation was calculated. The results, together with the "reference" strip, are displayed in Figures 6.3 and 6.4.

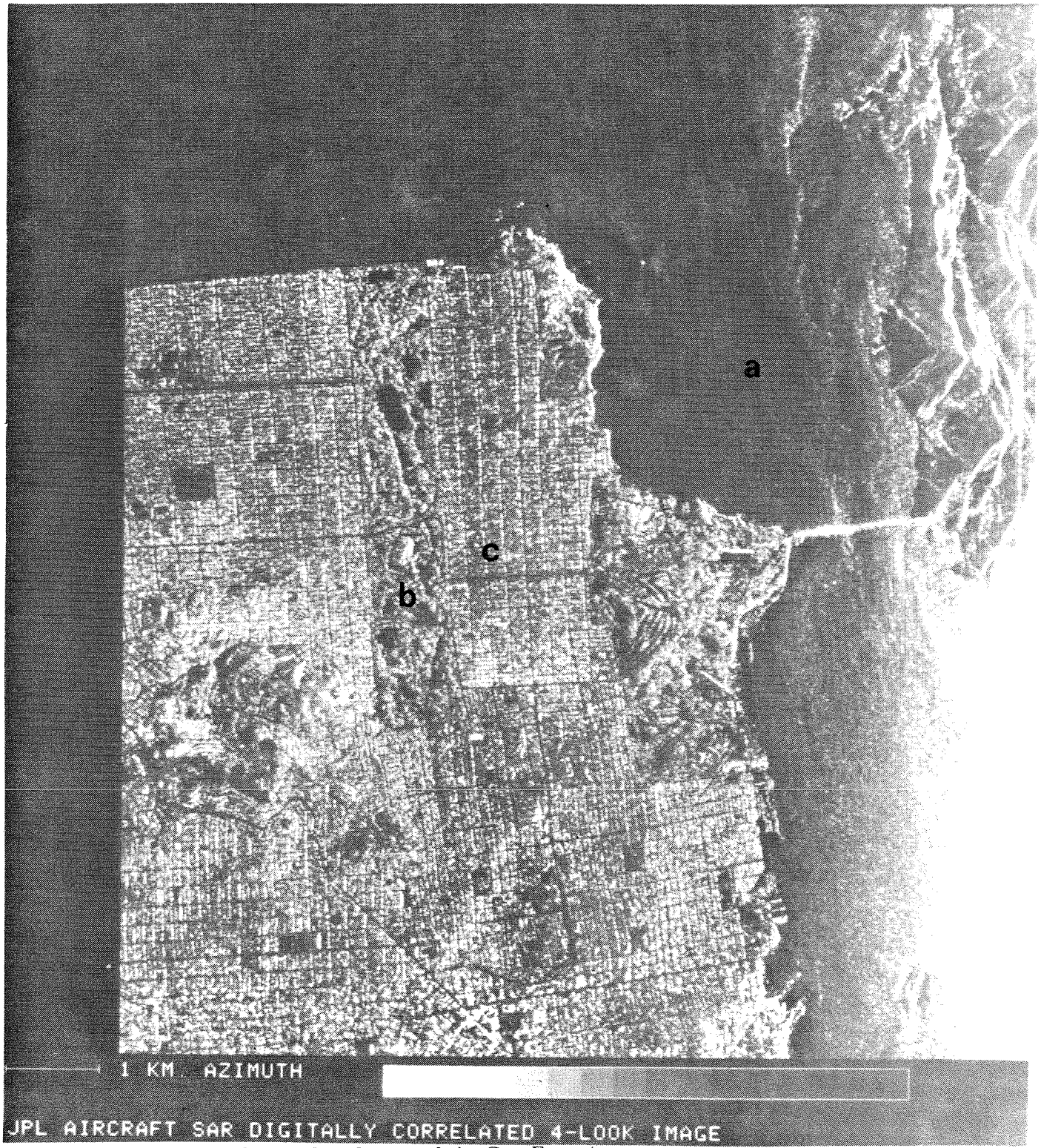

Figure 6.1. Image of the San Francisco area.

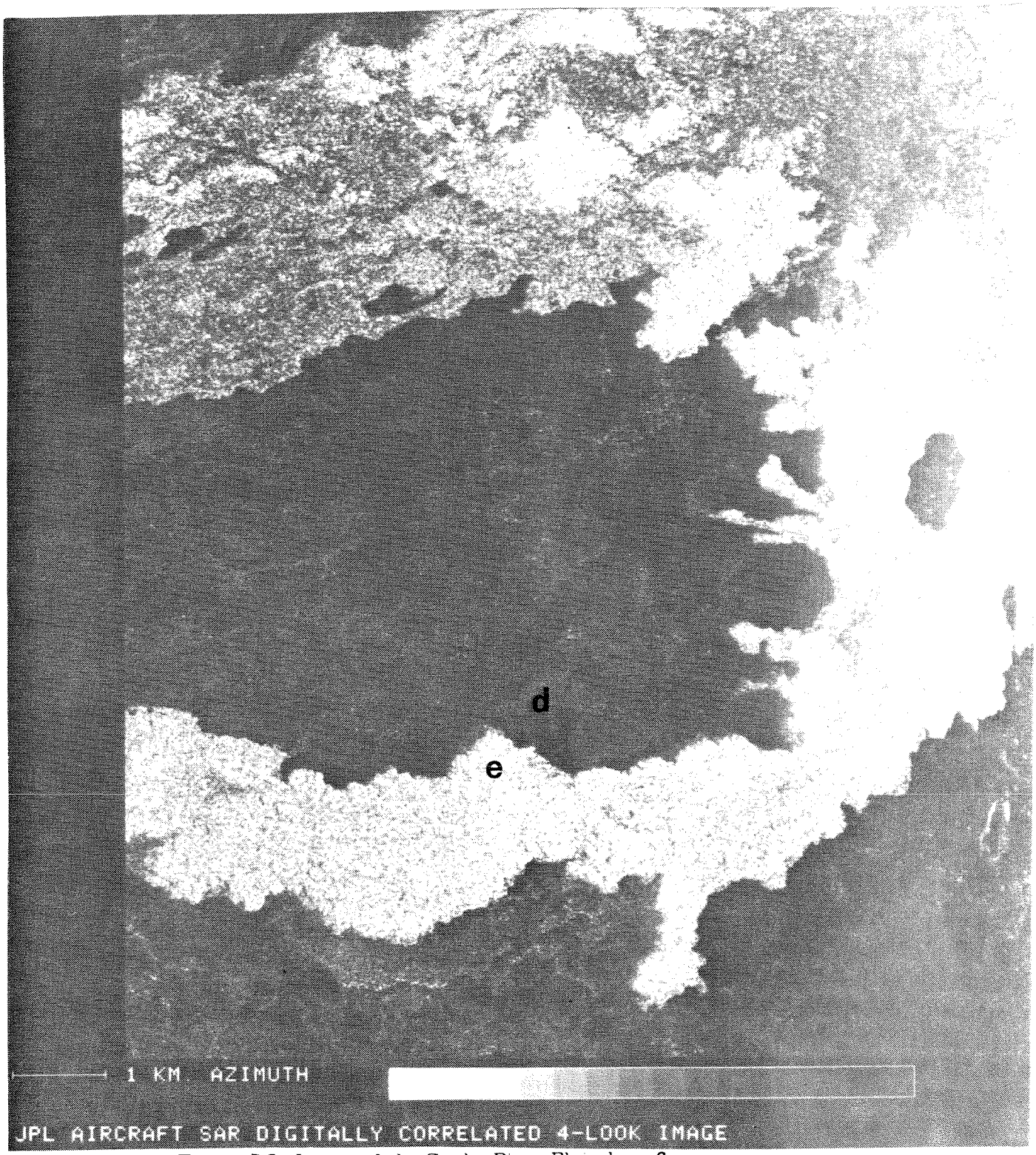

Figure 6.2. Image of the Snake River Plain lava flow area.

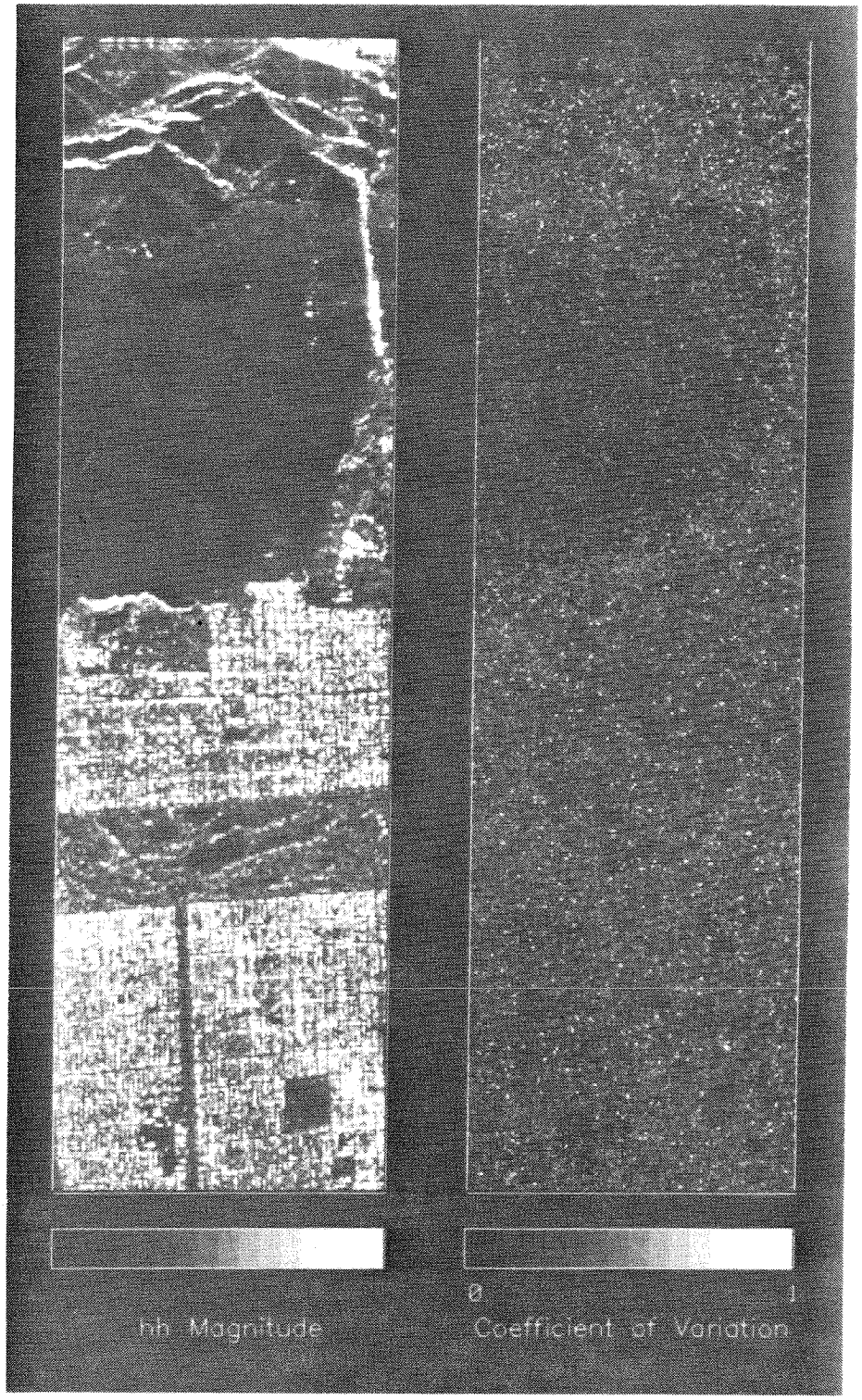

Figure 6.3. Coefficient of Variation for the San Francisco area.

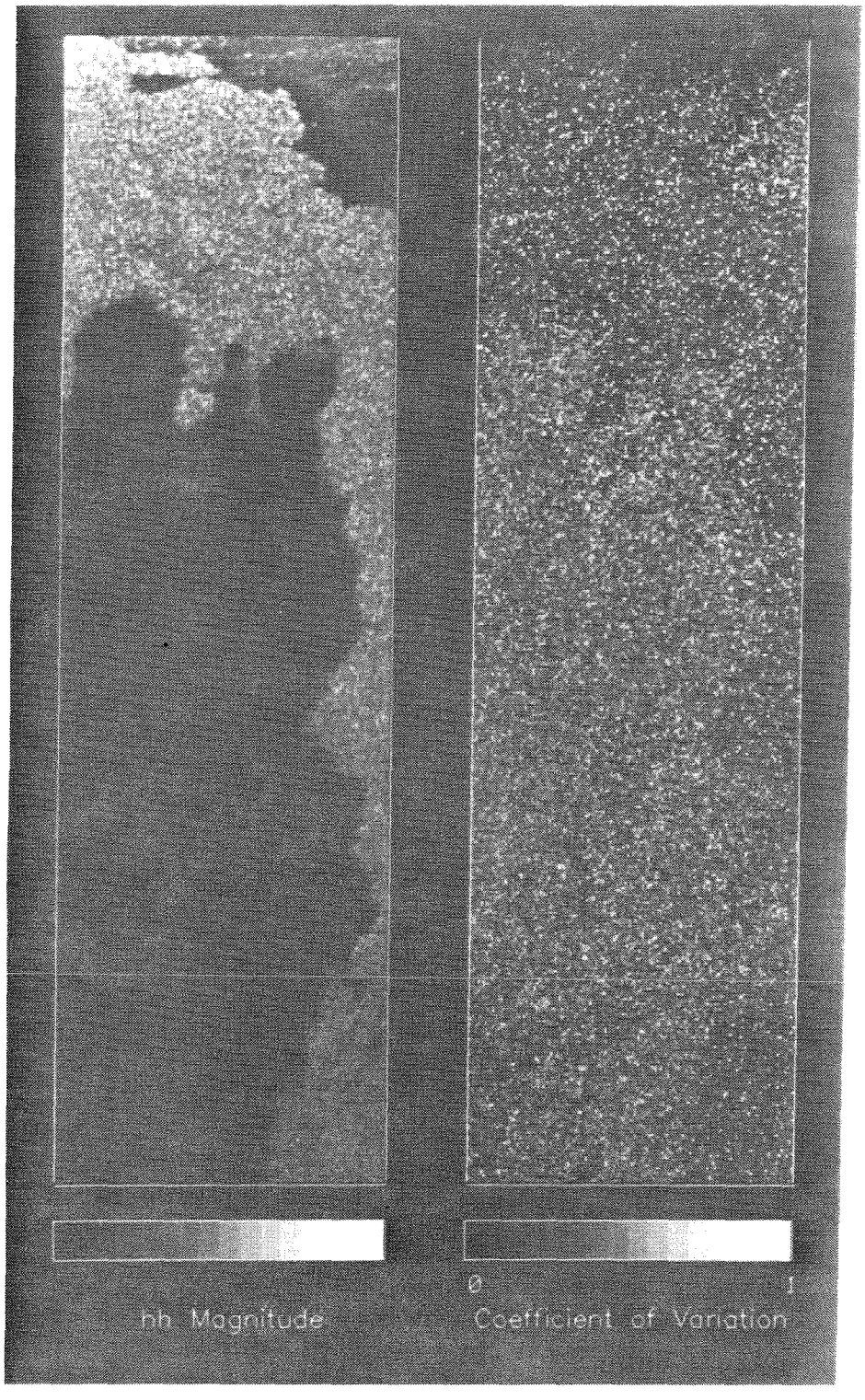

Figure 6.4. Coefficient of Variation for the Snake River Plain area.

In the San Francisco images, it is clear that, apart from the noisy character, as expected, the ocean has a lower coefficient of variation than the urban ares or the park areas. On this fairly small scale, there is very little difference between the coefficient of variation of the park area and that of the urban area, although the park area has a slightly higher coefficient of variation than the urban area. This is in accord with what should be expected, since urban scenes do not vary much over a 22m by 15m area.

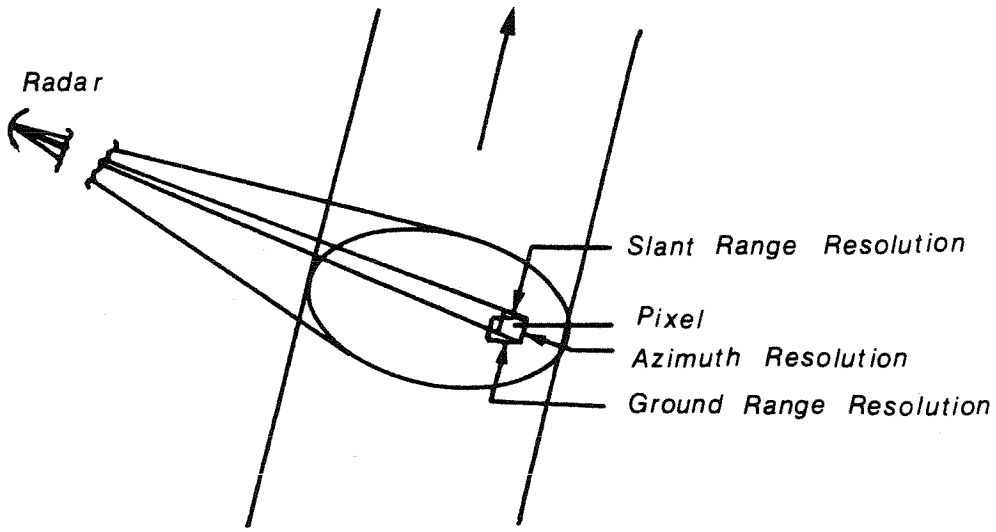

Figure 6.5. Measurement Geometry.

In the Snake River Plain images, it is clear that, on this fairly small scale, the smoother lava flow areas have a higher coefficient of variation than the rougher lava flow areas. While this may sound opposite to what one may expect, the higher variation for the smoother areas is probably due to the presence some vegetation (low bushes and grass) in the smoother areas. Since the received power for the smoother lava flows is very small, noise may also contribute to the higher coefficient of variation for these areas.

To investigate the character of the scattering processes in more detail, five "test" areas were selected from Figures 6.1 and 6.2. For each test area, the average Stokes Scattering Operator was calculated for an area of 90 metres (azimuth) by 132 metres (slant range). The polarization spectrums for each of these five test areas are shown in Figures 6.6 - 6.10. A comparison of some of the characteristics of these polarization spectrums is shown in Table 6.1.

TABLE 6.1 COMPARISON OF TEST AREAS.

Area	Image	Label	Max. "power"	Coef. of Var.
Ocean	San Francisco	a	.0232	.019
Park	San Francisco	b	.1035	.653
Urban	San Francisco	c	.1409	.421
"Smooth" lava	Snake River Plain	d	.0018	.145
Rough lava	Snake River Plain	e	.0155	.241

The results in Table 6.1 show that, on this medium scale, the ocean has very little variation in scattering properties, which corresponds with what one expects from the physical setup. The urban area has much more variation in scattering properties than the ocean, but less than the the park area. This is to be expected, since fairly large patches of urban areas exhibit the same scattering properties, while park areas covered with different types of vegetation show more variation in scattering properties on the medium scale.

Also, on the medium scale, the smoother lava flow shows less variation in scattering properties than the rough lava flow. On this scale, the effects of the relatively short bushes and grass are much smaller than that of the huge boulders found in the rougher flows. Also, the effects of noise is much smaller on the medium scale. Thus, it should be expected that, on a medium scale, the

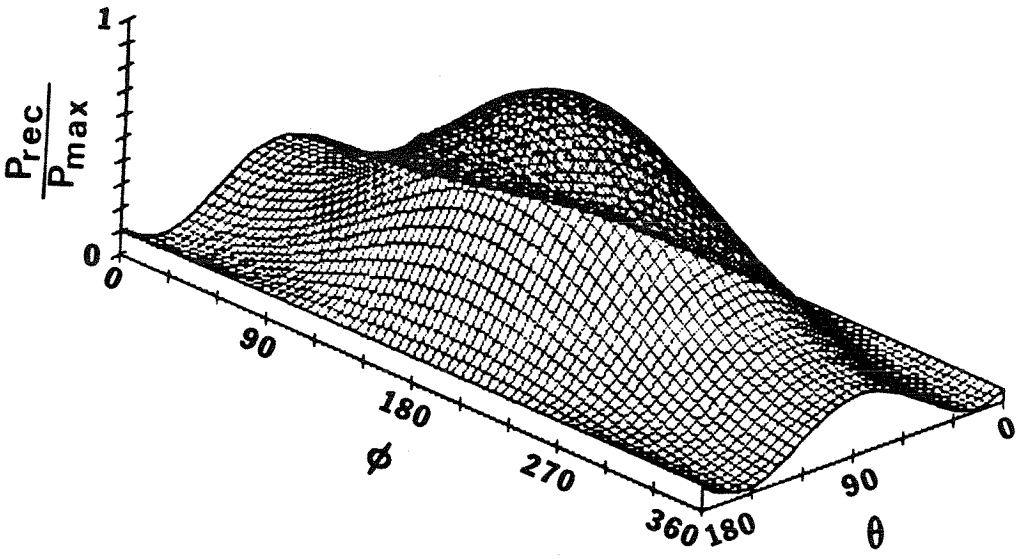

Figure 6.6. Polarization spectrum for ocean area.

rougher lava flows will show more variation in scattering properties than the smoother flows.

When the polarization spectra of the ocean area, the smoother lava flow and the rough lava flow are compared to that of a slightly rough ground surface calculated from Valenzuela's model [24], (Figure 2.7) it is clear that these four polarization spectrums are very similar. While it may be expected that the ocean, and even the smoother lava flow, may have spectrums that compare favorably with Valenzuela's model, it is surprising that the very rough lava flows have spectrums that look similar to Figure 2.7. It is clear that more work should be done in order to understand the dominating scattering processes when geological areas are imaged. More work is also needed to understand how the scattering process influences the form of the polarization spectrum.

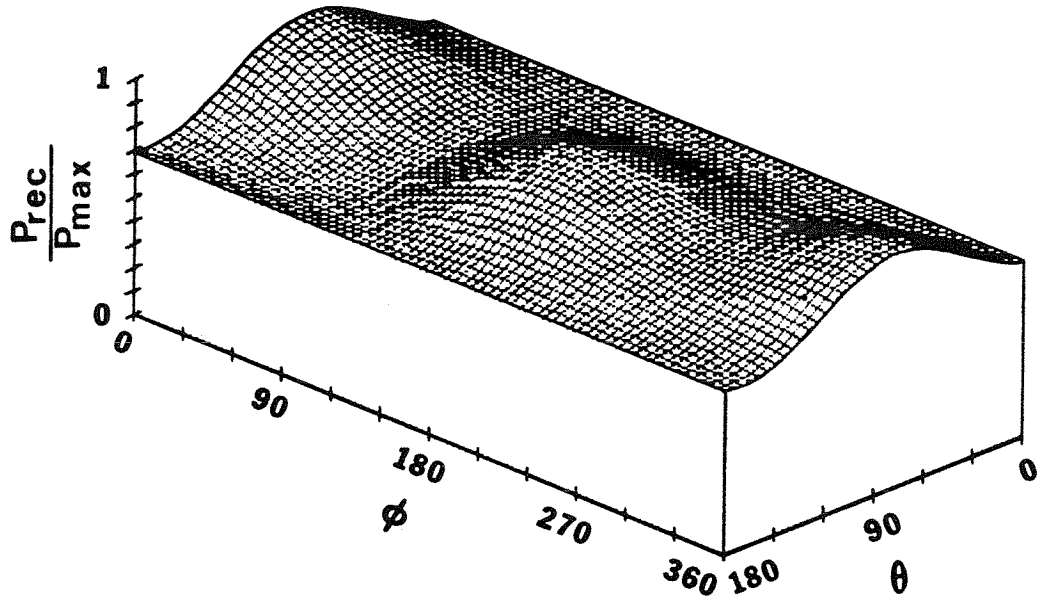

Figure 6.7. Polarization spectrum for park area.

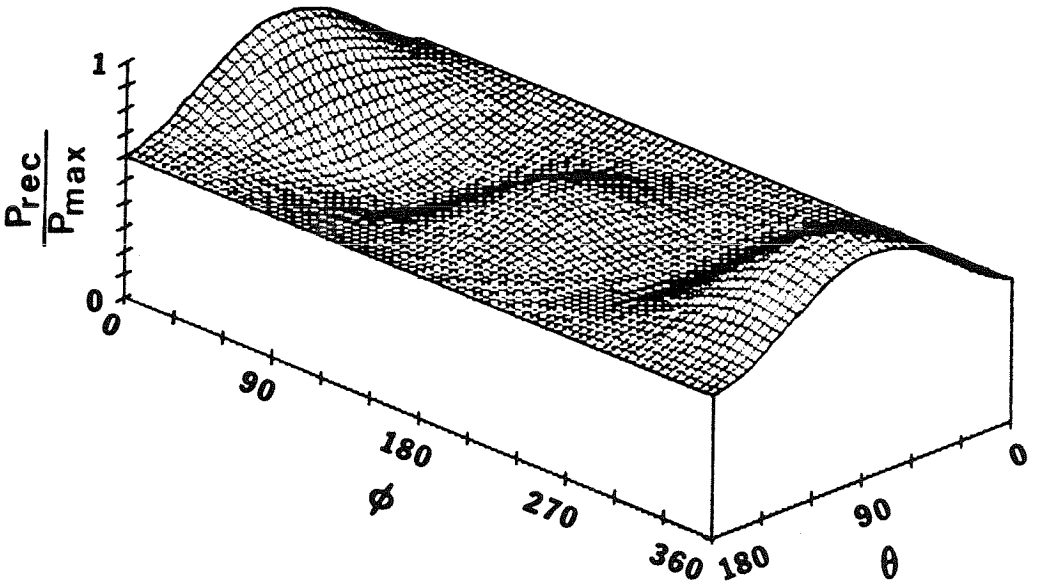

Figure 6.8. Polarization spectrum for urban area.

Next, consider the polarization spectrum of the urban area shown in Figure 6.8. This spectrum shows a maximum near horizontal polarization, minima near the 45 degrees and 135 degrees linear polarizations and a local maximum

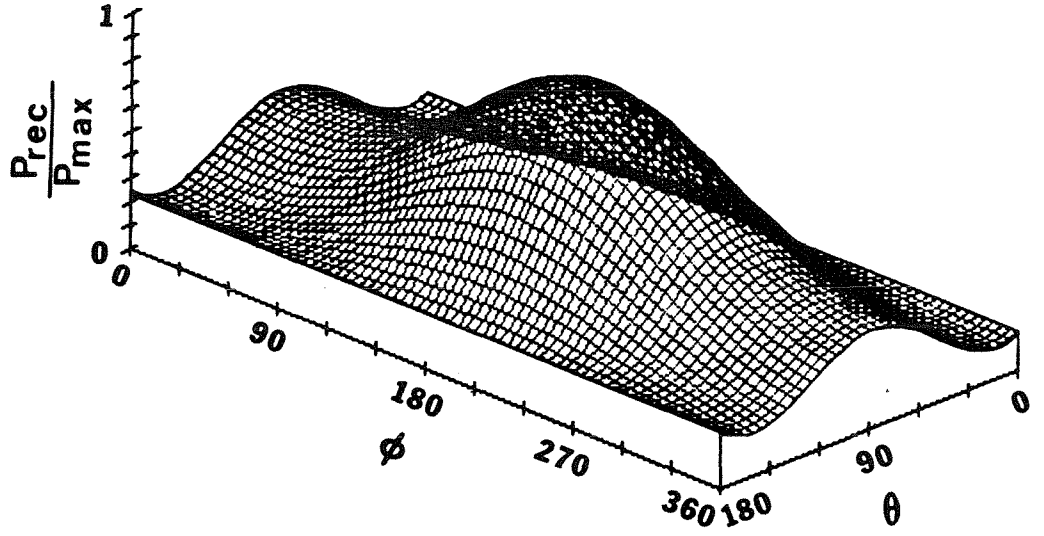

Figure 6.9. Polarization spectrum for smoother lava flow area.

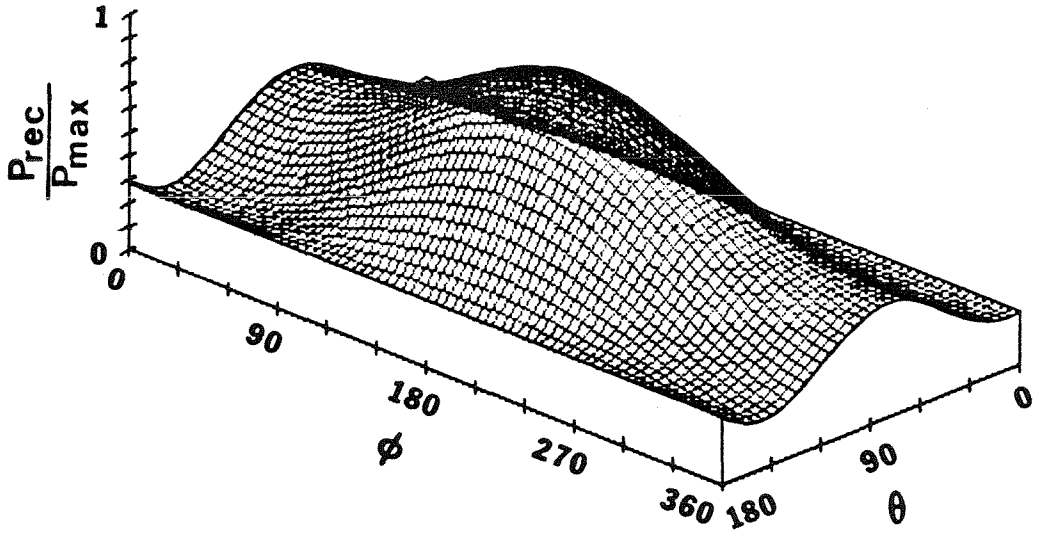

Figure 6.10. Polarization spectrum for rougher lava flow area.

near vertical polarization. Now, consider the case of a wave reflected as shown in Figure 6.11. For simplicity it is assumed that the reflecting surfaces are smooth when the double-bounce case is calculated. All surfaces are assumed to

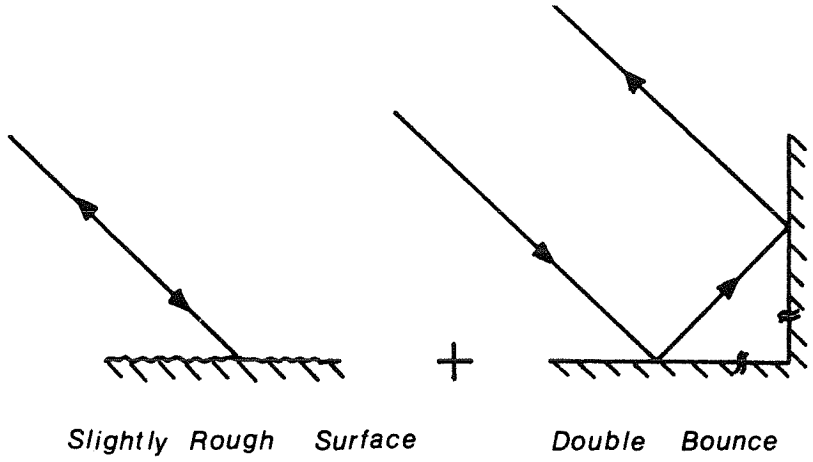

Figure 6.11. Model for scattering in urban areas.

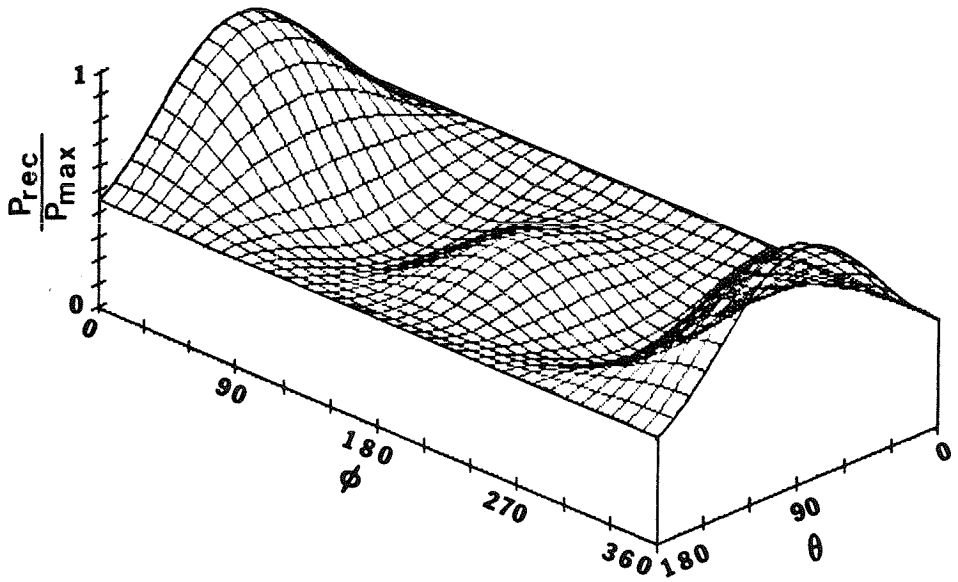

Figure 6.12. Polarization spectrum for model shown above.

have relative dielectric constants 6. The polarization spectrum of this scattering setup, assuming the power in the double-bounce wave is twice that of the wave reflected from the slightly rough surface, is shown in Figure 6.12. It is

clear that, apart from the offset caused by the variation in scattering properties, the polarization spectrum of the urban area exhibits the same behaviour as the polarization spectrum shown in Figure 6.12. This leads one to conclude that scattering in urban areas is dominated by double bounces.

In a similar way, it is possible to show that that the polarization spectrum of the park area is also a combination of the polarization spectrums of a slightly rough surface and that of a double bounce reflection. For the park areas, however, the double bounce reflections play a much smaller role than in the case of the urban areas.

At this point, a word of caution is in order. Since, as pointed out before, the polarization spectrum is not unique, it is conceivable that other combinations of scattering processes may also give spectrums which exhibit behaviours similar to that of the urban or park areas. When trying to explain the form of a polarization spectrum, one has to be careful in assuring that the explanatory processes chosen are physically possible for the area under consideration.

6.3 Conclusions.

In this chapter, some of the concepts introduced earlier were applied to real data. It is clear that the behaviour of all the parameters may be explained qualitatively, and all parameters were found to behave as expected. The polarization spectrum proved to be a valuable tool in deciding which scattering processes are important when different areas are imaged.

CHAPTER 7

CONCLUSIONS AND RECOMMENDATIONS.

In this thesis, the different characterizations of scatterers were discussed in detail. The problem of finding the polarizations that would yield an optimum amount of power received from the scatterer was solved for various different cases. It was shown that, in the most general case, six optimum polarizations may exist and not four as reported elsewhere in the literature.

The concept of a polarization spectrum was introduced and results, using real multipolarization synthetic aperture radar data, show the usefulness of this concept in understanding the scattering processes at work in radar imaging. Although this polarization spectrum concept was introduced with the same antenna used for transmission and reception, this is actually a very special case. Strictly speaking, one scatterer has infinitely many such polarization spectrums. For every transmit polarization, a spectrum may be calculated by varying the polarization of the receiving antenna. Although the same antenna is usually used for transmission and reception in practical radar systems, this limitation no longer exists when multipolarization synthetic aperture radar data are processed using digital computers.

In the same way, the definition of the coefficient of variation may be generalized. Instead of using the maximum and minimum powers in the spectrum when the same antenna is used for transmission and reception, one should use the absolute maximum and minimum amounts of power received from the scatterer when all possible polarizations are used for transmission and reception. When this is done for the areas shown in Table 6.1, the results shown in Table 7.1 are found.

TABLE 7.1 COMPARISON OF TEST AREAS.			
Area	Image	Label	Coef. of Var.
Ocean	San Francisco	a	.0085
Park	San Francisco	b	.2440
Urban	San Francisco	c	.1146
"Smooth" lava	Snake River Plain	d	.0293
Rough lava	Snake River Plain	e	.1001

This shows that the global coefficients of variation, which may be thought of as being proportional to the ratio of the diffuse- and coherent components of the received power, are much lower than the coefficient of variation calculated when the same antenna is used for transmission and reception. The results discussed in the previous chapter showed that the coefficient of variation may provide some information about the scale over which scattering properties vary in an area.

At present, no calibrated data are available for heavily vegetated areas. It is therefore not possible to compare the results of Chapter 4 with measured data. An image taken over the Raisin City area in California, which is an agricultural area, will be investigated in the near future and should provide the opportunity to compare the results of Chapter 4 with measured data.

In the introduction of Chapter 3 it was mentioned that it is hard to calculate multiple scattering results from the formulation given in that chapter. The results in Tables 6.1 and 7.1 seem to suggest that, at least for the five areas investigated, the diffuse component of the received power is fairly small. This would mean that multiple scattering is relatively unimportant in those areas

investigated. However, the only area with a reasonable amont of vegetation, the park area in the San Francisco image, has a diffuse component much larger than the other areas. This may suggest that multiple scattering may be important in heavily vegetated areas.

If it should prove to be necessary to calculate multiple scattering results, the well-known matrix addition and matrix doubling methods may be used [26],[27],[28],[29],[30]. It is easy to find the single scattering operators from the formulation given in Chapter 3. This single scattering operator is then used as an input to the matrix-doubling method to calculate the multiple scattering operator for a slab of arbitrary thickness. Finally, the matrix-addition method may be used to add a ground surface to the "vegetation" layer.

The results presented in this thesis clearly illustrate the importance of polarization in radar scattering problems. When the concepts started in this thesis are applied to the increasing volume of multipolarization synthetic aperture radar data, the present understanding of the scattering processes involved may be greatly improved.

APPENDIX A.

THE STOKES SCATTERING OPERATOR.

It will be assumed that the scatterer is characterized by a 2x2 bistatic scattering matrix as follows:

$$\begin{bmatrix} E_{x'}^{sc} \\ E_{y'}^{sc} \end{bmatrix} = \begin{bmatrix} S_{x'x} & S_{x'y} \\ S_{y'x} & S_{y'y} \end{bmatrix} \begin{bmatrix} E_x^{inc} \\ E_y^{inc} \end{bmatrix}. \tag{A-1}$$

It is easily shown that

$$\begin{bmatrix} E_{x'}^{sc}.E_{x'}^{sc*} \\ E_{y'}^{sc}.E_{y'}^{sc*} \\ E_{x'}^{sc}.E_{y'}^{sc*} \\ E_{y'}^{sc}.E_{x'}^{sc*} \end{bmatrix} = [\mathbf{W}] \begin{bmatrix} E_x^{rad}.E_x^{rad*} \\ E_y^{rad}.E_y^{rad*} \\ E_x^{rad}.E_y^{rad*} \\ E_y^{rad}.E_x^{rad*} \end{bmatrix}, \tag{A-2}$$

where

$$[\mathbf{W}] = \begin{bmatrix} S_{x'x}.S_{x'x}^{*} & S_{x'y}.S_{x'y}^{*} & S_{x'x}.S_{x'y}^{*} & S_{x'x}^{*}.S_{x'y} \\ S_{y'x}.S_{y'x}^{*} & S_{y'y}.S_{y'y}^{*} & S_{y'y}^{*}.S_{y'x} & S_{y'y}.S_{y'x}^{*} \\ S_{x'x}.S_{y'x}^{*} & S_{y'y}^{*}.S_{x'y} & S_{x'x}.S_{y'y}^{*} & S_{x'y}.S_{y'x}^{*} \\ S_{x'x}^{*}.S_{y'x} & S_{y'y}.S_{x'y}^{*} & S_{y'x}.S_{x'y}^{*} & S_{x'x}^{*}.S_{y'y} \end{bmatrix}. \tag{A-2a}$$

If the Stokes parameters of an electric field of the form

$$\mathbf{E}=\mathrm{Re}\left\{\left[E_x\mathbf{e}_x+E_y\mathbf{e}_y\right]e^{i(kr-\omega t)}\right\} \tag{A-3}$$

are defined to be

$$\begin{bmatrix} S_0 \\ S_1 \\ S_2 \\ S_3 \end{bmatrix} = \begin{bmatrix} E_x E_x^* + E_y E_y^* \\ E_x E_x^* - E_y E_y^* \\ 2\mathrm{Re}[E_x E_y^*] \\ 2\mathrm{Im}[E_x E_y^*] \end{bmatrix}, \tag{A-4}$$

it follows that one can write (A-4) as:

$$\mathbf{S(E)} = [\mathbf{R}]\mathbf{G(E)}\,, \tag{A-5}$$

where

$$[\mathbf{R}] \equiv \begin{bmatrix} 1 & 1 & 0 & 0 \\ 1 & -1 & 0 & 0 \\ 0 & 0 & 1 & 1 \\ 0 & 0 & -i & i \end{bmatrix} \tag{A-6}$$

and

$$\tilde{\mathbf{G}}\mathbf{(E)} = [\, E_x \cdot E_x^* \,;\, E_y \cdot E_y^* \,;\, E_x \cdot E_y^* \,;\, E_y \cdot E_x^* \,]\,. \tag{A-7}$$

Here, $\tilde{}$ means *transposed*. It then follows from (A-5) that

$$\mathbf{G(E)} = [\mathbf{R}]^{-1}\mathbf{S(E)}\,, \tag{A-8}$$

where

$$[\mathbf{R}]^{-1} = \tfrac{1}{2}\begin{bmatrix} 1 & 1 & 0 & 0 \\ 1 & -1 & 0 & 0 \\ 0 & 0 & 1 & i \\ 0 & 0 & 1 & -i \end{bmatrix}. \tag{A-9}$$

Using this notation, one may write:

$$\mathbf{G}(\mathbf{E}^{sc}) = [\mathbf{W}]\,\mathbf{G}(\mathbf{E}^{rad})\,, \tag{A-10}$$

where $[\mathbf{W}]$ is the 4x4 matrix in (A-2a). In Chapter 2 it is shown that

$$P_{rec} = K(\lambda,\vartheta,\varphi)\,|\mathbf{E}^{rad}\cdot\mathbf{E}^{sc}|^2\,. \tag{A-11}$$

Now, define

$$P'_{rec} \equiv (\mathbf{E}^{rad}.\mathbf{E}^{sc}).(\mathbf{E}^{rad}.\mathbf{E}^{sc})^* . \tag{A-12}$$

Expanding the right-hand side of (A-12), one finds

$$P'_{rec} = |E_x^{rad}.E_{x'}^{sc} + E_y^{rad}.E_{y'}^{sc}|^2$$

$$= \mathbf{G}(\mathbf{E}^{rad}).\mathbf{G}(\mathbf{E}^{sc})$$

$$= \tilde{\mathbf{G}}(\mathbf{E}^{rad})\,[\mathbf{W}]\,\mathbf{G}(\mathbf{E}^{rad})$$

$$= \tilde{\mathbf{S}}(\mathbf{E}^{rad})\,\widetilde{[\mathbf{R}]^{-1}}\,[\mathbf{W}]\,[\mathbf{R}]^{-1}\,\mathbf{S}(\mathbf{E}^{rad}) .$$

If it is now defined that

$$\mathbf{S}^{rad} = \mathbf{S}(\mathbf{E}^{rad}) \tag{A-13}$$

and

$$[\mathbf{M}] = \widetilde{[\mathbf{R}]^{-1}}\,[\mathbf{W}]\,[\mathbf{R}]^{-1} \tag{A-14}$$

it is clear that

$$P'_{rec} = |\mathbf{E}^{rad}.\mathbf{E}^{sc}|^2 = \mathbf{S}^{rad}.[\mathbf{M}]\mathbf{S}^{rad} \tag{A-15}$$

This 4x4 real matrix $[\mathbf{M}]$ will be called the Stokes Scattering Operator. If the matrix multiplication is carried out, the results shown in (2-17) are found.

APPENDIX B.

BISTATIC SCATTERING MATRIX OF A DIPOLE OF ARBITRARY ORIENTATION.

The scattering geometry to be considered is shown in Figure B.1.

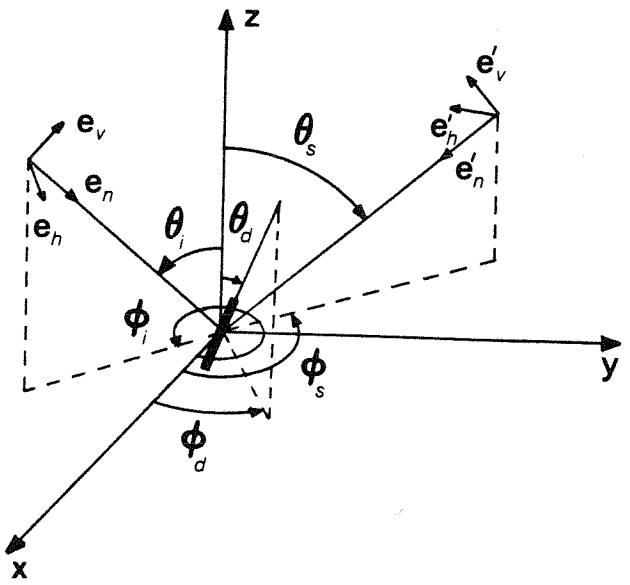

Figure B.1. Dipole of arbitrary orientation.

According to the definition in Chapter 3, the bistatic scattering matrix relates the scattered and incident electric fields in the following way:

$$\mathbf{E}^{sc}(\mathbf{r}) = [\mathbf{S}(\vartheta_i,\varphi_i,\vartheta_s,\varphi_s)]\, \mathbf{E}^{inc}(0)\, h(kr) \qquad \text{(B-1)}$$

where, as before,

$$h(kr) = \frac{e^{ikr}}{kr}. \qquad \text{(B-2)}$$

According to Figure B.1, the dipole may be described by:

$$\mathbf{p} = p\mathbf{e}_d$$

$$= p\,[\,\sin\vartheta_d\cos\varphi_d\,\mathbf{e}_x + \sin\vartheta_d\sin\varphi_d\,\mathbf{e}_y + \cos\vartheta_d\,\mathbf{e}_z\,]\,, \tag{B-3}$$

where p is the dipole moment of the dipole. The dipole moment created by an incident electric field, $\mathbf{E}^{inc}$, is given by [18],[19]:

$$\mathbf{p} = \varepsilon_0\chi_e(\mathbf{e}_d\cdot\mathbf{E}^{inc})\mathbf{e}_d \tag{B-4}$$

with χ_e the electric susceptibility of the material. The far-zone electric field radiated by this dipole is [18]:

$$\mathbf{E}^{sc} = \frac{k^2\,e^{ikr}}{4\pi\varepsilon_0 r}[(\mathbf{e}'_n\times\mathbf{p})\times\mathbf{e}'_n]\,. \tag{B-5}$$

Combining (B-4) and (B-5), one finds:

$$\mathbf{E}^{sc}(\mathbf{r}) = \frac{k^3\chi_e}{4\pi}[(\mathbf{e}'_n\times\mathbf{p})\times\mathbf{e}'_n]\,(\mathbf{e}_d\cdot\mathbf{E}^{inc})\,h(kr)\,. \tag{B-6}$$

It is easily shown, using some vector identities [20], that:

$$(\mathbf{e}'_n\times\mathbf{e}_d)\times\mathbf{e}'_n = \mathbf{e}_d - (\mathbf{e}'_n\cdot\mathbf{e}_d)\mathbf{e}'_n\,. \tag{B-7}$$

If this is expressed in the $\mathbf{e}'_h,\mathbf{e}'_v$ basis, one finds:

$$(\mathbf{e}'_n\times\mathbf{e}_d)\times\mathbf{e}'_n = (\mathbf{e}'_h\cdot\mathbf{e}_d)\mathbf{e}'_h + (\mathbf{e}'_v\cdot\mathbf{e}_d)\mathbf{e}'_v - (\mathbf{e}'_n\cdot\mathbf{e}_d)\mathbf{e}'_n \tag{B-8}$$

Using (B-8), (B-5) and (B-1), one finds that the elements of the scattering matrix are :

$$S_{h'h} = \frac{k^3\chi_e}{4\pi}W_i\,W_s \tag{B-9a}$$

$$S_{h'v} = \frac{k^3\chi_e}{4\pi}W_s\,Z_i \tag{B-9b}$$

$$S_{v'h} = \frac{k^3\chi_e}{4\pi}W_i\,Z_s \tag{B-9c}$$

$$S_{v'v} = \frac{k^3 \chi_e}{4\pi} Z_i Z_s , \tag{B-9d}$$

where

$$Z_x = \sin(\vartheta_x)\cos(\vartheta_d) - \cos(\varphi_d - \varphi_x)\sin(\vartheta_d)\cos(\vartheta_x) \tag{B-10a}$$

$$W_x = \sin(\vartheta_d)\sin(\varphi_d - \varphi_x) \tag{B-11b}$$

and x may be either i or s.

The effective area that this dipole exhibits to vertically polarized incident electric fields is, following the definition in [1]:

$$A_v(\vartheta_i,\varphi_i) = \frac{3\lambda^2}{8\pi} Z_i^2 . \tag{B-12}$$

This gives the attenuation constant for vertically polarized electric fields as:

$$\alpha_v^i = \frac{3\lambda^2}{16\pi} Z_i^2 . \tag{B-13a}$$

Similarly, the other attenuation constants are:

$$\alpha_v^s = \frac{3\lambda^2}{16\pi} Z_s^2 \tag{B-13b}$$

$$\alpha_h^i = \frac{3\lambda^2}{16\pi} W_i^2 \tag{B-13c}$$

$$\alpha_h^s = \frac{3\lambda^2}{16\pi} W_s^2 . \tag{B-13d}$$

APPENDIX C.

EFFECTIVE OPERATORS FOR A SLAB FILLED WITH CHIRAL OBJECTS.

As a chiral medium, a slab filled with small chiral objects as shown in Figure C.1 below, will be considered. It will be assumed that the chiral objects are spherically randomly oriented; i.e., all orientations are equally likely.

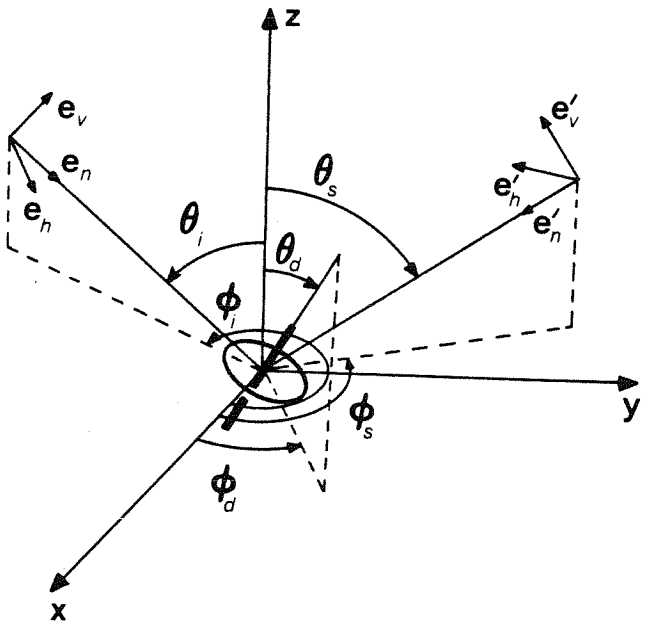

Figure C.1. Vectors indicating the directions and angles of incident and scattered waves and the orientation angles of the chiral object.

It is clear from Figure C.1 that:

$$\mathbf{e}_v = -\mathbf{e}_{\vartheta(\vartheta_i,\varphi_i)}$$

$$= -\cos(\vartheta_i)\cos(\varphi_i)\mathbf{e}_x - \cos(\vartheta_i)\sin(\varphi_i)\mathbf{e}_y + \sin(\vartheta_i)\mathbf{e}_z \qquad \text{(C-1a)}$$

$$\mathbf{e}_h = \mathbf{e}_{\varphi(\vartheta_i,\varphi_i)} = -\sin(\varphi_i)\mathbf{e}_x + \cos(\varphi_i)\mathbf{e}_y \qquad \text{(C-1b)}$$

$$\mathbf{e}'_v = -\mathbf{e}_{\vartheta(\vartheta_s,\varphi_s)}$$

$$= -\cos(\vartheta_s)\cos(\varphi_s)\mathbf{e}_x - \cos(\vartheta_s)\sin(\varphi_s)\mathbf{e}_y + \sin(\vartheta_s)\mathbf{e}_z \qquad \text{(C-1c)}$$

$$\mathbf{e}'_h = \mathbf{e}_{\varphi(\vartheta_s,\varphi_s)} = -\sin(\varphi_s)\mathbf{e}_x + \cos(\varphi_s)\mathbf{e}_y . \qquad \text{(C-1d)}$$

Now, in general, the incident plane wave has an electric field of the form:

$$\mathbf{E}^{inc} = [\, E_h\mathbf{e}_h + E_v\mathbf{e}_v \,]\, e^{-i(kr+\omega t)} , \qquad \text{(C-2a)}$$

and the magnetic filed of the incident plane wave may be expressed as [18]:

$$\mathbf{B}^{inc} = \frac{1}{c}(\, \mathbf{e}_n \times \mathbf{E}^{inc}) . \qquad \text{(C-2b)}$$

Here, c is the free-space velocity of light. This incident plane wave excites an electric and a magnetic dipole in the chiral object. In the limit where the chiral objects are small compared to the wavelength, these dipole moments are [18]:

$$\mathbf{p} = \varepsilon_0 [\, \chi_e(\mathbf{e}_d\cdot\mathbf{E}^{inc}) \pm i\chi_{em}c(\mathbf{e}_d\cdot\mathbf{B}^{inc}) \,]\mathbf{e}_d \equiv p\mathbf{e}_d \qquad \text{(C-3a)}$$

$$\mathbf{m} = -c\varepsilon_0 [\, \chi_m c(\mathbf{e}_d\cdot\mathbf{B}^{inc}) \pm i\chi_{me}(\mathbf{e}_d\cdot\mathbf{E}^{inc}) \,]\mathbf{e}_d \equiv m\mathbf{e}_d . \qquad \text{(C-3b)}$$

The upper (lower) signs correspond to the case of objects with right-handed (left-handed) chirality.

The electric field radiated by this combination is given by [18]:

$$\mathbf{E}^{sc}(\mathbf{r}) = \frac{k^3}{4\pi\varepsilon_0}[\, (\mathbf{e}'_n\times\mathbf{p})\times\mathbf{e}'_n + c^{-1}(\mathbf{e}'_n\times\mathbf{m}) \,]\frac{e^{ikr}}{kr} . \qquad \text{(C-4)}$$

It is easily shown that

$$(\mathbf{e}'_n \times \mathbf{e}_d) \times \mathbf{e}'_n = (\mathbf{e}'_h \cdot \mathbf{e}_d)\mathbf{e}'_h + (\mathbf{e}'_v \cdot \mathbf{e}_d)\mathbf{e}'_v - (\mathbf{e}'_n \cdot \mathbf{e}_d)\mathbf{e}'_n . \tag{C-5}$$

Thus, the transverse components of (C-4) may be written as:

$$\mathbf{E}^{sc}(\mathbf{r}) = \frac{k^3}{4\pi\varepsilon_0}\left\{ [(p\mathbf{e}_d + \frac{m}{c}\mathbf{e}'_n \times \mathbf{e}_d)\cdot \mathbf{e}'_h]\mathbf{e}'_h \right.$$

$$\left. + [(p\mathbf{e}_d + \frac{m}{c}\mathbf{e}'_n \times \mathbf{e}_d)\cdot \mathbf{e}'_v]\mathbf{e}'_v \right\} \frac{e^{ikr}}{kr} . \tag{C-6}$$

Going through some simple algebra, one finds that

$$\mathbf{e}_d \cdot \mathbf{e}'_h = \sin(\vartheta_d)\sin(\varphi_d - \varphi_s) \equiv W_s \tag{C-7a}$$

$$\mathbf{e}_d \cdot \mathbf{e}'_v = \sin(\vartheta_s)\cos(\vartheta_d) - \cos(\varphi_d - \varphi_s)\sin(\vartheta_d)\cos(\vartheta_s) \equiv Z_s \tag{C-7b}$$

$$(\mathbf{e}'_n \times \mathbf{e}_d)\cdot \mathbf{e}'_h = Z_s \tag{C-7c}$$

$$(\mathbf{e}'_n \times \mathbf{e}_d)\cdot \mathbf{e}'_v = -W_s . \tag{C-7d}$$

In the same way, it is easily shown that

$$\mathbf{p} = \varepsilon_0 \left\{ W_i[\chi_e E_h \pm i\chi_{em} E_v] + Z_i[\chi_e E_v - \pm i\chi_{em} E_h] \right\} \mathbf{e}_d \tag{C-8a}$$

$$\mathbf{m} = c\varepsilon_0 \left\{ W_i[-\chi_m E_v - \pm i\chi_{me} E_h] + Z_i[\chi_m E_h - \pm i\chi_{me} E_v] \right\} \mathbf{e}_d , \tag{C-8b}$$

where W_i and Z_i are given by (C-7a) and (C-7b), but with ϑ_s and φ_s replaced by ϑ_i and φ_i, respectively. Using (C-6), (C-7) and (C-8), the elements of the bistatic scattering matrix may be written as:

$$S_{h'h} = \frac{k^3}{4\pi}\left\{ [W_i W_s \chi_e + Z_i Z_s \chi_m] - \pm i[Z_i W_s \chi_{em} + W_i Z_s \chi_{me}] \right\} \tag{C-9a}$$

$$S_{v'h} = \frac{k^3}{4\pi}\left\{ [W_i Z_s \chi_e - Z_i W_s \chi_m] - \pm i[Z_i Z_s \chi_{em} - W_i W_s \chi_{me}] \right\} \quad \text{(C-9b)}$$

$$S_{h'v} = \frac{k^3}{4\pi}\left\{ [Z_i W_s \chi_e - W_i Z_s \chi_m] \pm i[W_i W_s \chi_{em} - Z_i Z_s \chi_{me}] \right\} \quad \text{(C-9c)}$$

$$S_{v'v} = \frac{k^3}{4\pi}\left\{ [Z_i Z_s \chi_e + W_i W_s \chi_m] \pm i[W_i Z_s \chi_{em} + Z_i W_s \chi_{me}] \right\}. \quad \text{(C-9d)}$$

It is easily seen that the results of appendix B is a special case of (C-9) with $\chi_m = \chi_{em} = \chi_{me} = 0$.

Using the definition of effective area as found in [1], it is found that the effective area may be written as:

$$A(\vartheta,\varphi) = \frac{\lambda^2 r^2 |\mathbf{E}^{rad}(\mathbf{r})|^2}{\int_0^{2\pi}\int_0^{\pi} |\mathbf{E}^{rad}(\mathbf{r})|^2 r^2 \sin(\vartheta)\, d\vartheta\, d\varphi}. \quad \text{(C-10)}$$

Since the amount of power radiated into all of space does not depend on the orientation of the chiral object, for the purpose of evaluating the integral in the denominator of (C-10) it will be assumed that the chiral object is oriented along the z-axis. From (C-6) and (C-7)

$$\mathbf{E}^{rad}(\mathbf{r}) = \frac{k^3}{4\pi\varepsilon_0}\left[p\sin(\vartheta)\mathbf{e}'_v - \frac{m}{c}\sin(\vartheta)\mathbf{e}'_h\right]\frac{e^{ikr}}{kr}. \quad \text{(C-11)}$$

Thus:

$$|\mathbf{E}^{rad}(\mathbf{r})|^2 = \left[\frac{k^2}{4\pi\varepsilon_0}\right]^2 \left[p^2 + \frac{m^2}{c^2}\right]\frac{\sin^2(\vartheta)}{r^2} \quad \text{(C-12)}$$

and

$$\int_0^{2\pi}\int_0^{\pi} r^2 |\mathbf{E}^{rad}(\mathbf{r})|^2 \sin(\vartheta)\, d\vartheta\, d\varphi = \frac{8\pi}{3}\left[\frac{k^2}{4\pi\varepsilon_0}\right]^2 [p^2+\frac{m^2}{c^2}] . \tag{C-13}$$

Using (C-13) in (C-11), one finds that

$$A(\vartheta,\varphi) = \frac{3\lambda^2}{8\pi}\left[\frac{4\pi\varepsilon_0}{k^2}\right]^2 \frac{r^2}{p^2+\frac{m^2}{c^2}} |\mathbf{E}^{rad}(\mathbf{r})|^2 . \tag{C-14}$$

Using the general result for $\mathbf{E}^{sc}$ given in (C-6), one finds:

$$A_v^x = \frac{3\lambda^2}{8\pi}\frac{1}{p^2+c^{-2}m^2}\left\{p^2 Z_x^2 + c^{-2}m^2 W_x^2 + \frac{mp}{c} W_x Z_x\right\} \tag{C-15a}$$

and

$$A_h^x = \frac{3\lambda^2}{8\pi}\frac{1}{p^2+c^{-2}m^2}\left\{p^2 W_x^2 + c^{-2}m^2 Z_x^2 + \frac{mp}{c} W_x Z_x\right\} , \tag{C-15b}$$

where x may be either i or s. The average effective areas are:

$$\langle A_y^x \rangle = \frac{1}{4\pi}\int_0^{2\pi}\int_0^{\pi} A_y^x \sin(\vartheta_d)\, d\vartheta_d\, d\varphi_d , \tag{C-16}$$

where y may be either v or h. Now,

$$\int_0^{2\pi}\int_0^{\pi} W_x^2 \sin(\vartheta_d)\, d\vartheta_d\, d\varphi_d = \frac{4}{3}\pi \tag{C-17a}$$

$$\int_0^{2\pi}\int_0^{\pi} Z_x^2 \sin(\vartheta_d)\, d\vartheta_d\, d\varphi_d = \frac{4}{3}\pi \tag{C-17b}$$

$$\int_0^{2\pi}\int_0^{\pi} Z_x W_x \sin(\vartheta_d)\, d\vartheta_d\, d\varphi_d = 0. \tag{C-17c}$$

Thus, the average attenuation constants are:

$$\langle \alpha_v^i \rangle = \langle \alpha_v^s \rangle = \langle \alpha_h^i \rangle = \langle \alpha_h^s \rangle = \frac{\lambda^2}{16\pi} . \tag{C-18}$$

In order to calculate the effective scattering operators, the following integrals are listed first:

$$\frac{1}{4\pi}\int_0^{2\pi}\int_0^{\pi} W_i W_s \sin(\vartheta_d)\, d\vartheta_d\, d\varphi_d = \frac{1}{3}\cos(\varphi_s-\varphi_i) \qquad \text{(C-19a)}$$

$$\frac{1}{4\pi}\int_0^{2\pi}\int_0^{\pi} W_i Z_s \sin(\vartheta_d)\, d\vartheta_d\, d\varphi_d = \frac{1}{3}\cos(\vartheta_s)\sin(\varphi_s-\varphi_i) \qquad \text{(C-19b)}$$

$$\frac{1}{4\pi}\int_0^{2\pi}\int_0^{\pi} W_s Z_i \sin(\vartheta_d)\, d\vartheta_d\, d\varphi_d = \frac{1}{3}\cos(\vartheta_i)\sin(\varphi_i-\varphi_s) \qquad \text{(C-19c)}$$

$$\frac{1}{4\pi}\int_0^{2\pi}\int_0^{\pi} Z_s Z_i \sin(\vartheta_d)\, d\vartheta_d\, d\varphi_d = \frac{1}{3} Z_{is} \qquad \text{(C-19d)}$$

$$\frac{1}{4\pi}\int_0^{2\pi}\int_0^{\pi} W_i^2 W_s^2 \sin(\vartheta_d)\, d\vartheta_d\, d\varphi_d = \frac{1}{15}[1+2\cos^2(\varphi_s-\varphi_i)] \qquad \text{(C-19e)}$$

$$\frac{1}{4\pi}\int_0^{2\pi}\int_0^{\pi} Z_i^2 Z_s^2 \sin(\vartheta_d)\, d\vartheta_d\, d\varphi_d = \frac{1}{15}[1+2Z_{is}^2] \qquad \text{(C-19f)}$$

$$\frac{1}{4\pi}\int_0^{2\pi}\int_0^{\pi} W_i^2 Z_s^2 \sin(\vartheta_d)\, d\vartheta_d\, d\varphi_d = \frac{1}{15}[1+2\sin^2(\varphi_s-\varphi_i)\cos^2(\vartheta_s)] \qquad \text{(C-19g)}$$

$$\frac{1}{4\pi}\int_0^{2\pi}\int_0^{\pi} Z_i^2 W_s^2 \sin(\vartheta_d)\, d\vartheta_d\, d\varphi_d = \frac{1}{15}[1+2\sin^2(\varphi_s-\varphi_i)\cos^2(\vartheta_i)] \qquad \text{(C-19h)}$$

$$\frac{1}{4\pi}\int_0^{2\pi}\int_0^{\pi} W_i W_s Z_i Z_s \sin(\vartheta_d)\, d\vartheta_d\, d\varphi_d = \frac{1}{15} Q_{is} \qquad \text{(C-19i)}$$

$$\frac{1}{4\pi}\int_0^{2\pi}\int_0^{\pi} W_i W_s^2 Z_i \sin(\vartheta_d)\, d\vartheta_d\, d\varphi_d = \frac{1}{15}\cos(\vartheta_i)\sin(2\varphi_s-2\varphi_i) \qquad \text{(C-19j)}$$

$$\frac{1}{4\pi}\int_0^{2\pi}\int_0^{\pi} W_i^2 W_s Z_s \sin(\vartheta_d)\, d\vartheta_d\, d\varphi_d = \frac{1}{15}\cos(\vartheta_s)\sin(2\varphi_i-2\varphi_s) \qquad \text{(C-19k)}$$

$$\frac{1}{4\pi}\int_0^{2\pi}\int_0^{\pi} W_i Z_i Z_s^2 \sin(\vartheta_d)\, d\vartheta_d\, d\varphi_d = \frac{2}{15}\sin(\varphi_i-\varphi_s)\cos(\vartheta_s) Z_{is} \qquad \text{(C-19l)}$$

$$\frac{1}{4\pi}\int_0^{2\pi}\int_0^{\pi} Z_i^2 W_s Z_s \sin(\vartheta_d)\, d\vartheta_d\, d\varphi_d = \frac{2}{15}\sin(\varphi_s-\varphi_i)\cos(\vartheta_i) Z_{is} \qquad \text{(C-19m)}$$

with

$$Z_{is} = \sin(\vartheta_i)\sin(\vartheta_s)+\cos(\varphi_s-\varphi_i)\cos(\vartheta_s)\cos(\vartheta_i) \qquad \text{(C-19n)}$$

$$Q_{is} = \cos(\vartheta_i)\cos(\vartheta_s)\cos2(\varphi_i-\varphi_s)+\sin(\vartheta_i)\sin(\vartheta_s)\cos(\varphi_s-\varphi_i)\,. \qquad \text{(C-19o)}$$

Using these, it is now easily shown that:

$$\langle S_{h'h}\rangle = \frac{k^3}{12\pi}\Big\{[\cos(\varphi_s-\varphi_i)\chi_e + Z_{is}\chi_m]$$

$$- \pm i[\cos(\vartheta_i)\sin(\varphi_i-\varphi_s)\chi_{em} + \cos(\vartheta_s)\sin(\varphi_s-\varphi_i)\chi_{me}]\Big\} \qquad \text{(C-20a)}$$

$$\langle S_{v'h}\rangle = \frac{k^3}{12\pi}\Big\{[\cos(\vartheta_s)\sin(\varphi_s-\varphi_i)\chi_e - \cos(\vartheta_i)\sin(\varphi_i-\varphi_s)\chi_m]$$

$$- \pm i[Z_{is}\chi_{em} - \cos(\varphi_s-\varphi_i)\chi_{me}]\Big\} \qquad \text{(C-20b)}$$

$$\langle S_{h'v}\rangle = \frac{k^3}{12\pi}\Big\{[\cos(\vartheta_i)\sin(\varphi_i-\varphi_s)\chi_e - \cos(\vartheta_s)\sin(\varphi_s-\varphi_i)\chi_m]$$

$$\pm i[\cos(\varphi_s-\varphi_i)\chi_{em} - Z_{is}\chi_{me}]\Big\} \qquad \text{(C-20c)}$$

$$\langle S_{v'v}\rangle = \frac{k^3}{12\pi}\Big\{[Z_{is}\chi_e + \cos(\varphi_s-\varphi_i)\chi_m]$$

$$\pm i[\cos(\vartheta_s)\sin(\varphi_s-\varphi_i)\chi_{em} + \cos(\vartheta_i)\sin(\varphi_i-\varphi_s)\chi_{me}]\Big\} \qquad \text{(C-20d)}$$

and

$$\langle|S_{h'h}|^2\rangle = \left(\frac{k^3}{4\pi}\right)^2\frac{1}{15}\Big\{\chi_e^2[1+2\cos^2(\varphi_s-\varphi_i)] + \chi_m^2[1+2Z_{is}^2]$$

$$+ \chi_{em}^2[1+2\sin^2(\varphi_s-\varphi_i)\cos^2(\vartheta_i)] + \chi_{me}^2[1+2\sin^2(\varphi_s-\varphi_i)\cos^2(\vartheta_s)]$$

$$+ \; 2[\chi_e\chi_m+\chi_{em}\chi_{me}]Q_{is} \Big\} \qquad \text{(C-21a)}$$

$$\langle|S_{h'v}|^2\rangle = \left(\frac{k^3}{4\pi}\right)^2 \frac{1}{15}\Big\{\chi_e^2[1+2\sin^2(\varphi_s-\varphi_i)\cos^2(\vartheta_i)]$$

$$+ \chi_m^2[1+2\sin^2(\varphi_s-\varphi_i)\cos^2(\vartheta_s)] + \chi_{em}^2[1+2\cos^2(\varphi_s-\varphi_i)]$$

$$+ \chi_{me}^2[1+2Z_{is}^2] - 2[\chi_e\chi_m+\chi_{em}\chi_{me}]Q_{is} \Big\} \qquad \text{(C-21b)}$$

$$\langle|S_{v'h}|^2\rangle = \left(\frac{k^3}{4\pi}\right)^2 \frac{1}{15}\Big\{\chi_e^2[1+2\sin^2(\varphi_s-\varphi_i)\cos^2(\vartheta_s)]$$

$$+ \chi_m^2[1+2\sin^2(\varphi_s-\varphi_i)\cos^2(\vartheta_i)] + \chi_{me}^2[1+2\cos^2(\varphi_s-\varphi_i)]$$

$$+ \chi_{em}^2[1+2Z_{is}^2] - 2[\chi_e\chi_m+\chi_{em}\chi_{me}]Q_{is} \Big\} \qquad \text{(C-21c)}$$

$$\langle|S_{v'v}|^2\rangle = \left(\frac{k^3}{4\pi}\right)^2 \frac{1}{15}\Big\{\chi_e^2[1+Z_{is}^2] + \chi_m^2[1+2\cos^2(\varphi_s-\varphi_i)]$$

$$+ \chi_{em}^2[1+2\sin^2(\varphi_s-\varphi_i)\cos^2(\vartheta_s)] + \chi_{me}^2[1+2\sin^2(\varphi_s-\varphi_i)\cos^2(\vartheta_i)]$$

$$+ \; 2[\chi_e\chi_m+\chi_{em}\chi_{me}]Q_{is} \Big\} \qquad \text{(C-21d)}$$

$$\mathrm{Re}[\langle S_{h'h}^* S_{h'v}\rangle] = \left(\frac{k^3}{4\pi}\right)^2 \frac{2}{15}\Big\{[\chi_e^2-\chi_{em}^2]\cos(\vartheta_i)\sin(\varphi_s-\varphi_i)\cos(\varphi_s-\varphi_i)$$

$$- \; [\chi_m^2-\chi_{me}^2]\sin(\varphi_i-\varphi_s)\cos(\vartheta_s)Z_{is}$$

$$- [\chi_e\chi_m+\chi_{em}\chi_{me}]\sin(\varphi_s-\varphi_i)V_{is}\Big\} \qquad \text{(C-21e)}$$

$$\mathrm{Im}[\langle S^*_{h'h}S_{h'v}\rangle] = \pm\left(\frac{k^3}{4\pi}\right)^2\frac{2}{15}\Big\{\chi_e\chi_{em}[1+\cos^2(\varphi_s-\varphi_i)+\sin^2(\varphi_s-\varphi_i)\cos^2(\vartheta_i)]$$

$$- \chi_m\chi_{me}[1+\sin^2(\varphi_s-\varphi_i)\cos^2(\vartheta_s)+Z^2_{is}]\Big\} \qquad \text{(C-21f)}$$

$$\mathrm{Re}[\langle S^*_{h'h}S_{v'h}\rangle] = \left(\frac{k^3}{4\pi}\right)^2\frac{2}{15}\Big\{[\chi_e^2-\chi_{me}^2]\cos(\vartheta_s)\sin(\varphi_i-\varphi_s)\cos(\varphi_s-\varphi_i)$$

$$+ [\chi_{em}^2-\chi_m^2]\sin(\varphi_s-\varphi_i)\cos(\vartheta_i)Z_{is}$$

$$+ [\chi_e\chi_m+\chi_{em}\chi_{me}]\sin(\varphi_i-\varphi_s)V_{si}\Big\} \qquad \text{(C-21g)}$$

$$\mathrm{Im}[\langle S^*_{h'h}S_{v'h}\rangle] = \pm\left(\frac{k^3}{4\pi}\right)^2\frac{2}{15}\Big\{\chi_e\chi_{me}[1+\cos^2(\varphi_s-\varphi_i)+\sin^2(\varphi_s-\varphi_i)\cos^2(\vartheta_s)]$$

$$- \chi_m\chi_{em}[1+\sin^2(\varphi_s-\varphi_i)\cos^2(\vartheta_i)+Z^2_{is}]\Big\} \qquad \text{(C-21h)}$$

$$\mathrm{Re}[\langle S_{v'v}S^*_{h'v}\rangle] = \left(\frac{k^3}{4\pi}\right)^2\frac{2}{15}\Big\{[\chi_e^2-\chi_{me}^2]\cos(\vartheta_i)\sin(\varphi_s-\varphi_i)Z_{is}$$

$$+ [\chi_{em}^2-\chi_m^2]\sin(\varphi_i-\varphi_s)\cos(\vartheta_s)\cos(\varphi_s-\varphi_i)$$

$$+ [\chi_e\chi_m+\chi_{em}\chi_{me}]\sin(\varphi_s-\varphi_i)V_{si}\Big\} \qquad \text{(C-21i)}$$

$$\mathrm{Im}[\langle S_{v'v}S^*_{h'v}\rangle] = \pm\left(\frac{k^3}{4\pi}\right)^2\frac{2}{15}\Big\{\chi_e\chi_{me}[1+\sin^2(\varphi_s-\varphi_i)\cos^2(\vartheta_i)+Z^2_{is}]$$

$$- \chi_m\chi_{em}[1+\cos^2(\varphi_s-\varphi_i)+\sin^2(\varphi_s-\varphi_i)\cos^2(\vartheta_s)]\Big\} \qquad \text{(C-21j)}$$

$$\mathrm{Re}[\langle S_{v'v}S^*_{v'h}\rangle] = \left(\frac{k^3}{4\pi}\right)^2 \frac{2}{15}\Big\{[\chi_e^2-\chi_{em}^2]\cos(\vartheta_s)\sin(\varphi_i-\varphi_s)Z_{is}$$

$$+ [\chi_{me}^2-\chi_m^2]\sin(\varphi_s-\varphi_i)\cos(\vartheta_i)\cos(\varphi_s-\varphi_i)$$

$$- [\chi_e\chi_m+\chi_{em}\chi_{me}]\sin(\varphi_i-\varphi_s)V_{is}\Big\} \qquad \text{(C-21k)}$$

$$\mathrm{Im}[\langle S_{v'v}S^*_{v'h}\rangle] = \pm\left(\frac{k^3}{4\pi}\right)^2 \frac{2}{15}\Big\{\chi_e\chi_{em}[1+\sin^2(\varphi_s-\varphi_i)\cos^2(\vartheta_s)+Z_{is}^2]$$

$$- \chi_m\chi_{me}[1+\cos^2(\varphi_s-\varphi_i)+\sin^2(\varphi_s-\varphi_i)\cos^2(\vartheta_i)]\Big\} \qquad \text{(C-21l)}$$

$$\mathrm{Re}[\langle S_{v'v}S^*_{h'h}\rangle] = \left(\frac{k^3}{4\pi}\right)^2 \frac{1}{15}\Big\{[\chi_e^2-\chi_{em}^2+\chi_m^2-\chi_{me}^2]Q_{is}$$

$$+ 2\chi_e\chi_m[1+\cos^2(\varphi_s-\varphi_i)+Z_{is}^2]$$

$$- 2\chi_{em}\chi_{me}[1+\sin^2(\varphi_s-\varphi_i)(\cos^2(\vartheta_s)+\cos^2(\vartheta_i))]\Big\} \qquad \text{(C-21m)}$$

$$\mathrm{Im}[\langle S_{v'v}S^*_{h'h}\rangle] = \pm\left(\frac{k^3}{4\pi}\right)^2 \frac{2}{15}\Big\{[\chi_e\chi_{em}+\chi_m\chi_{me}]\sin(\varphi_s-\varphi_i)U_{is}$$

$$+ [\chi_e\chi_{me}+\chi_m\chi_{em}]\sin(\varphi_i-\varphi_s)U_{si}\Big\} \qquad \text{(C-21n)}$$

$$\mathrm{Re}[\langle S_{v'h}S^*_{h'v}\rangle] = \left(\frac{k^3}{4\pi}\right)^2 \frac{1}{15}\Big\{[\chi_e^2-\chi_{em}^2+\chi_m^2-\chi_{me}^2]Q_{is}$$

$$- 2\chi_e\chi_m[1+\sin^2(\varphi_s-\varphi_i)(\cos^2(\vartheta_s)+\cos^2(\vartheta_i))]$$

$$+ 2\chi_{em}\chi_{me}[1+\cos^2(\varphi_s-\varphi_i)+Z_{is}^2]\Big\} \qquad \text{(C-21o)}$$

$$\mathrm{Im}[\langle S_{v'h}S_{h'v}^{*}\rangle] = \pm\left(\frac{k^3}{4\pi}\right)^2\frac{2}{15}\Big\{[\chi_e\chi_{em}+\chi_m\chi_{me}]\sin(\varphi_s-\varphi_i)U_{is}$$

$$- [\chi_e\chi_{me}+\chi_m\chi_{em}]\sin(\varphi_i-\varphi_s)U_{si}\Big\}, \qquad \text{(C-21p)}$$

where

$$V_{is} = \cos(\vartheta_i)\sin(\vartheta_i)\sin(\vartheta_s)+\cos(\varphi_s-\varphi_i)\cos(\vartheta_s)[\cos^2(\vartheta_i)+1]$$

$$V_{si} = \cos(\vartheta_s)\sin(\vartheta_i)\sin(\vartheta_s)+\cos(\varphi_s-\varphi_i)\cos(\vartheta_i)[\cos^2(\vartheta_s)+1]$$

$$U_{is} = \cos(\vartheta_i)\sin(\vartheta_i)\sin(\vartheta_s)+\cos(\varphi_s-\varphi_i)\cos(\vartheta_s)[\cos^2(\vartheta_i)-1]$$

$$U_{si} = \cos(\vartheta_s)\sin(\vartheta_i)\sin(\vartheta_s)+\cos(\varphi_s-\varphi_i)\cos(\vartheta_i)[\cos^2(\vartheta_s)-1].$$

The use of these expressions, together with the results of Chapter 3 now allows one to calculate the effective bistatic scattering operators for the slab filled with the small chiral objects.

Again, it is clear that if $\chi_m = \chi_{em} = \chi_{me} = 0$ are used in (C-20) and (C-21), the results are the same as that of appendix B.

APPENDIX D.

OPTIMUM POLARIZATIONS WHEN TWO ANTENNAS ARE USED.

In this appendix, the general problem of finding the optimum polarizations for power reception from a scatterer when two different antennas are used for transmission and reception, will be considered. While it may not be practical to use two different antennas in a radar instrument, there is no reason why only one "antenna" should be used when the measured results are processed in a computer.

In order to solve this problem, the Stokes Scattering Operator of the scatterer is written as:

$$[\mathbf{M}] = \begin{bmatrix} M_{11} & \tilde{\mathbf{v}} \\ \mathbf{u} & [\mathbf{Q}] \end{bmatrix}, \tag{D-1}$$

where $\mathbf{u}$ and $\mathbf{v}$ are vectors with three coefficients and $[\mathbf{Q}]$ is a 3x3 matrix. To optimize the amount of power received from the scatterer, one must consider the function

$$F(\mathbf{y},\mathbf{x}) = \begin{bmatrix} 1 \\ y_1 \\ y_2 \\ y_3 \end{bmatrix} \cdot \begin{bmatrix} M_{11} & \tilde{\mathbf{v}} \\ \mathbf{u} & [\mathbf{Q}] \end{bmatrix} \begin{bmatrix} 1 \\ x_1 \\ x_2 \\ x_3 \end{bmatrix}. \tag{D-2}$$

Since both $\mathbf{x}$ and $\mathbf{y}$ are Stokes vectors, they must satisfy

$$\mathbf{x}\cdot\mathbf{x} = \begin{bmatrix} x_1 \\ x_2 \\ x_3 \end{bmatrix} \cdot \begin{bmatrix} x_1 \\ x_2 \\ x_3 \end{bmatrix} = 1. \tag{D-3a}$$

and

$$\mathbf{y}\cdot\mathbf{y} = \begin{bmatrix} y_1 \\ y_2 \\ y_3 \end{bmatrix} \cdot \begin{bmatrix} y_1 \\ y_2 \\ y_3 \end{bmatrix} = 1. \qquad \text{(D-3b)}$$

Lagrange Multiplier Method: To solve this problem with this method, the auxiliary function $G(\mathbf{y},\mathbf{x})$ is formed

$$G(\mathbf{y},\mathbf{x}) = M_{11} + \mathbf{v}\cdot\mathbf{x} + \mathbf{u}\cdot\mathbf{y} + \mathbf{y}\cdot[\mathbf{Q}]\mathbf{x} + \nu(1-\mathbf{x}\cdot\mathbf{x}) + \mu(1-\mathbf{y}\cdot\mathbf{y}) . \qquad \text{(D-4)}$$

It is then required that

$$\frac{\partial G(\mathbf{y},\mathbf{x})}{\partial x_i} = 0. \quad ; \quad \frac{\partial G(\mathbf{y},\mathbf{x})}{\partial y_i} = 0. \quad ; \quad i=1,2,3 . \qquad \text{(D-5)}$$

Performing these differentiations, one finds that the optimum polarizations are the solutions to

$$[\tilde{\mathbf{Q}}]\mathbf{y} + \mathbf{v} = 2\nu\mathbf{x} \qquad \text{(D-6a)}$$

and

$$[\mathbf{Q}]\mathbf{x} + \mathbf{u} = 2\mu\mathbf{y} . \qquad \text{(D-6b)}$$

Here, $\tilde{}$ means *transposed*. If (D-6a) is multiplied by $[\mathbf{Q}]$ and the results of (D-6b) are used, one finds:

$$[\mathbf{Q}\tilde{\mathbf{Q}} - 4\mu\nu\mathbf{I}]\mathbf{y} = -[\mathbf{Q}]\mathbf{v} - 2\nu\mathbf{u} , \qquad \text{(D-7)}$$

where I is the 3x3 identity matrix. Similarly, one finds for $\mathbf{x}$ that

$$[\tilde{\mathbf{Q}}\mathbf{Q} - 4\mu\nu\mathbf{I}]\mathbf{x} = -[\tilde{\mathbf{Q}}]\mathbf{u} - 2\mu\mathbf{v} . \qquad \text{(D-8)}$$

If $4\mu\nu$ is not an eigenvalue of either $[\tilde{\mathbf{Q}}\mathbf{Q}]$ or $[\mathbf{Q}\tilde{\mathbf{Q}}]$, both (D-7) and (D-8) have unique solutions given by:

$$\mathbf{x} = -[\tilde{\mathbf{Q}}\mathbf{Q} - 4\mu\nu\mathbf{I}]^{-1}([\tilde{\mathbf{Q}}]\mathbf{u} + 2\mu\mathbf{v}) \qquad \text{(D-9a)}$$

$$\mathbf{y} = -[\mathbf{Q}\tilde{\mathbf{Q}} - 4\mu\nu\mathbf{I}]^{-1}([\mathbf{Q}]\mathbf{v} + 2\nu\mathbf{u}) . \qquad \text{(D-9b)}$$

Thus, once the values of μ and ν are known, both **x** and **y** can be found. To find the values of μ and ν, one uses the conditions given in (D-3). This would give two non-linear equations in the two unknowns μ and ν. Once the solutions of these two non-linear equations are known, the problem is essentially solved.

If both **u** and **v** are zero, it follows that the optimum polarizations **x** and **y** are the eigenvectors of $[\tilde{\mathbf{Q}}\mathbf{Q}]$ and $[\mathbf{Q}\tilde{\mathbf{Q}}]$, respectively.

Direct Method: The direct method, as in Chapter 2, involves realizing that **x** and **y** may be written as:

$$\mathbf{x} = \begin{bmatrix} \cos(\varphi_x)\sin(\vartheta_x) \\ \sin(\varphi_x)\sin(\vartheta_x) \\ \cos(\vartheta_x) \end{bmatrix} \tag{D-10a}$$

$$\mathbf{y} = \begin{bmatrix} \cos(\varphi_y)\sin(\vartheta_y) \\ \sin(\varphi_y)\sin(\vartheta_y) \\ \cos(\vartheta_y) \end{bmatrix}. \tag{D-10b}$$

Using these in (D-2) and taking the partial derivatives of $F(\mathbf{y},\mathbf{x})$ with respect to $\varphi_x, \varphi_y, \vartheta_x$ and ϑ_y, one finds that the angles of the optimum polarization vectors are the solutions to the following four non-linear equations:

$$\begin{aligned} &[M_{23}\cos(\varphi_y)+M_{33}\sin(\varphi_y)]\cos(\varphi_x)\sin(\vartheta_y) \\ &-[M_{22}\cos(\varphi_y)+M_{32}\sin(\varphi_y)]\sin(\varphi_x)\sin(\vartheta_y) \\ &+M_{13}\cos(\varphi_x)-M_{12}\sin(\varphi_x)+[M_{43}\cos(\varphi_x)-M_{42}\sin(\varphi_x)]\cos(\vartheta_y) = 0. \end{aligned} \tag{D-11a}$$

$$\begin{aligned} &[M_{32}\cos(\varphi_x)+M_{33}\sin(\varphi_x)]\cos(\varphi_y)\sin(\vartheta_x) \\ &-[M_{22}\cos(\varphi_x)+M_{23}\sin(\varphi_x)]\sin(\varphi_y)\sin(\vartheta_x) \end{aligned}$$

$$+M_{31}\cos(\varphi_y)-M_{21}\sin(\varphi_y)+[M_{34}\cos(\varphi_y)-M_{24}\sin(\varphi_y)]\cos(\vartheta_x) = 0. \qquad \text{(D-11b)}$$

$$[M_{12}\cos(\varphi_x)+M_{13}\sin(\varphi_x)]\cos(\vartheta_x)-M_{14}\sin(\vartheta_x)$$

$$+[M_{22}\cos(\varphi_y)+M_{32}\sin(\varphi_y)]\cos(\varphi_x)\sin(\vartheta_y)\cos(\vartheta_x)$$

$$+[M_{23}\cos(\varphi_y)+M_{33}\sin(\varphi_y)]\sin(\varphi_x)\sin(\vartheta_y)\cos(\vartheta_x)$$

$$-[[M_{24}\cos(\varphi_y)+M_{34}\sin(\varphi_y)]\sin(\vartheta_y)+M_{44}\cos(\vartheta_y)]\sin(\vartheta_x)$$

$$+ [M_{42}\cos(\varphi_x)+M_{43}\sin(\varphi_x)]\cos(\vartheta_x)\cos(\vartheta_y) = 0. \qquad \text{(D-11c)}$$

$$[M_{21}\cos(\varphi_y)+M_{31}\sin(\varphi_y)]\cos(\vartheta_y)-M_{41}\sin(\vartheta_y)$$

$$+[M_{22}\cos(\varphi_x)+M_{23}\sin(\varphi_x)]\cos(\varphi_y)\sin(\vartheta_x)\cos(\vartheta_y)$$

$$+[M_{32}\cos(\varphi_x)+M_{33}\sin(\varphi_x)]\sin(\varphi_y)\sin(\vartheta_x)\cos(\vartheta_y)$$

$$-[[M_{42}\cos(\varphi_x)+M_{43}\sin(\varphi_x)]\sin(\vartheta_x)+M_{44}\cos(\vartheta_x)]\sin(\vartheta_y)$$

$$+ [M_{24}\cos(\varphi_y)+M_{34}\sin(\varphi_y)]\cos(\vartheta_x)\cos(\vartheta_y) = 0. \qquad \text{(D-11d)}$$

The problem of finding the optimum polarizations, using two antennas to discriminate between two scatterers, has been solved by Ioannidis and Hammers [12] and will not be considered here.

ORTHOGONALLY POLARIZED ANTENNAS. One special case where two "antennas" may be used will be discussed in more detail. In this case, the two "antennas" are orthogonally polarized. It is easily shown [2] that, in this case,

$$\mathbf{y} = -\mathbf{x} . \tag{D-12}$$

Lagrange Multiplier Method. The function $G(\mathbf{y},\mathbf{x})$ for these cross-polarized "antennas" is

$$G_c(\mathbf{x}) = M_{11} + \mathbf{v}\cdot\mathbf{x} - \mathbf{u}\cdot\mathbf{x} - \mathbf{x}\cdot[\mathbf{Q}]\mathbf{x} + \nu(1-\mathbf{x}\cdot\mathbf{x}) . \tag{D-13}$$

It is then required that

$$\frac{\partial G_c(\mathbf{x})}{\partial x_i} = 0. \quad ; \quad i=1,2,3 . \tag{D-14}$$

It is then easily shown that the optimum polarizations are the solutions to

$$[\tfrac{1}{2}\mathbf{Q}+\tfrac{1}{2}\tilde{\mathbf{Q}}+\nu\mathbf{I}]\mathbf{x} = \tfrac{1}{2}\mathbf{v}-\tfrac{1}{2}\mathbf{u} . \tag{D-15}$$

If $-\nu$ is not an eigenvalue of $\frac{1}{2}[\mathbf{Q}+\tilde{\mathbf{Q}}]$, then (D-15) has a unique solution, given by

$$\mathbf{x} = \tfrac{1}{2}[\tfrac{1}{2}\mathbf{Q}+\tfrac{1}{2}\tilde{\mathbf{Q}}+\nu\mathbf{I}]^{-1}(\mathbf{v}-\mathbf{u}) . \tag{D-16}$$

To find the values of ν that may be used in (D-16), one uses the condition

$$\mathbf{x}\cdot\mathbf{x} = 1. \tag{D-17}$$

The result of this is that the values of ν that may be used in (D-16) are the real roots of

$$p(\nu) = \nu^6 + d_1\nu^5 + d_2\nu^4 + d_3\nu^3 + d_4\nu^2 + d_5\nu + d_6 = 0, \tag{D-18}$$

where

$$d_1 = 2c_1 \tag{D-19a}$$

$$d_2 = c_1^2 - q_{01}^2 - q_{02}^2 - q_{03}^2 + 2c_2 \tag{D-19b}$$

$$d_3 = 2[c_1c_2 - q_{01}q_{11} - q_{02}q_{12} - q_{03}q_{13} + c_3] \tag{D-19c}$$

$$d_4 = c_2^2 - q_{11}^2 - q_{12}^2 - q_{13}^2 + 2[c_1c_3 - q_{01}q_{21} - q_{02}q_{22} - q_{03}q_{23}] \tag{D-19d}$$

$$d_5 = 2[c_2c_3 - q_{11}q_{21} - q_{12}q_{22} - q_{13}q_{23}] \qquad \text{(D-19e)}$$

$$d_6 = c_3^2 - q_{21}^2 - q_{22}^2 - q_{23}^2 \qquad \text{(D-19f)}$$

and

$$c_1 = M_{22} + M_{33} + M_{44}$$

$$c_2 = -\frac{1}{4}\left[(M_{23}+M_{32})^2 + (M_{24}+M_{42})^2 + (M_{34}+M_{43})^2\right]$$

$$+M_{33}M_{44} + M_{22}M_{33} + M_{22}M_{44}$$

$$c_3 = M_{22}M_{33}M_{44} + \frac{1}{4}\left[(M_{23}+M_{32})(M_{24}+M_{42})(M_{34}+M_{43})\right.$$

$$\left. -M_{22}(M_{34}+M_{43})^2 - M_{33}(M_{24}+M_{42})^2 - M_{44}(M_{23}+M_{32})^2\right]$$

$$q_{01} = \tfrac{1}{2}(M_{12} - M_{21})$$

$$q_{11} = -\frac{1}{4}\left[(M_{13}-M_{31})(M_{23}+M_{32}) + (M_{14}-M_{41})(M_{24}+M_{42})\right]$$

$$+\tfrac{1}{2}(M_{12}-M_{21})(M_{33}+M_{44})$$

$$q_{21} = \tfrac{1}{2}(M_{12}-M_{21})\left[M_{33}M_{44} - \frac{1}{4}(M_{34}+M_{43})^2\right]$$

$$+\tfrac{1}{2}(M_{13}-M_{31})\left[\frac{1}{4}(M_{24}+M_{42})(M_{34}+M_{43}) - \tfrac{1}{2}M_{44}(M_{23}+M_{32})\right]$$

$$+\tfrac{1}{2}(M_{14}-M_{41})\left[\tfrac{1}{4}(M_{23}+M_{32})(M_{34}+M_{43})-\tfrac{1}{2}M_{33}(M_{24}+M_{42})\right]$$

$$q_{02} = \tfrac{1}{2}(M_{13}-M_{31})$$

$$q_{12} = -\tfrac{1}{4}\left[(M_{12}-M_{21})(M_{23}+M_{32})+(M_{14}-M_{41})(M_{34}+M_{43})\right]$$

$$+\tfrac{1}{2}(M_{13}-M_{31})(M_{22}+M_{44})$$

$$q_{22} = \tfrac{1}{2}(M_{12}-M_{21})\left[\tfrac{1}{4}(M_{24}+M_{42})(M_{34}+M_{43})-\tfrac{1}{2}M_{44}(M_{23}+M_{32})\right]$$

$$+\tfrac{1}{2}(M_{13}-M_{31})\left[M_{22}M_{44}-\tfrac{1}{4}(M_{24}+M_{42})^2\right]$$

$$+\tfrac{1}{2}(M_{14}-M_{41})\left[\tfrac{1}{4}(M_{23}+M_{32})(M_{24}+M_{42})-\tfrac{1}{2}M_{22}(M_{34}+M_{43})\right]$$

$$q_{03} = \tfrac{1}{2}(M_{14}-M_{41})$$

$$q_{13} = -\tfrac{1}{4}\left[(M_{12}-M_{21})(M_{24}+M_{42})+(M_{13}-M_{31})(M_{34}+M_{43})\right]$$

$$+\tfrac{1}{2}(M_{14}-M_{41})(M_{22}+M_{33})$$

$$q_{23} = \tfrac{1}{2}(M_{12}-M_{21})\left[\tfrac{1}{4}(M_{23}+M_{32})(M_{34}+M_{43})-\tfrac{1}{2}M_{33}(M_{24}+M_{42})\right]$$

$$+\tfrac{1}{2}(M_{13}-M_{31})\left[\tfrac{1}{4}(M_{24}+M_{42})(M_{23}+M_{32})-\tfrac{1}{2}M_{22}(M_{34}+M_{43})\right]$$

$$+\tfrac{1}{2}(M_{14}-M_{41})\left[M_{22}M_{33}-\frac{1}{4}(M_{23}+M_{32})^2\right].$$

Direct Method. As before, the direct method involves writing the transmit polarization in terms of the two spherical polar angles. The optimum polarizations then are the solutions to the following two non-linear equations:

$$\begin{aligned}&[(M_{12}-M_{21})\cos(\varphi)+(M_{13}-M_{31})\sin(\varphi)]\cos(\vartheta)-(M_{14}-M_{41})\sin(\vartheta)\\&-2(M_{23}+M_{32})\sin(\vartheta)\cos(\vartheta)\sin(\varphi)\cos(\varphi)-[(M_{24}+M_{42})\cos(\varphi)\\&+(M_{34}+M_{43})\sin(\varphi)](\cos^2(\vartheta)-\sin^2(\vartheta))-[M_{22}\cos^2(\varphi)\\&+M_{33}\sin^2(\varphi)-M_{44}]2\sin(\vartheta)\cos(\vartheta) = 0.\end{aligned} \tag{D-20}$$

and

$$\begin{aligned}&[(M_{13}-M_{31})\cos(\varphi)-(M_{12}-M_{21})\sin(\varphi)]-(M_{23}+M_{32})\sin(\vartheta)\cos(2\varphi)\\&-[(M_{34}+M_{43})\cos(\varphi)-(M_{24}+M_{42})\sin(\varphi)]\cos(\vartheta)\\&-(M_{33}-M_{22})\sin(\vartheta)\sin(2\varphi) = 0.\end{aligned} \tag{D-21}$$

To find the optimum polarization for discrimination between two scatterers when orthogonally polarized antennas are used for transmission and reception, the same procedure as described in Chapter 2 may be followed.

REFERENCES

[1] C.H. Papas, Theory of Electromagnetic Wave Propagation, McGraw - Hill, New York, 1965.

[2] J.R. Huynen, "Phenomenological Theory of Radar Targets," Ph.D. Dissertation, Drukkerij Bronder-Offset, N.V., Rotterdam, 1970.

[3] W-M. Boerner, M.B. El-Arini, C-Y. Chan and P.M. Mastoris, "Polarization Dependence in Electromagnetic Inverse Problems," *IEEE Transactions on Antennas and Propagation*, Vol. AP-29, pp. 262-270, March 1981.

[4] G.C. McCormick and A. Hendry, "Optimum Polarizations for Partially Polarized Backscatter," *IEEE Transactions on Antennas and Propagation*, Vol. AP-33, pp. 33-39, January 1985.

[5] M. Born and E. Wolf, Principles of Optics, Sixth Edition, Pergamon Press, New York, 1980.

[6] S. Chandrasekhar, Radiative Transfer, Dover, New York, 1960.

[7] H.C. van de Hulst, Light Scattering by Small Particles, Dover, New York, 1981.

[8] M.R. Spiegel, Advanced Calculus, Schaum's Outline Series, McGraw - Hill, New York, 1974.

[9] H. Mieras, "Optimum Polarizations of Simple Compound Targets," *IEEE Transactions on Antennas and Propagation*, Vol. AP-31, pp. 996-999, November 1983.

[10] E.M. Kennaugh, "Polarization Dependence of RCS - A Geometrical Interpretation," *IEEE Transactions on Antennas and Propagation*, Vol. AP-29, pp. 412-413, March 1981.

[11] J.J. van Zyl, N. Engheta, C.H. Papas, C. Elachi and H. Zebker, "Modelling of Backscatter from Vegetation Layers," *1985 Geoscience and Remote Sensing Symposium Digest*, Volume I, pp. 389-394, 1985.

[12] G.A. Ioannidis and D.E. Hammers, "Optimum Antenna Polarization for Target Discrimination in Clutter," *IEEE Transactions on Antennas and Propagation*, Vol. AP-27, pp. 357-363, May 1979.

[13] V. Twersky, "On Scattering of Waves by Random Distributions. I. Free-Space Scatterer Formalism," *Journal of Mathematical Physics*, Vol. 3, No. 4, pp. 700-715, July-August 1962.

[14] G.T. Ruck, D.E. Barrick, W.D. Stuart and C.K. Krichbaum, Radar Cross Section Handbook, Volume I, Plenum Press, New York - London, 1970.

[15] N. Engheta, C.H. Papas and C. Elachi, "On the Polarization Properties of the Far-Zone Radiation Fields of Primary and Secondary Electromagnetic Sources," *IEEE Antennas and Propagation Society 1984 International Symposium Digest*, Volume II, pp. 543-545, 1984.

[16] H.F. Mathis, "A Short Proof that an Isotropic Antenna is Impossible," *Proc. IRE*, Vol. 39, pp. 970 , 1951.

[17] C.J. Bouwkamp and H.B.G. Casimir, "On Multipole Expansions in the Theory of Electromagnetic Radiation," *Physica*, Vol. 20, pp. 539 , 1954.

[18] D.L Jaggard, A.R. Michelson and C.H. Papas, "On Electromagnetic Waves in Chiral Media," *Applied Physics (Springer - Verlag)*, Vol. 18, pp. 211-216, February 1979.

[19] W.H. Hayt, Jr, Engineering Electromagnetics, Third Edition, McGraw - Hill, New York, 1974.

[20] I.S. Gradshteyn and I.M. Ryzhik, Table of Integrals, Series, and Products, Corrected and Enlarged Edition, Chapter 10, Academic Press, New York, 1980.

[21] S.A. Schelkunoff and H.T. Friis, Antennas Theory and Practice, John Wiley and Sons, Inc., New York, 1952.

[22] J.D. Nespor, A.P. Agrawal and W-M. Boerner, "Development of a Model-free Clutter Description based on a Coherency Matrix Formulation," *IEEE Antennas and Propagation Society 1984 International Symposium Digest*, Volume I, pp. 37-40, 1984.

[23] D.E. Barrick, "Rough Surfaces," in Radar Cross Section Handbook, Volume II, G.T. Ruck Ed., Plenum Press, New York - London, 1970.

[24] G.R. Valenzuela, "Depolarization of EM Waves by Slightly Rough Surfaces," *IEEE Transactions on Antennas and Propagation*, Vol. AP-15, pp. 552-557, July 1967.

[25] D.N. Held, "The NASA/JPL Multipolarization SAR Aircraft Program," *1985 Geoscience and Remote Sensing Symposium Digest*, Volume I, pp. 454-457, 1985.

[26] R. Redheffer, "On the relation of Transmission-line Theory to Scattering and Transfer," *J. Math. Phys.*, Vol. 41, No. 1, pp. 1-41, 1962.

[27] G.N. Plass, G.W. Kattawar and F.E. Catchings, "Matrix Operator Theory of Radiative Transfer. 1: Rayleigh Scattering," *Applied Optics*, Vol. 12, No. 2, pp. 314-329, February 1973.

[28] J.C. Leader, "Polarization Dependence in EM Scattering from Rayleigh Scatterers Embedded in a Dielectric Slab," *Journal of Applied Physics*, Vol. 46, No. 10, pp. 4371-4391, October 1975.

[29] A.K.Fung and H.J. Eom, "Multiple Scattering and Depolarization by a Randomly Rough Kirchoff Surface," *IEEE Transactions on Antennas and Propagation*, Vol. AP-29, pp. 463-471, May 1981.

[30] H.J. Eom, "Scattering from a Layered Medium Connected with Rough Interfaces: Matrix Doubling Method," *1985 Geoscience and Remote Sensing Symposium Digest*, Volume I, pp. 496-504, 1985.